REPUBLIC OF TURKEY
ACIBADEM MEHMET ALİ AYDINLAR UNIVERSITY
INSTITUTE OF HEALTH SCIENCES

COMPARISON OF DNA REPAIR KINETICS AFTER RADIO- AND PARTICLE-THERAPY IN P53 RELEVANT B-CELL LYMPHOMA CELL MODELS

FATMA PINAR

MASTER THESIS

DEPARTMENT of MEDICAL BIOTECHNOLOGY

SUPERVISOR

Prof. Dr. İkbal Agah İnce

ISTANBUL - 2019

REPUBLIC OF TURKEY
ACIBADEM MEHMET ALİ AYDINLAR UNIVERSITY
INSTITUTE OF HEALTH SCIENCES

COMPARISON OF DNA REPAIR KINETICS AFTER RADIO- AND PARTICLE-THERAPY IN P53 RELEVANT B-CELL LYMPHOMA CELL MODELS

FATMA PINAR

MASTER THESIS

DEPARTMENT of MEDICAL BIOTECHNOLOGY

SUPERVISOR

Prof. Dr. İkbal Agah İnce

ISTANBUL - 2019

Department:	Medical Biotechnology
Program:	Medical Biotechnology
Thesis Title:	Comparison of DNA Repair Kinetics After Radio- and Particle Therapy in p53 Relevant B-cell Lymphoma Cell Models
Student's name and Surname:	Fatma Pınar
Date of Defance:	02/08/2019

This is to certify that Ihave examined this copy of master thesis. I have found that she/he prepared after fulfilling requirements specifed in the associated legislalations before the final examining committee whose signatures are below.

Jury president	Prof. Dr. Tanıl Kocagöz Acibadem Mehmegt Ali Aydinlar University	İmza 
Supervisor of the thesis	Prof. Dr. İkbal Agah İnce Acibadem Mehmet Ali Aydinlar University	İmza 
Jury Member	Assist Prof. Dr. Arzu Özgen Istanbul Gelisim University	İmza 

DECLARATION

I hereby declare that this thesis has been written by me based on the data obtained in line with the scientific rules and ethical principles of responsible conduct of research. All information, data, comments and analyses have been collected and processed in a scientific, academic manner, and the literature used has been duly shown by giving reference to the original sources in accordance with publication ethics. I also announce and emphasize that I have not violated any rules secured by patents and copyrights during the conduct and writing of this research.

Signature:

Name, Last name: Fatma Pınar

Date: 02.08.2019

ACKNOWLEDGEMENT

As a master's degree student, I wish to express my appreciation and gratitude to my university, my reputable advisors, my beloved colleague-friends and my dear family. First and foremost, I would like to thank my supervisor Prof. Dr. Ikbal Agah Ince for accepting me as his student 3 years ago. His supreme guidance provided golden opportunities to me and my fellow students. I would also like to express my gratitude to my second supervisor, Dr. Ali Nowrouzi for enabling me to perform this thesis in his research group as well as continuous support throughout this thesis. I am deeply grateful for his belief in me and his supervision and mentoring advice. I would like to express my gratitude to Dr. Amir Abdollahi for accepting that this thesis was performed in the division of Translational Radiooncology of the German Cancer Research Center. I also would like to express my gratitude to Dr. Mahdi Akbarpour for his patience with my endless questions and his help to analyze the data presented within this thesis. Further, my special thanks go to Dr. Ayca Zeynep Ilter for her insightful comments and suggestions which were of great help.

This study was carried out at the department of Translational Radiationoncology, in the German Cancer Research Center (DKFZ) in the Research Group of Dr. Ali Nowrouzi of the Heidelberg Institute of Radiation Oncology (HIRO). I am also very thankful to Acıbadem Mehmet Ali Aydınlar University for giving us the opportunity and scholarship to experience their world-class laboratories. Many of my fellow students, as well as my family, have encouraged me to not give up and supported me by providing helpful critiques. More than anything, I feel very lucky to have precious friends. First of all, I graciously thank Ömer Faruk Taştan for his infinite assistance with the laboratory work. I have always felt his support and continuous help through this journey. Moreover, I am grateful to have Jonas Poβmann who brings joy to my life and is my endorsement on technical issues by helping me with my endless requests. Finally, I appreciate having Süleyman Bozkurt, Kübra Doğan, Gülin Baran, Burcu Taluğ, Ayşegül Ekmekçioğlu, Hazal

Yılmaz and Tuba Polat as my best friends, who were there for me during the tough times and cheered me up with them with humor.

TABLE OF CONTENTS

Page

LIST OF ABBREVIATIONS

BL	: Burkitt lymphoma
DDR	: DNA damage response
DNA-PK	: DNA dependent protein kinases
DSBs	: Double-strand breaks
EBV	: Epstein-Bar-Virus
Gy	: Gray
HIT	: Heidelberg Ion Therapy Center
HR	: Homologous recombination
HIV	: Human immunodeficiency virus
IgH	: IgG heavy chain
IMRT	: Intensity modulated radiation therapy
IGK or IGL	: Immunoglobulin light chains
IRIF	: Ionizing radiation-induced foci
HIMAC	: Ion Medical Accelerator in Chiba
LET	: Linear Energy Transfer
NHLs	: Non-Hodgkin lymphomas
NHEJ	: Non-homologous end-joining
PIKK	: Phosphoinositide three-kinase-related protein kinases
RT	: Radiotherapy
ROS	: Reactive Oxygen Species
RBE	: Relative biological effectiveness
S15	: Serine 15
S18	: Serine 18
SSBs	: Single strand breaks
SOBP	: Spread Out Bragg-Peak

LIST OF FIGURES

Page

LIST OF TABLES

Page

SUMMARY

The induction of DNA-double-strand-breaks (DSB) is a hallmark of radiation-induced cytotoxicity. Upon induction of DSBs, the cellular DNA repair machinery detects these lesions and activates signaling cascades which induce the repair of DSBs. A key component in DNA repair is the histone protein H2AX, which is rapidly phosphorylated on a serine four residue from the carboxyl terminus, forming γH2AX at nascent DSB sites. After cells are exposed to ionizing radiation (IR) or heavy ion particles, a large number of γH2AX molecules form so called radiation-induced foci (RIF), where DNA repair proteins accumulate to promote the repair of DSBs. The microscopic visualization of RIF using immunohistochemistry is therefore considered a surrogate for measuring the radiobiological effects (RBE) of radiation therapy. Sequential quantification of RIFs after exposure to IR can also serve as a surrogate for measuring DNA repair kinetics, as it is proportional to the complexity of DNA damage, and the intrinsic ability of the cell to efficiently repair RIF. hIn this study, Human and mouse temperature-sensitive p53 B-cell lymphoma cell models were used to measure and compare the presence of DSBs after IR with photon, proton and carbon beams. The uniqueness of this approach relies on the fact that the effects of p53 mutant (p53-Val135) and p53 wild type in myc-driven lymphomas can be measured in parallel and with the same genetic background. The application of particle radiation to the cells used in this thesis was carried out at the Heidelberg-ion beam therapy center (HIT). HIT is one of the few locations in the world where the radiobiological effects of photons, protons and especially carbon beams can be measured simultaneously.

In summary, the quantification of RIF has been used as a molecular surrogate to measure the RBEs of photon, proton and carbon beams as a function of DNA repair kinetics and functionality of p53, providing molecular and radiobiological insights into radio- and particle-therapy for B-cell lymphomas. Finally, this study aims to show the role of p53 and the effect of radiation on B-cell lymphoma,

which in the future could provide a new treatment method for patients with lymphoma.

Keywords: DNA double strand breaks, p53 protein, B-cell lymphoma, radiotherapy, γ-H2AX

ÖZET

Radyoterapi ve Partikül Terapisi ile P53 Ilişkili B-Hücreli Lenfoma Hücre Modellerinde DNA Tamir Mekanizması Kinetiğinin Karşılaştırılması

DNA-çift sarmal kırıklarının (DSB) indüksiyonu, radyasyona bağlı sitotoksisitenin bir işaretidir. DSB'lerin indüklenmesi üzerine, hücresel DNA onarım mekanizması bu lezyonları tespit eder ve DSB'lerin onarımını indükleyen sinyal kaskadlarını aktive eder. DNA tamir mekanizmasında kilit rol oynayan histon proteini, H2AX, DNA çift sarmal kırık bölgelerinde karboksil terminalinden serin dört kalıntısı üzerine fosforile olarak γ-H2AX'e dönüşür. Hücrelerin iyonlaştırıcı radyasyona (IR) veya ağır iyon partiküllerine maruz bırakılmasından sonra, çok sayıda γH2AX molekülü radyasyona bağlı odakları (RIF) oluştur. Buna bağlı olarak DNA tamir proteinlerinin birikir ve DNA onarım mekanizması başlatılır. Bu nedenle immünohistokimya yöntemi kullanılarak RIF'in mikroskobik görüntülenmesi, radyasyon tedavisinin radyo biyolojik etkilerini (RBE) ölçmek için bir araç olarak düşünülmektedir. Mikroskobik görüntülemenin yanısıra, hücrelerin IR'ye maruz bırakılmasından sonra DNA hasarı ile orantılı olan sıralı RIF ölçümü, DNA onarım kinetiğini belirlemek için kullanılır. Foton, proton ve karbon ışınları arasındaki IR kaynaklı DSB'nin indüksiyonunu ölçmek ve karşılaştırmak için sıcaklığa duyarlı p53 B-hücreli lenfoma insan ve fare hücre modeli kullanıldı. Bu yaklaşımın özgünlüğü, p53 mutantın (p53-Val135) ve p53 yabani tipinin, myc kaynaklı lenfomalar üzerindeki etkilerinin eş genetik arka plan kullanılarak ölçülebilmesine dayandırılmaktadır. Bu tez çalışmasında kullanılan, hücrelere parçacık radyasyonun uygulanması Heidelberg-iyon ışını terapi merkezinde (HIT) gerçekleştirilmiştir. HIT, foton, proton ve özellikle karbon ışınlarının radyobiyolojik etkilerinin aynı anda ölçülebildiği, dünyada bulunan az sayıdaki bölgeden biridir.

Özet olarak, RIF ölçümü, DNA onarım kinetiğinin bir fonksiyonu olarak foton, proton ve karbon ışınlarının RBE'lerini ölçmek için moleküler aracı olarak kullanılmıştır. Ek olarak, B-hücreli lenfomalar için radyoterapi ve partikül terapisi p53'ün işlevselliğini ölçmek için kullanılmıştır. Son olarak, bu çalışma p53'ün ve

radyasyonun B-hücreli lenfoma üzerindeki etkisini göstererek, gelecekte lenfoma hastaları için yeni bir tedavi yöntemi geliştirilebilmesini amaçlamıştır.

Anahtar Kelimeler: DNA çift iplikli kırık, p53 proteini, B-hücreli lenfoma, radyoterapi, γ-H2AX

1. AIM OF STUDY

Over 50% of cancer patients undergo radiation therapy. The direct radiobiological effects (RBE) of Radiation therapy rely on the induction of DNA double strand breaks which eventually induce senescence and apoptosis of tumor cells upon a specific threshold or radiation dose. Particle therapy in contrast to conventional Photon therapy describes a technology by which beams of energetic protons, neutrons and ions are used to irradiate cells and tumors. Particle therapy provides a higher precision due to the fact that the dose increases while the particle penetrates the tissue until the Bragg peak. Moreover, from the radiation biology standpoint especially carbon ions have the advantage that they provide a higher relative biological effectiveness (RBE) which can be measured by sequential analyses and quantification of γ-H2AX-foci which serves as a surrogate for DSB induction and repair. Within this thesis the RBE of Photon, Proton and Carbon beams was analyzed and compared in a human and mouse temperature sensitive p53 B-cell lymphoma cell model using microscopy of γ-H2AX-foci sequentially after exposure to the three radiation qualities. We hypothesized that in this cell model the superior RBE of Proton and Carbon beams would be measurable based on the kinetics of DNA repair and that the re-expression of wild type p53 protein increases the RBE of radiation and particle therapy substantially. To address these questions the following aims were successfully implemented within this master thesis:

1. Irradiation of human and mouse B-cell lymphoma cells expressing mutant p53 and wild type p53 with Photon, Proton and Carbon beams.
2. Cytospin and immunostaining of γ-H2AX-foci 1 h, 24 h and 72 h post radiation exposure.
3. High-throughput microscopy of γ-H2AX-foci samples.
4. Analyzes and quantification of γ-H2AX-foci form all samples using in house developed ImageJ macros.

The analyses and comparison in the kinetics of DNA repair based on the quantification of γ-H2AX-foci 1, 24, and 72 hours post exposure to Photon,

Proton and Carbon beams verified the superior RBEs of Proton and Carbon beams compared to Photon beams and showed that reactivation of wtp53 in lymphoma lines increases the RBE of radiation therapy in general substantially.

2.INTRODUCTION

2.1. Burkitt Lymphoma

Lymphomas are a diverse group of neoplastic disorders of lymphocytes and the World Health Organization (WHO) classifies lymphomas according to their biological, clinical characteristics and origin as neoplasms of B-cell or T-cell origin. In general, lymphomas are considered as the non-Hodgkin lymphomas (NHLs) and Hodgkin lymphomas separately (1) (2). In the classification of lymphoid neoplasm, Burkitt lymphoma (BL) is defined as a highly aggressive mature B-cell neoplasm, a form of non-Hodgkin's lymphoma and includes endemic, sporadic and immunodeficiency clinical variants. Endemic type is associated with infection of Epstein-Bar-Virus (EBV), mostly seen in Africa. It is estimated that this type accounts for 30 to 50% of all childhood cancers in Africa and the incidence is 3-6 cases per 100,000 children in a year (2). The second variant of BL is sporadic which has histopathological features of endemic BL and constitutes 1-2% of all adult lymphomas in United States and Europe (3). Even though, the frequency of sporadic BL in the United States and Europe (approximately 2.2 cases per million) is increasing every year, the incidence is still much lower than Africa. The third variant constitutes 20% of BL and is associated with infections with the human immunodeficiency virus (HIV), thereby, is defined as immunodeficiency BL (2).

Burkitt Lymphoma is characterized by overexpression of MYC transcription factor through the translocation of *c-myc* gene to one of the immunoglobulin loci (4) (5). The MYC gene family consist of oncogenes and regulator genes that encode transcription factors and responsible for regulating pathways including cell growth and proliferation, DNA replication, differentiation and apoptosis (6). The translocation of the *c-myc* gene on chromosome 8 occurs in 95% of BL cases. In case of translocation, MYC oncogene is relocated juxtaposed to the promoter sequence of the immunoglobulin IgG heavy chain (IgH) on chromosome 14. The t(8;14) (q24;q32) is the most common translocation in BL, occurring in 70% to 80% of all the cases. Other translocations also occurred in the immunoglobulin

light chains (IGK or IGL) on chromosome 2 or 22 caused the dysregulation of the MYC. In addition to translocations of *c-myc*, several other mutations are also caused BL development. These mutations are truncating alterations of PTEN, NOTCH, and ATM, amplifications of RAF1, MDM2, KRAS, IKBKE, deletion of CDKN2A, and CCND3 activating mutations. Besides that, it is not uncommon for tumor suppressor gene TP53 to be mutated in the neoplastic cells of BL (7).

Cancers like Burkitt lymphoma can be caused also by various chemicals. Even some patients who have undergone long-term chemotherapy for another cancer type have a higher risk of developing Burkitt lymphoma than those who never had chemotherapy. In the treatment of Burkitt lymphoma, radiotherapy and chemotherapy have been used for many years. In reported clinical trials, the prognosis for BL is generally favorable, with median survivals of 75% to 90% with modern chemoimmunotherapy regimens (8). Recently, immunotherapy and chemotherapy with the addition of rituximab display as an important treatment when used with radiotherapy against lymphoma (9).

2.2. Chemotherapy and Radiotherapy

Two of the most commonly used type of cancer treatments are chemotherapy and radiotherapy. The term of chemotherapy refers to the use of chemical drugs to treat the cancer. The chemotherapy drugs affect mostly the cancer cells. As cancer cells divide faster than normal cells, they are more prone to be affected by the cytotoxic effect of chemotherapy. These chemicals can be DNA damaging agents, antimetabolites or mitosis inhibitors. Apart from their toxicity to cancer cells, these chemicals have also an effect on normal cells, thereby, causing unintended side effects on patients (10)

Radiotherapy (RT) is the use of ionizing radiation to destroy tumor while preserving normal tissues. Many cancer patients receive radiotherapy, using X-ray and other radiation qualities. The success of this therapy depends on the dosage and frequency of the treatment, and the level of the cancer of the patient (11). Ideally, it is expected that multiple doses of radiation would kill only cancerous

cells, however, RT may lead to undesired side effects on normal cells. In rare cases, damage to normal cells can be repaired incorrectly, which can cause new cancer (12). It can be used alone as well as with surgery and chemotherapy. The aim of radiotherapy is to treat the cancer and minimizing damage to normal tissues (13). In addition, radiation makes it possible to target the tumor with high accuracy by using high doses and this makes RT an alternative to surgery (14). In conclusion, the reason that radiotherapy is still commonly used is that the benefits are much greater than the potential negative effects.

2.3. Ionizing Radiation and other Radiation Qualities

Radiation therapy kills cancer cells by depositing high physical energy and this radiation called ionizing radiation (15). Through the removing of electron, the atom or electron increase the higher level and it's called extinction. Ionization is the energy state of radiation required to remove and excite one or more electrons from the orbit of the atom and molecule. The most important feature of ionizing radiation is the localized release of large amounts of energy. Ionizing radiation can act in two ways: directly and indirectly (Figure 2.1). If any form of radiation is absorbed in the biological material, the radiation interacts directly with the main target and it results in ionization of target atoms in the cell. High linear energy transfer (LET) such as neutrons or alpha particles perform direct action. The radiation interacts with other atoms and molecules in the cell through produce free radicals to reach the main targets and cause harm. It produces free radicals that are used to achieve and harm the main targets. While providing this, it interacts with other atoms and molecules is called the indirect action of radiation (16).

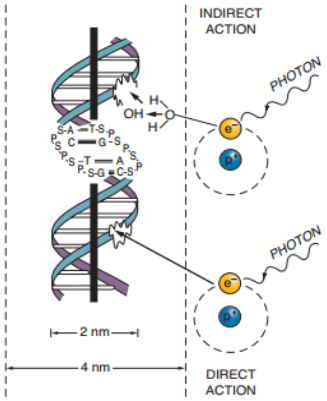

Figure 2.1. Direct and indirect actions.

Ref (16): Hall EJ, Giaccia AJ. Radiobiology for the Radiobiologist. 2012, 7. p.9-10.

Low LET radiation such as X-rays and gamma-rays is caused 60% of cellular damage by this indirect effect of radiation. The Linear Energy Transfer (LET), defined as the biological activity of ionizing radiation, often expressed in keV / µm, is the amount of energy released by the particle over the decay length. This amount of energy is divided into two depending on the energy density of the emitted particle as high and low LET radiation (15). The difference between low and high LET radiation is the number of particles necessary to deposit a certain energy dose (17). As an example of low LET radiation Photons can be given and is the most common type of radiation used in many cancer treatments (18). Photon radiation penetrates highly while entering into the tumor and normal tissue. Dosing less than optimal is made to restrict the effect of radiation on normal tissue (19). With Photon beams, intensity modulated radiation therapy (IMRT) is the most advanced method for delivering high doses. IMRT provides radiation to the target tumor through the crossing of multiple shaped beams of various intensities. Within this way, radiosensitive or adjacent tumors can be spared (20). An alternative method is to use heavy-particle radiation, this way the dose increasing can be provided while sparing normal tissue. Proton and Carbon ions can be given as examples of heavy particles. These particles deposit minimal radiation dose upon entry into tumor tissue. The radiation dose increases with greater depth and lower speed, suddenly rising to a peak, called the Bragg peak,

when heavy particles are stopped (19). Biological effects of charged particle beams increase depending on the dose of radiation as in photon treatment. There are differences in this absorbed energy accumulation arrangement at the microscopic level between heavy particles and Photon beams (16). Due to charged particles interact differently with tissues, they cause more pronounced biological effects when administered at the same dose as the Photons (20). This relative biological effectiveness (RBE) is defined as an absorbed dose of an amount of radiation, physical quantity with the unit of gray (Gy) (16). The biological effectiveness of radiation depends on; the linear energy transfer, the number of fractions, total dose, and radio sensitivity of the targeted cells or tissues (15). The heavy particles have different RBE and dose distribution characteristics. For example, while the Proton RBE is about 1.1, Carbon ions have been reported to have an RBE of around 3 (20). After heavy particles enter the tissue at a high rate, the collision between them has made the particles to slow down and stop. Thus, they gather a large part of their energy at the point called the Bragg peak (21). The Bragg peaks for the particles (Proton and Carbon beams) are very sharp and afterward, the beams need to be spread out uniform. This uniform spread is achieved by overlapping different Bragg peak points with specific densities and energies, and the resulting dose distribution is called Spread Out-Bragg-Peak (SOBP). For heavy particles, the depth-dose profile can be observed by a sharp Bragg peak, however it is occurred in the Photon beam (Figure 2.2) (22).

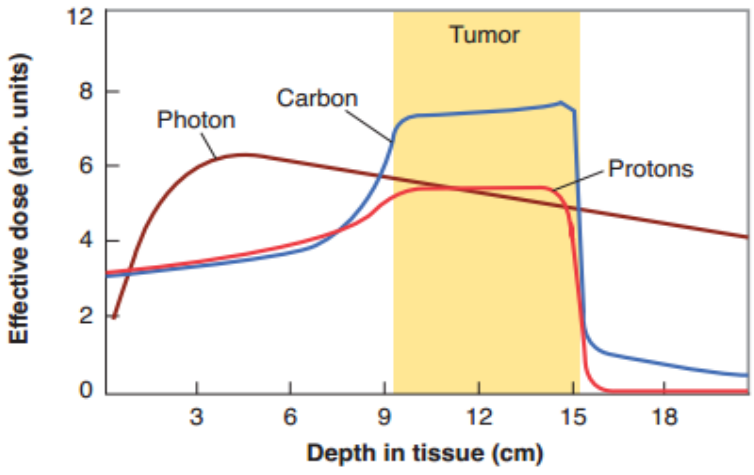

Figure 2.2. Comparing of Photon, Proton and Carbon ions the depth-dose profiles. While protons and carbon ions form Bragg peaks, this peak can spread at any depth to cover the tumor. Since carbon ions have high LET, SOBP is higher than other ions.
Ref (26): Hall EJ, Giaccia AJ. Radiobiology for the Radiobiologist. 2012, 7. p.9-10.

Protons have a low LET property because they sparsely ionize after entering the tissue. As it enters deeper into the tissue, they gradually release their kinetic energies. Within the speed increases, the time between successive events of energy accumulation shortens. When the Proton beams approach the end of the path, it releases all its energy at some point (Bragg peak) thus increases the LET and the RBE increases in turn. Because of these properties, Proton beams do not have a constant biological activity during their progression (23).

Transmission is another physical difference between Protons and Carbon ions. Due to their 12-fold higher mass, Carbon ions compared to Protons, tend to travel straighter until they stop in the tissue. Hence, Protons have the ability "halo" or penumbra to produce around the target region. Carbon ions with smaller penumbra are more advantageous to treat more sensitive tissues such as optic nerve or prostatic urethra (21). In cases where the tumor is difficult to treat (which are radioresistant tumors, or those present deeper in the body), high LET particles such as Carbon are used. Carbon ion-based RT was applied for the first time in the Heavy Ion Medical Accelerator (HIMAC) in Chiba, Japan in 1994. After Japan, Germany opened the Heidelberg Ion Therapy Center (HIT) in 2009 (24). The treatments in this thesis using Carbon-ion based IR were performed at HIT.

2.4. Radiation-Induced Critical DNA Damages

The free radicals that mediate to damage when ionizing radiation induces the biological effect are called Reactive Oxygen Species (ROS) (25). ROS has an important role in the damaging effects of low LET ionizing radiation. The hydroxyl radical formed as a result of radiolysis is joined to damage DNA (26). Oxidants and radicals, such as ROS produced during radiation, can damage proteins that ensure correct repair of DNA damage (27). Besides, ROS produce damage to DNA not only directly damage to DNA's sugar spine during radiation but also do indirectly damage through with free radicals such as mostly OH ion.

Furthermore, ROS can induce DNA damage through the oxidizing nucleoside base. This damage may cause G-T or G-A transversions if not repaired. Oxidized bases are recognized and repaired by the DNA repair mechanism. However, when it occurs in opposing strands, it cannot be repaired and causes DSB to form (28).

IR is caused DNA lesions per cell detected immediately after a dose. As result of this, more than 1000 base damage, approximately 1000 single-strand breaks (SSBs) and 40 Double-strand breaks (DSBs) per cell per gray can be produced (29). Breaks caused by IR in a single strand are called SSBs and it can occur as a function of dose when the DNA is denatured. During repair of SSBs, the other strand is used as a template and repaired easily. If damage occurs in the two strands, the breaks are opposite one another or separated by only a few base pairs, this causes DSBs. As a result of this, chromatin separates into two pieces (30-16). Although DSBs have effects such as cell death, mutation, genomic instability and carcinogen, the problems associated with the repair of high LET-induced DSBs are not fully understood. Therefore, it is important to investigate γ-H2AX induction and time-dependent loss, which is an indicator of DSBs (31).

2.5. γH2AX and Its Use as a Biomarker for the Determination of DNA Double

-Strand Breaks

IR causes the accumulation of many DNA damage response proteins in the DSB region, while it forms foci known as ionizing radiation-induced foci (IRIF) and it can be monitored by fluorescence microscopy (32). IRIF is required for accurate DNA repair (33). In addition, the main regulator of IRIF formation is the histone subtype H2A isoform X, which is a component of the cell nucleus structure and phosphorylation of this protein provides to quantify DNA damage response to sites of DNA damage (34). Using a fluorescent antibody specific for the γ-H2AX, discrete nuclear foci can be visualized at sites of DSBs.

H2A belongs to the protein family including histone proteins, such as H1, H3, H4 and play a part in chromatin organization by packaging eukaryotic DNA. H2AX is a member of the H2A family, and two H2As are found in each nucleosome, which is a basic subunit of chromatin (35). Although there are several histone modifications associated with DNA damage, the most focusing is the modification of the H2A variant, H2AX. This located different level (2 up to 25%) in chromatin depending on cell and tissue type (36).

One of the earliest events in the damage response is phosphorylation of H2AX (37). DSBs trigger the activation of PI3K-like kinases such as ataxia telangiectasia mutated (ATM), ATR (ataxia telangiectasia and Rad3-related), and DNA-PK (DNA-dependent protein kinase) (24). Upon the activation of the proteins, H2AX protein phosphorylates by DNA repair mechanism proteins at Serine 139 site and this phosphorylated form of H2AX is referred to as γH2AX (37) (38). The first-time form of phosphorylated H2AX was observed after exposure to γ-rays, thus it is called γ-H2AX (39). In more detail, ATM is activated by its autophosphorylation at Serine1981 position, which leads to dissociation of the inactive ATM dimers into single protein molecules with increased kinase activity. At Serine1981 position, ATM can be activated by its autophosphorylation and it leads to increasing kinase activity of ATM (40). In normal physiology, ATM is the main kinase for the phosphorylation of H2AX, among three kinases. Following the first phosphorylation of ATM, MRN complex (MRE11-RAD50-NBS1) makes further activate ATM. After recognizing DNA damage by MRN complex, Nibrin protein (NBS1) and mediator protein 1 (MDc1) alert ATM. The binding of NBS1 and MDc1 to γH2AX leads to the accumulation of repair proteins at the DSB sites (Figure 2.3) (36). ATM phosphorylates not only H2AX but also phosphorylates other response proteins such as BRCA1, 53BP1, and MDC1 as well as checkpoint proteins, Chk1 and Chk2. The aim of the phosphorylation of checkpoint proteins is to stop the cell cycle and to activate proteins responsible for DNA repair. Moreover, H2AX can also be phosphorylated by ATR and DNA dependent protein kinases (DNA-PK). In

addition to DSB dependent H2AX phosphorylation, in case of stress in replication, such as replication fork arrest, ATR lead single-stranded breaks (SSBs) dependent H2AX phosphorylation (41). DNA-PK is a mediator of phosphorylation of H2AX during hypertonic condition or apoptotic DNA fragmentation of cells (40).

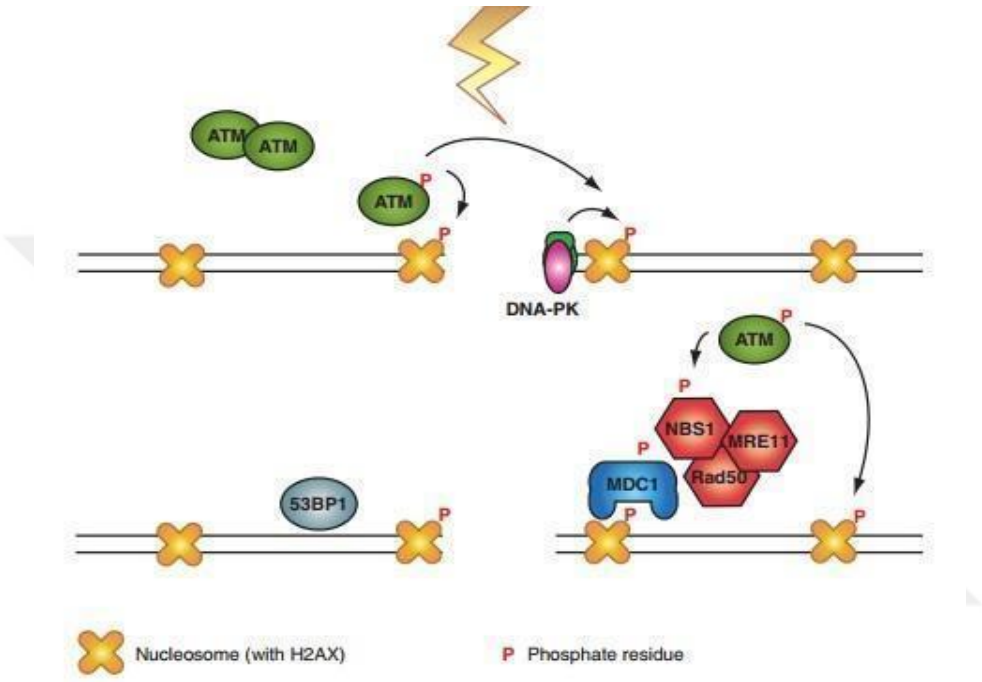

Figure 2.3. DSBs related to γH2AX signal signaling pathways.

Ref (36): Kinner A1, Wu W, Staudt C, Iliakis G. γ-H2AX in recognition and signaling of DNA double-strand breaks in the context of chromatin17, Nucleic Acids Res. 2008, 36. 5678-94.

There are two ways by which γH2AX formation can be used to visualize DSBs: 1) immunostaining of γH2AX foci followed by software aided counting, and 2) measurement of gamma H2AX protein levels by Western blot (37). The immunostaining of phosphorylated γH2AX proteins bound to chromatin is the most commonly used method to detect and quantify the induction and repair of DSB (38). Although the determination of non-DSB lesions can be done through fluorescence microscopy, this method has a disadvantage due to some DNA lesions cannot be monitored, such as 1-20 bp DNA lesions (42). Moreover,

immunofluorescence microscopic approaches using targeted antibodies could be used to visualize DNA lesions (24). DSB is induced not only by cancer development but also by cancer treatment, and this leads to the use of γH2AX as a potential biomarker for diagnosis, and a target for treatment (43). Thus, γH2AX can be used for the interpretation of treatment progress and to monitor cancer growth (44). Therefore, γH2AX can be used for both diagnoses, and for the evaluation of the impact of diverse factors on DNA damage.

2.6. DNA Damage Response and Repair Mechanisms

Non-repair of DSBs breaks causes genome instability and activates tumorigenesis. Therefore, the cells have mechanisms that consist of control points responsible for the recognition and activation of DNA damage (40). DNA damage response (DDR) is a signal transduction pathway that perceives DNA damage and stress and also protects the cell and repairs the damage (45). This mechanism also protects genomic integrity through multiple DNA repair pathways, cell-cycle checkpoints, and damage tolerance processes (46). Firstly, DNA damage/chromatin change is detected via sensor proteins from repair pathway. Following this, the signal is transmitted by transducers proteins, which are kinases that amplify the signal DDR. The DDR is regulated by the phosphoinositide three-kinase-related protein kinases (PIKK). PIKK is responsible for signaling the presence of DNA damage and includes ATM, ATR, and DNA-PKcs. In addition, all three kinases are taken into the DNA lesion site that supports kinase activation. Thus, PIKK phosphorylates hundreds of proteins that maintain genome integrity through cellular senescence, apoptosis, DNA repair (47). The occurrence of DNA damage causes many DDR proteins such as MRE11 / NBS1 / RAD50, MDC1, 53BP1 and BRCA1 to be re-localized in their nuclear foci where they previously interacted with γH2AX. γH2AX foci attract other repair proteins to the DSB region, resulting in higher repair. Other repair proteins recognize γH2AX in the presence of protein domains that bind to the phosphorylated carboxy terminus of γH2AX (40).

Unrepaired DSB may be sufficient to induce cell death by apoptosis. To prevent this, there are two main pathways for DSB repair, homologous recombination (HR) and non-homologous end-joining (NHEJ), which are error-free and error-prone, respectively. HR is observed in simple eukaryotes such as yeast, while NHEJ occurs in mammals. Another difference occurs in the NHEJ G0 / G1 cell cycle phase, whereas HR occurs in late S and G2 phases (48).

2.6.1. Non-homologous end joining

NHEJ repairs DSB by blunt end ligation using enzymes such as Ku70/80, DNA-PKcs, and DNA ligase IV. This repair mechanism has fast kinetics and is error prone but has a protecting role in suppressing genomic instability. The heterodimeric complex Ku70/80 binds to DNA ends and thus it protects the DNA from exonuclease digestion. After binding to DNA, Ku heterodimer produce DNA-PK holoenzyme by the association of subunit of DNA-PK. The interaction with single-strand DNA at the site of DSB activates DNA-PKcs. The XRCC4 (49) which is the target of activated DNA-PKcs, produce a complex with DNA ligase IV. LIG4 and XRCC4 together form the ligase complex and following activation of this complex, the DNA ends are linked (48). However, for re-ligation by XRCC4–ligase IV complex, processing of DSBs are required and re-ligation mainly performed by the integration of the MRE11-Rad50-NBS1 complex which displays exonuclease, endonuclease and helicase activity and includes FEN1 and Artemis. The MRE11-Rad50-NBS1 complex is responsible for removing excess DNA at 3' flaps while the flap endonuclease 1 (FEN1) is responsible for 5 'flap removal. The deficiency of this protein leads to a reduction in the use of the NHEJ pathway (48).

A protein called Artemis is responsible for overhangs during NHEJ, acting in a complex with DNA-PKcs. After forming a complex with and being phosphorylated by DNA–PKcs, gains endonuclease activity, degrading single-strand overhangs, and hairpins which is required for 5’ and 3’- overhangs during NHEJ (50).

2.6.2. Homologous recombination

Homologous recombination follows the slow kinetics in contrast to NHEJ. HR requires a sister chromatid for the repair of DSB and dominates in the mid-S and mid-G2 cell cycle phases, where the amount of DNA replication is highest and when the sister template is available. The repair is initiated by 5' to 3' nucleolytic resection of the DSB ends by the MRE11-Rad50-NBS1 (MRN) (80). Following this, 3 single-stranded DNA is bound by heptameric ring complex which is formed by Rad52 proteins. These proteins compete with Ku complex during the attachment DNA ends. This will determine whether the DSB will be repaired with HR or NHEJ.

Interaction of Rad52 with Rad51 and RPA stimulates DNA strand exchange activity of Rad51. The strand-exchange events are catalyzed by Rad51. The exchange events with the complementary strand in which the damaged DNA molecule invades the undamaged DNA duplex, displacing one strand as D-loop. The assembly of the Rad51 occurs with five different paralogues of Rad51 (Rad51B, C and D; and XRCC2 and XRCC3). Another protein is RPA which interacts with Rad51. It is known that RPA stabilized Rad51-mediated DNA pairing by binding to the displaced DNA strand. Following the recognition of DSB and strand exchanging by Rad proteins, there are structures which are resolved according to the classical model of Holliday (48) (51).

There is another protein called p53 which is linked to both repair pathways, NHEJ and HR, with the interaction of RAD51, DNA-PK which are able to modulate the function of p53 (52).

2.7. The Role of p53 Protein in the DNA Repair Mechanism

One of the best-known tumor suppressors is p53. It has a very short half-life in normal cells, whereas its half-life is dramatically prolonged in human tumor cells. The activation of p53 includes nutrient stress, hypoxic conditions, activation of oncogenes, DNA damage, oxidative stress from reactive oxygen species (ROS) and also a variety of stressful situations, such as telomere erosion, hypoxia,

mutational activation, and radiation, as a result, increase the activity of p53 (81). Depending on the extent of the damage, p53 can then promote apoptosis, cell cycle arrest, metabolic alterations. The variety of responses to a wide range of stresses, such as repairing defects and killing defective cells, reveals the tumor suppressor phenotype of the TP53 gene in p53 (53). Moreover, p53 encodes by the TP53 gene. The role of p53 extends well beyond its role as a tumor suppressor; it displays as an important regulator of metabolic homeostasis, pivotal in most major cell processes (81).

The induction of p53 in response to DNA damage is coordinated by the ATM and ATR protein kinases, which mediate the rapid destruction of MDM2 and MDM4. MDM2 and MDM4 act as a negative regulator, allowing the accumulation of the stable active state of p53 (54). As described above, ATM and ATR coordinate a complex signaling network in response to various forms of DNA damage (47). ATM plays a crucial part in the immediate response to double-strand breaks by coordinating the activation and execution of checkpoint pathways and repair pathways. ATR plays a role in replication stress and DNA crosslinking. There is an association between the pathways regulated by these molecules, and they have similar downstream targets in the repair and checkpoint pathways such as the transducer kinases CHK1 and CHK2, component of the p53 pathway. ATM and ATR induce various post-transcriptional modification with one damage signaling an appropriate and proportionate manner according to the nature of the damage and the intensity of the stress. There are two important phosphorylation sites in p53: Serine 15 (S15) and Serine 18 (S18). S15 and S18 both have a role in inducing the interaction of p53 with the transcriptional machinery, and they can inhibit the interaction of p53 and MDM2 (54).

The mutation is as important as the induction of p53. Over 50% of human cancers show the loss of function mutations in the p53 gene and also, Donehower et al showed the deficiency of p53 caused cancers on mice (82). There are differences between mutant p53 and wild type p53. The wild type p53 is short-lived (20 min) whereas mutant p53 has a prolonged half-life (2 to 12 h) with

oncogenic potential. Furthermore, the wild type p53 protein responds to chemotherapy and radiation treatments and repair and protection of normal cells (homeostasis) are achieved. As such, p53 based therapy also provides the differential toxicity observed in therapies between normal cells and cancer cells, leading to cell death upon treatment (53). Thus, it is quite important to develop a novel strategy to eliminate the negative effect of mutant p53 on wild type p53 for efficient chemotherapy (83).

Radiation-induced death is called radio sensitivity, the wild type p53 (wtp53) plays an important role in mediating radio sensitivity. Fei et al stated that p53 has responsible from the cell's fate to live by inducing cell arrest, coupled with DNA repair, or to die by inducing apoptosis (52). Thus, p53 target genes summarized into two aspects. The first target genes (PUMA, P53AIP1, DR5, and others) (84) that directly mediate cell death by contributing to the radio sensitivity. Other genes (APAF1, caspase 6, BID and others) (85) lower cell death threshold to allow sensitizing radio or chemosensitivity. The IR dose is also important for determining cell fate. In the presence of low doses, it initiates reversible cell growth arrest and at high doses IR is the trigger for apoptosis. There are several possible responses to IR before passed to p53 radiation response. One possible response is the phosphorylation of Ser345 on CHK1 and has been found that it is associated with a p53-dependent cell cycle arrest pathway. Additionally, Ser1423 phosphorylation on BRCA1 has a role ATM-dependent G2/M arrest after IR. These two responses indicate whether the cells have entered arrest or apoptosis by stimulating p53 signals. Factors like this may play a role in modifying the choice of outcome. In addition, the intensity of DNA damage plays an important role in determining cell fate after radiation (52).

Regarding radiation, p53 is the main regulator of DNA repair mechanisms and does so by promoting protein translation and inhibition of protein degradation (86). At the same time, p53 contains two transcriptional activation domains that can enhance the transcription of downstream target genes as a transcription factor. Following radiation, activation of DDR caused the increasing of p53 protein level

in the nucleus. As a result of the accumulation of p53 protein caused the signaling pathway activation, apoptosis can be induced, which also takes the cell to replication arrest. Therefore, p53 plays a crucial role in controlling cellular fate after irradiation (35).

Future studies on p53 functioning at the switch from reversible arrest to induced apoptosis may offer a greater understanding of radio resistance and radio sensitivity.

3. MATERIALS AND METHODS

3.1. Cell Cultures

BL41 wild type p53, BL41 mutated p53 and J3D wild type p53, J3D mutated p53 cell, cell lines were cultured in a humidified incubator at 5% CO_2 and 37˚C. Cells were maintained in Roswell Park Memorial Institute (RPMI) medium (Thermo Fisher, 11875101) and supplemented with 10% (v/v) fetal bovine serum (FBS, Merck, S0615) and 1% (v/v) Penicillin-Streptomycin (Roth, 15140122). Stock J3D and BL41 cells were taken from the liquid container and warmed up to 37 ˚C. The cell suspension was collected into a sterile 15ml falcon tube and 9 mL RPMI growth medium was added dropwise to the cell suspension. Cells were centrifuged at 800 rpm for 5 minutes, and the supernatant was discarded. The cell pellet was resuspended in 10mL RPMI growth medium and transferred into a T175 cell culture flask containing 10mL growth medium then incubated in a mammalian cell incubator at 37˚C and 5 % CO2. Cell passaging was performed when cells reached 70% confluency. During the experiment, temperature-wild type p53 was activated by reducing the temperature to 32°C. For long term storage, 1x 10^6 cells were resuspended in 500µL freezing medium containing 30% (v/v) FBS, 15% (v/v) Dimethyl sulfoxide (DMSO, PAN Biotech, P60-36720100) and 55 % RPMI growth medium and were frozen at -80˚C using an isopropanol tank and transferred to a liquid nitrogen container the following day.

3.2. Irradiation

1 Gy and 3 Gy Carbon irradiation was performed with 248.9-284.8 MeV/u (median LET: 55keV/µm, ranging from 45-150 keV/µm), corresponding to a median of 135 mm water equivalent depth within a 35 mm wide SOBP. For 2Gy and 5 Gy proton irradiation the same SOBP constraints were utilized by energies ranging between 129.3-148.2 MeV/u and median LET: 3.5 keV/µm (ranging from 2.9-7.9 keV/µm). All particle irradiations were carried out at the Heidelberg Ion Beam Therapy Centre (HIT, University Hospital, Heidelberg, Germany), using a

raster-scanning technique. 2 and 5 Gy Photon Irradiation was performed at the DKFZ using a Siemens linear accelerator (LINAC, Artist 6mV) system.

3.3. Cytospins and Immunofluorescence staining

To monitor the ionizing radiation induced DNA damage foci, γ-H2AX staining was performed for 1 hour, 24 hours, and 72 hours post-irradiation time points and untreated cells as the control.

Firstly, cells were counted as $1x10^6$ cells/ml and kept on ice. Before adding cell suspension, cytospin chambers were equilibrated using 100 µl of DPBS and centrifuged at 750 rpm for 1 min at 4°C. Following the equilibration, 100 µl of cell suspension was added to chamber tubes and the chambers were centrifuged at 750 rpm for 3 min at 4°C. Chambers were removed and spots were marked with a hydrophobic pap pen. Cold fixation buffer (4% (w/v) PFA in PBS) was added to (the) spots and incubated at room temperature (RT) for 20 mins. After twenty mins, the incubation spots were washed with DPBS. Cell spots were washed using DPBS containing 0.1% (w/v) BSA and slides were placed in 15 cm petri dishes.

Cell spots were washed twice using DPBS and were incubated at RT for 30 mins in 50µL blocking buffer, containing 3% (w/v) Bovine Serum Albumin (BSA) and0.1% (v/v) Triton X in DPBS. The permeabilization step was performed by incubation of cells with buffer containing 0.1% (v/v) Triton and 3% (w/v) BSA in DPBS for 30 minutes. Cells were washed by washing buffer which was a dilution of blocking buffer in PBS at a ratio of 1:3. Primary antibody against γ-H2AX (STA-321, Cell Biolabs) was diluted 1:100 in washing buffer and incubated overnight in a humid chamber at 4°C. The next day, cells were washed 3 times with DPBS and secondary antibody (A21424, Alexa Flour555 Goat anti mouse, Invitrogen) was added at a ratio of 1:400 in washing buffer followed by incubation for 1 hour at RT. Cells were washed three times with DPBS and one time with ddH_2O, then mounted with ProLong Gold Antifade Mountant.

3.4. Screening and Analysis

Imaging was performed using Olympus Cell-R fluorescent microscopy at the light microscopy facility (LMF) of DKFZ. At least six images of different non-overlapping fields per sample were quantified. The final analysis was performed in SUMO which gives histogram and number of cell count, cell with foci, sum foci, foci area and foci intensity.

Following this, foci numbers/cell were calculated for each replicate divided of sum foci to cell count and normalized to non-treatment control calculation. For data processing and quantification of radiation-induced foci (RIF), Fiji (Rasband, W.S., ImageJ, U.S. National Institutes of Health, Bethesda, Maryland, USA. https://imagej.nih.gov/ij/, 1997-2016) software was used and we also applied inhouse developed macros and SUMO (http://angiogenesis.dkfz.de/oncoexpress/software/ software implemented by Dr. Christian Schwager). The frequency of γ-H2AX foci was measured in irradiated and non-irradiated cells.

3.5. Statistical Analysis by T-test

Represented data were derived from two replicates and showed as the mean ± standard deviation (S.D). In addition, the t-distribution is a continuous probability distribution that arises when estimating the mean of a normally distributed population. In the comparison between samples, p-values were displayed two-tailed and as a type of t-test, two-sample assuming unequal variance were performed. P values under 0.05 were considered as statistically significant.

4.RESULTS

4.1. Determination of DNA Damage Repair-Kinetics γH2AX Foci in Response to Ionizing Radiation in Lymphoma Cell Lines

γ-H2AX foci are used as a reliable marker to quantify DSBs as well as an applicable tool to study DNA damage repair kinetics. In normal cells, the induced γ-H2AX foci mostly disappear within 24-72h post-irradiation. In this thesis, we aimed to compare the frequency of radiation-induced γ-H2AX foci in lymphoma cell lines using three different radiation qualities (Photon, Proton, and Carbon). In addition, we analyzed and compared the effects of wtp53 vs mutant p53 on DNA repair kinetics in the same cell lines. In order to determine the frequency of DSB and the kinetics of DNA, we exposed human BL41 and J3D lymphoma cell lines to a dose series of Photon, Proton and Carbon radiations at the Heidelberg Ion-Beam Therapy Center (HIT) repair (Figure 4.1.).

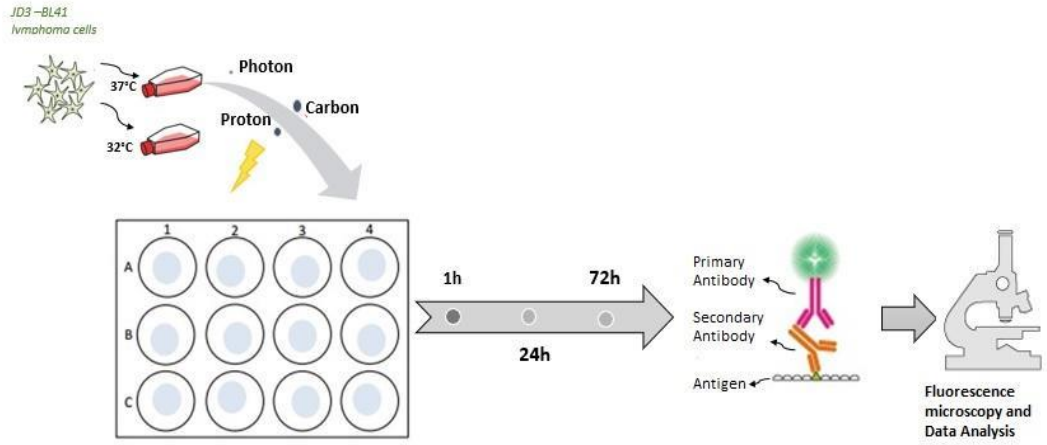

Figure 4.1. Outline of the performed experiments. To quantify radiation induced DSB γH2AX antibody was used. For a conformational change, cells incubation temperature shift to 32°C induces the wild type configuration of p53 and at 37°C, cells conformation is the mutated form (described in Section 3.3.1). After this, BL41 and J3D wild type and mutant cells were seeded on cytospin chambers at 10^6 cells/ well density in triplicates. Cells were exposed to graded doses of different types of ionizing radiation (IR). Fixed, permeabilized cells were incubated with Anti-Phospho-Histone H2AX (Ser139) antibody and nuclei were counterstained with DAPI at 1 h, 24 h and 72 hours post-treatment. Cell death was compared to untreated samples after the indicated

treatments. Images of γ-H2AX foci number, foci area, and foci intensity were analyzed using the Image J program with SUMO software.

Plates were incubated overnight at 37°C-32°C and irradiations were performed using doses of 2 Gy and 5 Gy of Photon and Proton beams and 1 Gy and 3 Gy Carbon beams in the following morning. After 1 h, 24 h and 72 h, corresponding cells were fixed, and staining were performed with a γ-H2AX antibody. Finally, florescence microscopy was used to analyze the images with regards to γ-H2AX foci formation (Figure 4.1.). Based on cell viability of the BL41 and J3D lymphoma cell lines were investigated after 32°C culture conditions in which p53 is mostly expressed in the wild type conformation and at 37°C which conditions p53 is predominantly expressed in the p53-Val135 mutant configuration (55). This difference between the two cell lines was first demonstrated by comparing the cell numbers obtained from the Image J analysis. For both BL41 and also J3D mutant and wtp53 cell lines, the total cell numbers obtained at each time point and exposed to each radiation quality were calculated, and these cell numbers are shown in Tables 1 and 2. BL41 mutant p53 cell numbers were higher than BL41 wild type cell numbers ($p < 0{,}0001$), whereas the number of J3D mutant p53 cell number were no significant ($p > 0.05$) difference with J3D wild type p53 cell numbers (Figure 4.2).

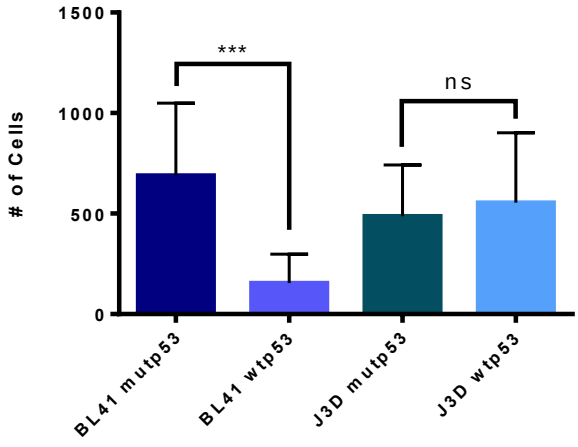

Figure 4.2. Overview of number of cells analyzed. Average of the cell numbers obtained from the foci analysis using ImageJ with compatible macros and the in house developed software, SUMO. The standard deviations are displayed by the error bars for independent duplicates per time point.

p-values were determined using t-test. Symbols used in charts means; when p values were found higher than 0.05 shown as ns, $p \leq 0.05$ (*), $p \leq 0.01$ (**) and $p \leq 0.001$ demonstrated as (***).

The number of cells obtained in the dose and post-irradiation time values used for both BL41 and J3D mutant p53 and wild type p53 cell lines and the number of cells containing foci are shown in Table 4.1 and Table 4.2. Following exposure to three different radiation, the percentages of foci positive cells at all time points were calculated based on the average of total cell numbers and cell numbers which were foci positive. The counting cells which have foci independent of the foci frequency, size, intensity were in BL41 mutant p53 and wtp53 has been shown both Table 4.1 and also Figure 4.2. Considering the values shown in Table 4.1, Figure 4.3 and 4.4, we evaluated BL41 mutant p53 and wtp53 values separately with Photon, Proton and Carbon IR. After radiation, first observation is that the frequency of foci positive cells decreased sequentially after 1 h, 24 h, and 72 h. Foci positive percentages of Photon 2 Gy treated BL41 mutant p53 cells at 1 h post-irradiation were shown as 78% when foci positive levels were presented as 61% at 24 h and at 72 h post-irradiation was 42%. After increasing the dose, to Photon 5 Gy the percentage of foci positive cells were determined as 92% at 1 h post-irradiation and it decreased to 82% and 45% after 24 h and 72 h post-irradiation (Table 4.1-Figure 4.3). Following this, in Proton 2 Gy treated BL41 mutant p53 cells, the percentage of foci positive cells were found at 1 h post-irradiation as 95% while at 24 h and 72 h post-irradiation 39% and 26%, respectively. Likewise, although Proton 5 Gy the percentage of foci positive cells also decreased over time. Likewise, Carbon 1 Gy, and 3 Gy treated foci positive levels decreased over time (Table 4.1). In BL41 mutant p53 cells, at 1h post-irradiation, Photon 5 Gy the percentage of foci positive cells were significantly ($p \leq 0.01$) higher than Photon 2 Gy cells numbers and it can be observed that there were no significant ($p > 0.05$) differences in the frequency of foci positive cells at 24 h and 72 h post-irradiation. Despite this, there were significant ($p \leq 0.05$) differences between doses Carbon IR (1 Gy-3 Gy) at 1 h and 72 h post-irradiation whereas there were no significant ($p > 0.05$) differences between Carbon 1 Gy and 3 Gy cells numbers (Table 4.1-Figure 4.3).

Table 4.1. BL41 wild type versus mutant p53 cells, overview of the cell numbers and percentages of foci.

Cell Type	Radiation Type	Dose	Post RT	Cell Number	%Foci Positive
BL41 mutp53	Photon	2	1	565	78
BL41 mutp53	Photon	2	24	1155	61
BL41 mutp53	Photon	2	72	432	42
BL41 mutp53	Photon	5	1	1167	92
BL41 mutp53	Photon	5	24	1348	82
BL41 mutp53	Photon	5	72	191	45
BL41 mutp53	Proton	2	1	603	95
BL41 mutp53	Proton	2	24	425	39
BL41 mutp53	Proton	2	72	425	26
BL41 mutp53	Proton	5	1	857	99
BL41 mutp53	Proton	5	24	600	62
BL41 mutp53	Proton	5	72	401	12
BL41 mutp53	Carbon	1	1	501	96
BL41 mutp53	Carbon	1	24	1108	68
BL41 mutp53	Carbon	1	72	355	8
BL41 mutp53	Carbon	3	1	837	99
BL41 mutp53	Carbon	3	24	904	57
BL41 mutp53	Carbon	3	72	389	20
BL41 wtp53	Photon	2	1	37	89
BL41 wtp53	Photon	2	24	234	59
BL41 wtp53	Photon	2	72	309	32
BL41 wtp53	Photon	5	1	98	95
BL41 wtp53	Photon	5	24	66	63
BL41 wtp53	Photon	5	72	70	47
BL41 wtp53	Proton	2	1	76	96
BL41 wtp53	Proton	2	24	0	0
BL41 wtp53	Proton	2	72	537	54
BL41 wtp53	Proton	5	1	92	91
BL41 wtp53	Proton	5	24	39	78
BL41 wtp53	Proton	5	72	222	75
BL41 wtp53	Carbon	1	1	148	96
BL41 wtp53	Carbon	1	24	62	72
BL41 wtp53	Carbon	1	72	395	67
BL41 wtp53	Carbon	3	1	98	98
BL41 wtp53	Carbon	3	24	67	78
BL41 wtp53	Carbon	3	72	164	86

As in BL41 mutant p53 cells levels, BL41 wtp53 cells the percentage of foci positive cells was the highest in 1 h post-irradiation of all radiation qualities. Photon 2 Gy 1 h post-irradiation was detected as 89% in BL41 wtp53 cells while 24 h and 72 h post-irradiation values were 59% and 32%, respectively. Besides that, Photon 5 Gy the percentage of foci positive cells was recorded at 1 h post-irradiation as 95% and 24 h and 72 h post-irradiation were found to be 63% and 47%, respectively (Figure 4.4). Proton 2 Gy treated BL41 wtp53 cells the percentage of foci positive cells were determined as 96% at 1 h post-irradiation and 54% after 72 h. Although at 1 h post-irradiation the percentage of foci positive cells were demonstrated higher ($p \leq 0.05$) than 24 h and 72 h post-irradiation levels, there was no major difference ($p > 0.05$) between 24 h and 72 h post-irradiation the percentage of foci positive cells in Carbon 1 Gy treated BL41 wtp53 cells. After the increasing the dose to Carbon 3 Gy in BL41 wtp53 cells the percentage of foci positive cells at 1 h post-irradiation were significantly ($p \leq 0.001$) higher than levels at 24 h post-irradiation (Table 4.1-Figure 4.4).

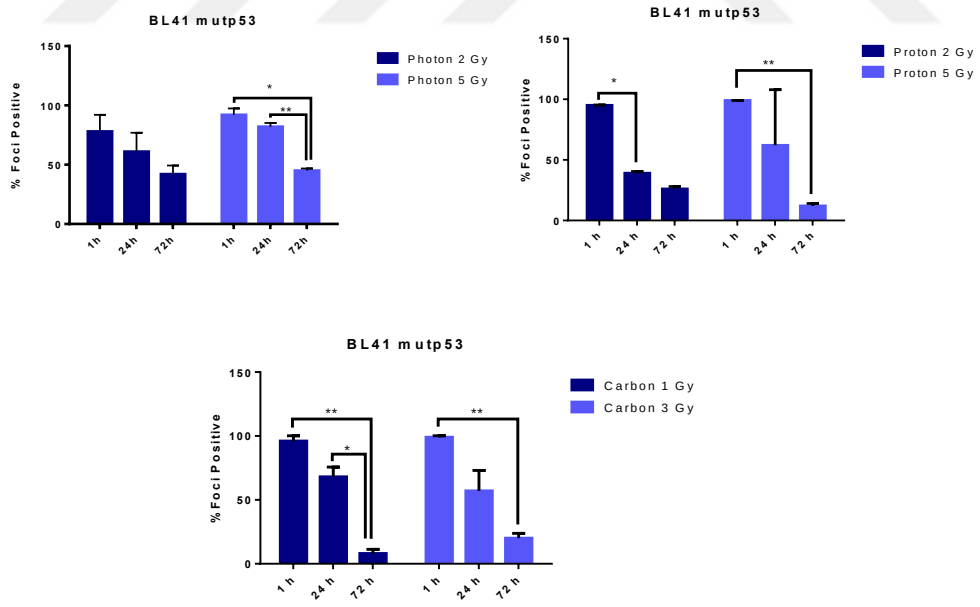

Figure 4.3. Comparison of foci percentages levels at 1h, 24 h and 72 h post-irradiation of three different radiation qualities in the BL41 mutant p53 cell lines. Foci percentages levels were calculated based on the cell numbers and cell with foci. p-values were determined using t-test. Symbols used in charts means; when p values were found higher than 0.05 shown as ns, $p \leq 0.05$ (*), $p \leq 0.01$ (**) and $p \leq 0.001$ demonstrated as (***).

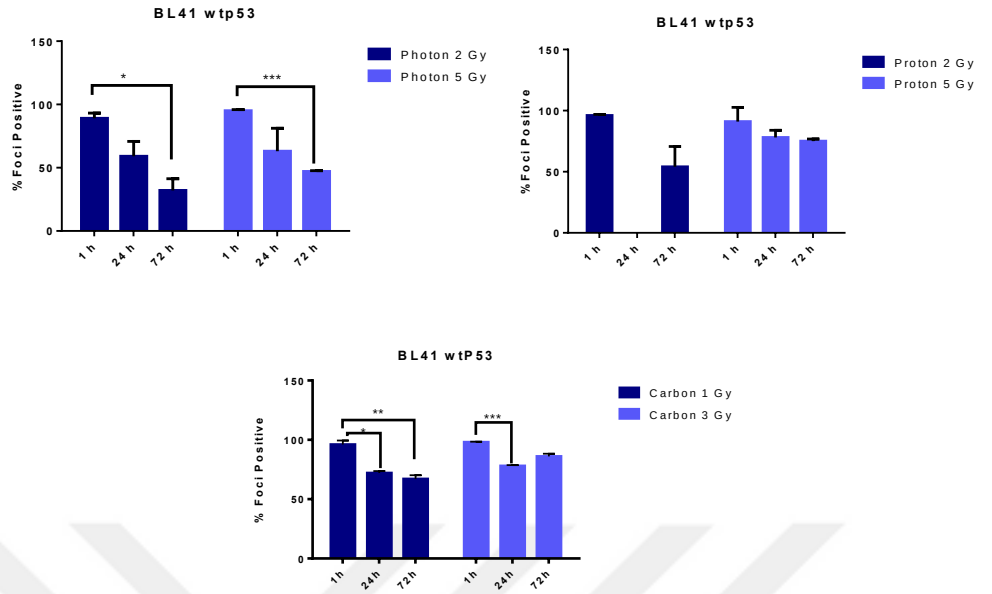

Figure 4.4. Comparison of foci percentages levels at 1h, 24 h and 72 h post-irradiation of three different radiation qualities in the BL41 wild type p53 cell lines. Foci percentages levels were calculated based on the cell numbers and cell with foci. p-values were determined using t-test. Symbols used in charts means; when p values were found higher than 0.05 shown as ns, $p \leq 0.05$ (*), $p \leq 0.01$ (**) and $p \leq 0.001$ demonstrated as (***).

Similar to BL41 mutant p53 and wild type p53 cells the percentage of foci positive cells were shown in Table 4.2 and Figure 4.5 and 4.6. The cells which have foci and number of cells were counted independent of the other parameters. The percentage of foci positive cells were calculated based on the number of cells. When J3D mutant p53 cells were examined, the highest level of the percentage of foci positive cells in Photon 5 Gy IR was found to be 94% at 1 h post-irradiation whereas 24 h and 72 h post-irradiation the percentage of foci positive cells were 44% and 25%, respectively. Proton 2 Gy the percentage of foci positive cells over time in J3D mutant p53 cells. Following this, the percentage of foci positive cells l of Proton 5 Gy was found to be 94 %, 62% and 26% at 1h, 24 h and 72 h post-irradiation, respectively (Table 4.2) (Figure 4.5). In the case of Carbon 1 Gy at 1h post-irradiation the percentage of foci positive cells ls led to a marked decrease to 54% at 24 h post-irradiation and 39% at 72h post-irradiation (Figure 4.5) (Table 4.2).

Table 4.2. J3D mutantp53 and wtp53 cells overview of the cell numbers and with foci percentages.

Cell Type	Radiation Type	Dose	Post RT	Cell Number	%Foci Positive
J3D mutp53	Photon	2	1	367	49
J3D mutp53	Photon	2	24	0	0
J3D mutp53	Photon	2	72	450	21
J3D mutp53	Photon	5	1	733	94
J3D mutp53	Photon	5	24	31	44
J3D mutp53	Photon	5	72	390	25
J3D mutp53	Proton	2	1	86	53
J3D mutp53	Proton	2	24	685	53
J3D mutp53	Proton	2	72	995	27
J3D mutp53	Proton	5	1	434	94
J3D mutp53	Proton	5	24	654	62
J3D mutp53	Proton	5	72	654	26
J3D mutp53	Carbon	1	1	560	95
J3D mutp53	Carbon	1	24	658	54
J3D mutp53	Carbon	1	72	303	39
J3D mutp53	Carbon	3	1	505	92
J3D mutp53	Carbon	3	24	429	61
J3D mutp53	Carbon	3	72	137	26
J3D wtp53	Photon	2	1	945	78
J3D wtp53	Photon	2	24	0	0
J3D wtp53	Photon	2	72	265	30
J3D wtp53	Photon	5	1	259	94
J3D wtp53	Photon	5	24	191	70
J3D wtp53	Photon	5	72	521	50
J3D wtp53	Proton	2	1	399	82
J3D wtp53	Proton	2	24	703	60
J3D wtp53	Proton	2	72	575	76
J3D wtp53	Proton	5	1	469	89
J3D wtp53	Proton	5	24	480	65
J3D wtp53	Proton	5	72	1262	64
J3D wtp53	Carbon	1	1	496	86
J3D wtp53	Carbon	1	24	579	67
J3D wtp53	Carbon	1	72	345	63
J3D wtp53	Carbon	3	1	650	90
J3D wtp53	Carbon	3	24	704	51
J3D wtp53	Carbon	3	72	258	78

We also observed a decrease in the frequency of foci positive cells in J3D wild type cells as a function of time in all different radiation qualities (Figure 4.6.). Interestingly, Proton 2 Gy at 1 h post-irradiation the percentage of foci positive cells were recorded as 82% and at 24 h and 72 h post-irradiation were found to be 60% and 76 %, respectively in J3D wtp53 cells. Likewise, Carbon 1 Gy the percentage of foci positive cells were found significant difference ($p \leq 0.05$) between at 1 h and 72 h post-irradiation the percentage of foci positive cells. Carbon 3 Gy IR led to an increase from 51% to 78% at 24 h and 72h post-irradiation. (Table 4.2) (Figure 4.6).

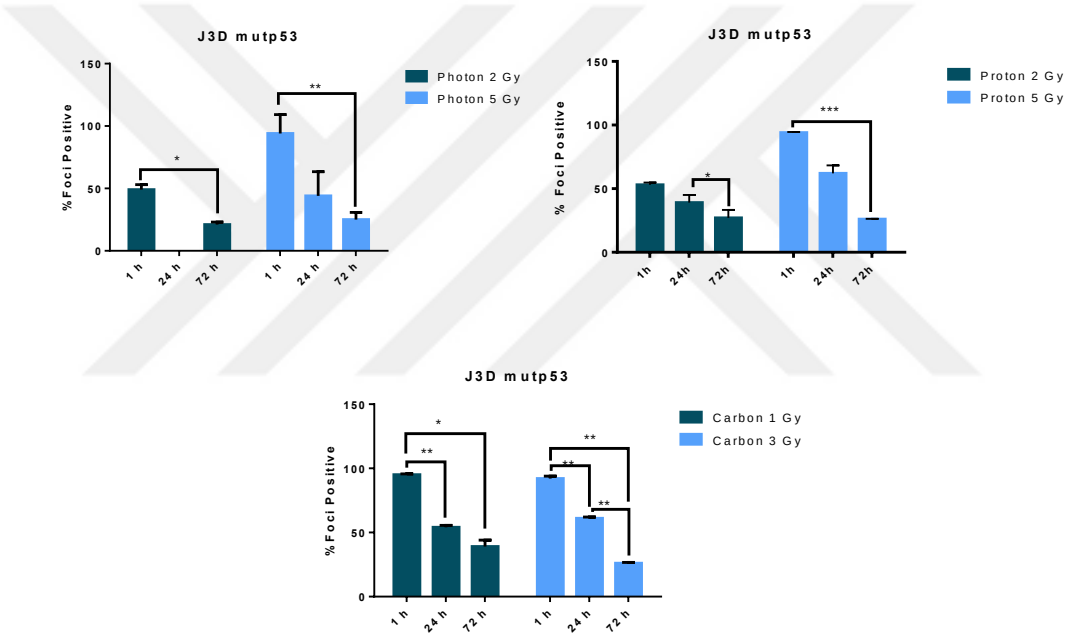

Figure 4.5. Quantification of foci positive percentage levels of γH2AX foci in the J3D mutant p53 cell lines. Foci percentages levels were calculated based on the cell numbers and cell with foci. Symbols used in charts means; when p values were found higher than 0.05 shown as ns, $p \leq 0.05$ (*), $p \leq 0.01$ (**) and $p \leq 0.001$ demonstrated as (***).

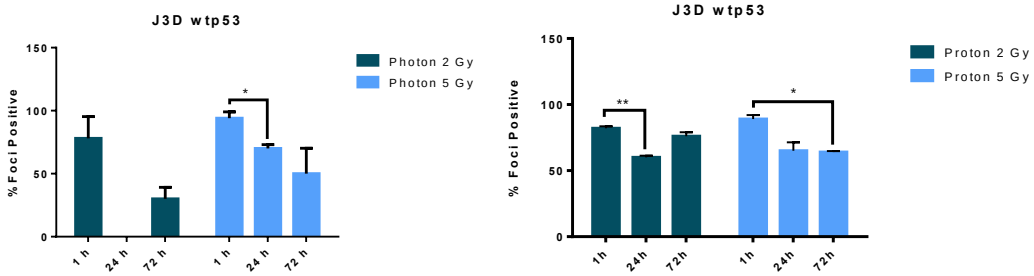

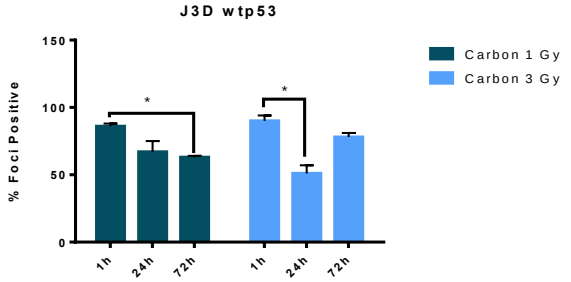

Figure 4.6. Quantification of foci percentage levels of γH2AX foci in the J3D wtp53 cell lines. Foci percentages levels were calculated based on the cell numbers and cell with foci. Symbols used in charts means; when p values were found higher than 0.05 shown as ns, $p \leq 0.05$ (*), $p \leq 0.01$ (**) and $p \leq 0.001$ demonstrated as (***).

4.2. The Comparison of Background Levels for Mutant p53 and Wild type p53 Cells Based on Foci per Nucleus, Foci Area and Foci Intensity

In this study, the frequency of γ-H2AX foci based on three different parameters were analyzed: foci number, foci area and the intensity of foci, which are representative of number, extent and size of DNA double strand breaks, respectively.

To investigate whether the functional status of p53 has an influence on the genomic stability of the cells, the backgrounds levels of γ-H2AX foci of lymphoma cells which express wild type versus those with mutated p53 were compared by counting foci, number, area and intensity (Figure 4.7). In unirradiated samples of BL41 wtp53 cells, the frequency of γ-H2AX foci per nucleus foci per nucleuswas found to be approximately 3-fold higher than in BL41 mutant p53 cells. In addition, the foci area levels of BL41 wtp53 were 6-fold higher which was not significant due to there was high variance between replicates. The foci intensity levels 12-fold higher than in BL41 mutant p53 cells.

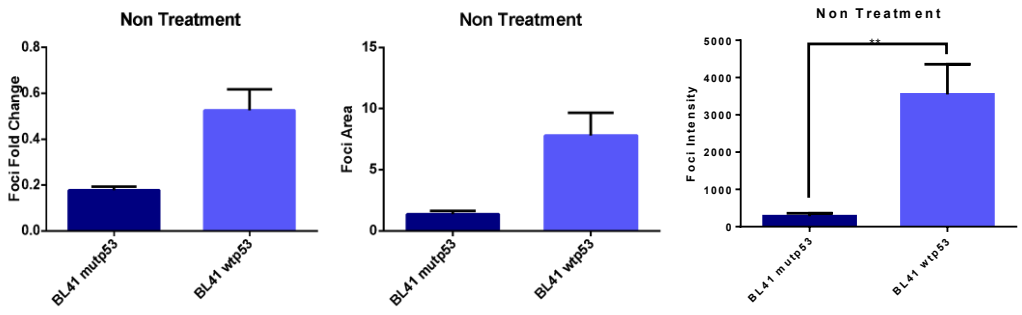

Figure 4.7. γH2AX foci per nucleus, area and foci intensity per cell of the background level comparing in BL41 mutp53 and wtp53. The foci per nucleus was calculated by dividing the sum of the foci by the cell number. Area and Intensity were divided by the cell number counted to calculate the average of each time point. The standard deviation is indicated by the error bars for independent replicates per time point. Symbols used in charts means; when p values were found higher than 0.05 shown as ns, $p \leq 0.05$ (*), $p \leq 0.01$ (**) and $p \leq 0.001$ demonstrated as (***).

As shown in figure 4.8, J3D wtp53 cells the frequency of foci per nucleus was found to be 1.5-fold higher than J3D mutant p53, moreover foci area levels and foci intensity levels were 2.1 -fold and 1.1-fold higher, respectively. However, these fold changes were not found significant.

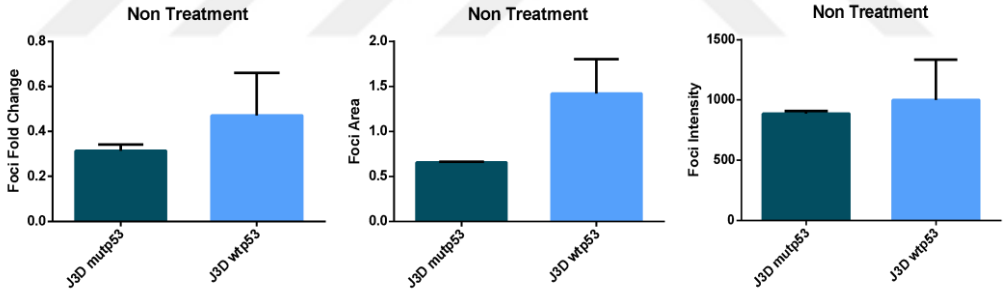

.

Figure 4.8. γH2AX foci per nucleus, area and foci intensity per cell of the background levels comparing in J3D mutp53 and wtp53. The foci per nucleus was calculated by dividing the sum of the foci by the cell number. Area and Intensity were divided by the cell number counted to calculate the average of each time point. The standard deviation is indicated by the error bars for independent replicates per time point. Symbols used in charts means; when p values were found higher than 0.05 shown as ns, $p \leq 0.05$ (*), $p \leq 0.01$ (**) and $p \leq 0.001$ demonstrated as (***).

4.3. Analyses of the Increase of γ-H2AX Foci in Response to Photon, Proton and Carbon Irradiation Foci per Nucleus in BL41 and J3D Cells

In respect of investigating the increase of γ-H2AX-foci in response to irradiation, we determined the frequency γ-H2AX-foci per nucleus in BL41

mutant p53 cell lines and compared them foci per nucleus with values obtained from BL41 wtp53 cell lines (Figure 4.9A.). To determinate foci values per cell, the data, which was obtained by Image J analysis, was divided by the total cell number of each replicate. Later for normalization, foci values were divided to background levels for each cell lines which was shown as Norm to 0 Gy in Figure 4.9. and the fluorescence microscopy images were analyzed in respect to γ-H2AX foci formation (Figure 4.9).

First, the foci per nucleus levels BL41 was compared between mutant p53 and wtp53 cells. Analysis of BL41 wtp53 cells showed that the γ-H2AX foci per nucleus levels at 24 h and 72 h post-irradiation, BL41 mutant p53 cells levels were found 2.2-fold and 6-fold higher than BL41 wtp53 cells levels, respectively. In the case of Photon 5 Gy, the foci per nucleus levels in BL41 mutant p53 cells were recorded as 2-fold and 3-fold higher than BL41 wtp53 cells levels at 24 h and 72 h post-irradiation, respectively (Figure 4.9.A).

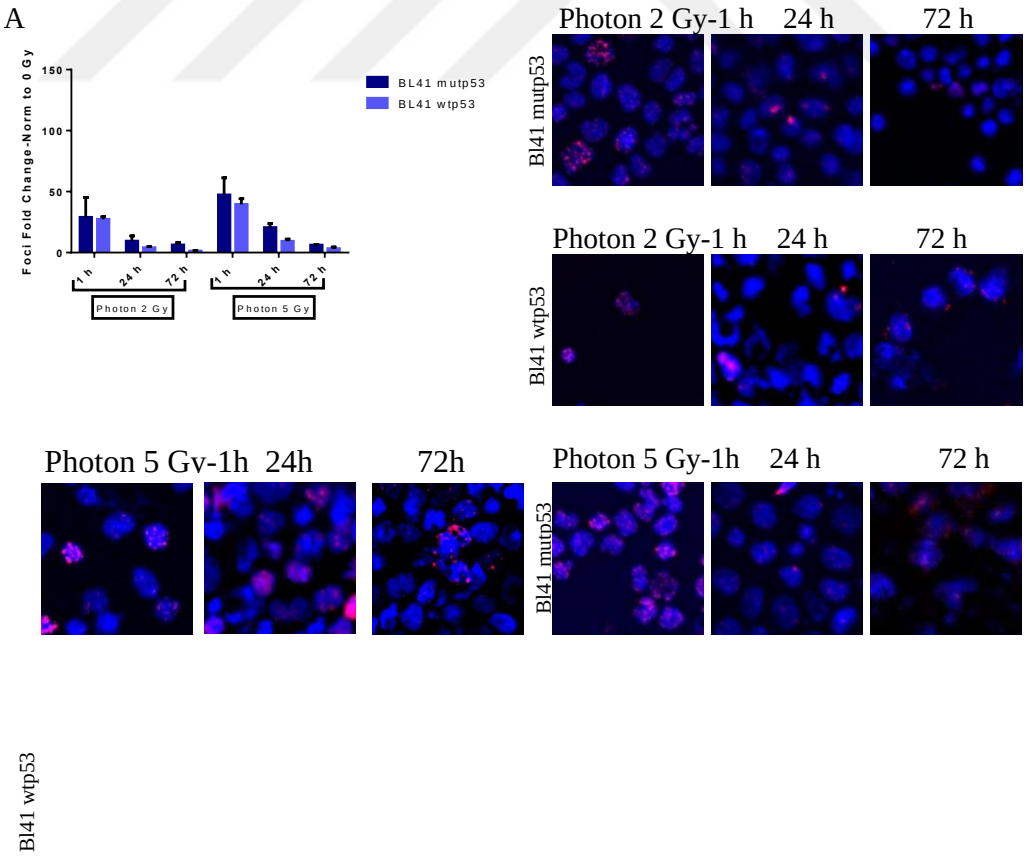

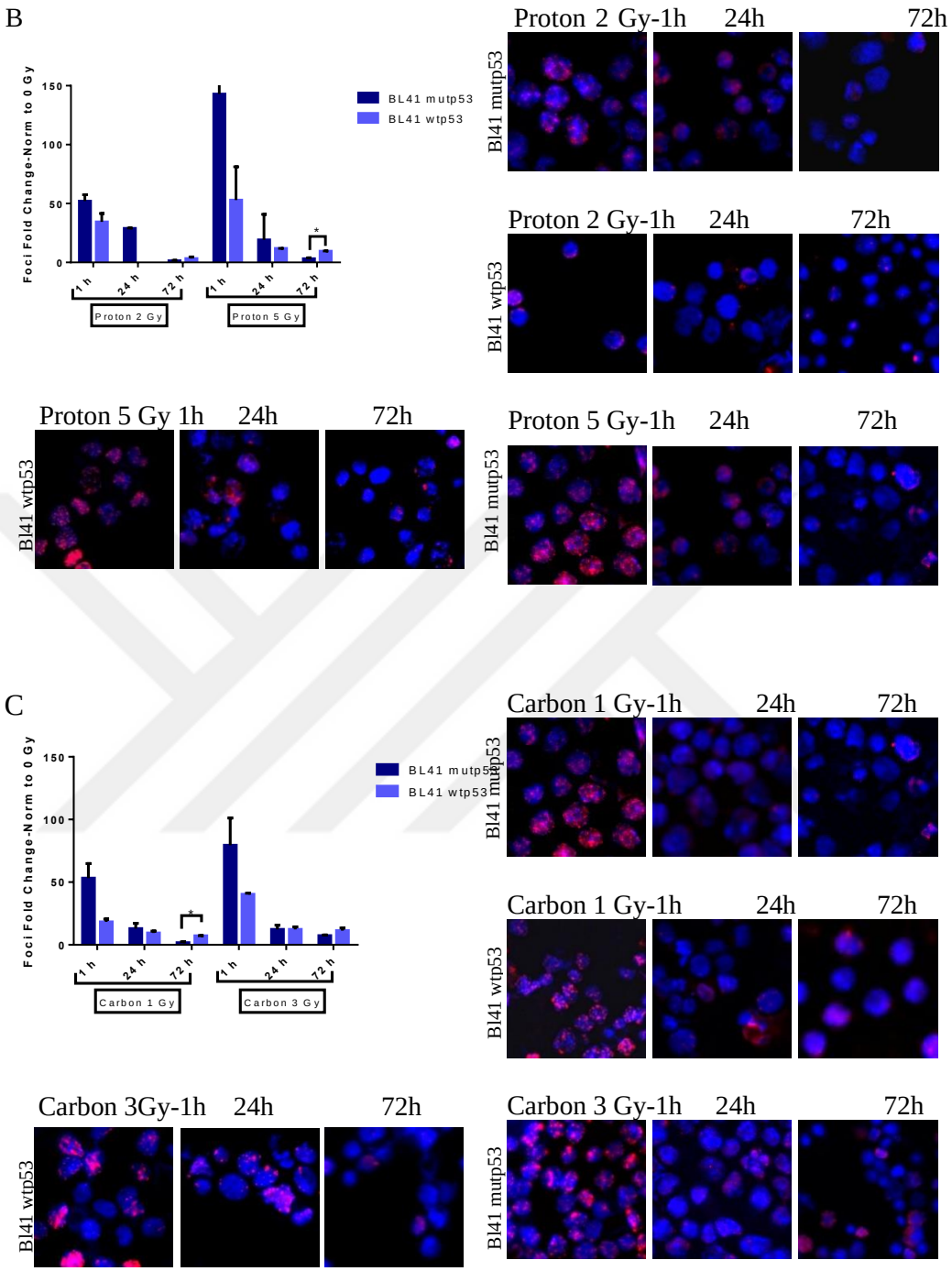

Figure 4.9 A, B, C. The Frequency of γH2AX foci per cell in human BL41 lymphoma cell lines expressing wild type and mutated p53 after photon, proton and Carbon irradiation. The sum of foci was divided by the total number of cells counted to calculate the average of each time point from two replicates. For normalization the data from the untreated-background levels of γH2AX foci were used for the whole data to enable the comparison of the DNA repair kinetics of the BL41 mutant p53 and wtp53 cell lines. The standard deviation is represented by the error bars for independent replicates per time point. Images were analyzed using time dependent thresholds.

Staining with γH2AX and DAPI for monitoring on fluorescence microscopy was done at 1h, 24h and 72h post irradiation. The fluorescence microscopy of the slides was done by Olympus Cell R microscope at the light microscopy facility of DKFZ. In total, 12 images per time point per cell line were used. The thresholds used were based on radiation qualities and doses. The images were analyzed by ImageJ.

In Figure 4.9.B, although at 1 h post-irradiation after Proton 2 Gy treated BL41 mutant p53 cells foci per nucleus levels were found to be 1.6-fold higher than BL41 wtp53 cells foci per nucleus levels, ($p > 0.05$). In BL41 mutant p53 cells, Proton 5 Gy foci per nucleus levels at 1 h post-irradiation was recorded as 2.6-fold higher than BL41 wtp53 cells foci per nucleus levels. After 24 hours in Proton 5 Gy, the foci per nucleus levels of BL41 mutant p53 cells were 1.7-fold higher than BL41 wtp53 cells levels (Figure 4.9B). In a similar manner, Carbon 1 Gy and Carbon 3 Gy foci per nucleus levels in BL41 mutant p53 cells were demonstrated higher than BL41 wtp53 cells foci per nucleus levels. Carbon 1 Gy treated BL41 wtp53 cells levels were significantly ($p \leq 0.05$) higher than BL41 mutant p53 cells levels at 72 h post-irradiation (Figure 4.9.C).

Another observation from Figure 4.19 is that in BL41 mutant p53 cells, Proton 5 Gy were demonstrated significantly higher than Proton 2 Gy levels at 1 h post-irradiation. In the case of increasing the dose from Carbon 1 Gy to Carbon 3 Gy resulted as significant ($p \leq 0.01$) increasing in BL41 mutant p53 cells at 72 h post-irradiation. In BL41 wtp53 cells, Carbon 3 Gy levels were found significantly ($p \leq 0.01$) higher than Carbon 1 Gy levels at 1 h post-irradiation.

The overall observation from the comparison of Figure 4.A, 4.B and 4.C is; Carbon IR and Proton IR foci per nucleus levels are higher than Photon IR foci per nucleus levels. Significant differences are; in BL41 mutant p53 cells Proton 5 Gy foci per nucleus levels were recorded significantly higher than Photon 5 Gy levels at 1 h ($p \leq 0.01$) post-irradiation. Following this, in BL41 wtp53 cells, Carbon 1 Gy foci per nucleus levels were demonstrated significantly higher than Photon 2 Gy levels at 1 h ($p \leq 0.001$) and 72 h ($p \leq 0.01$) post-irradiation (Figure 4.9).

To improve our understanding of the p53 effect on lymphoma, we systematically analyzed the pattern of radiation response. In regard, the foci per nucleus levels which presented in Figure 4.10, normalization was performed using mutant p53 backgrounds for the calculation of wtp53 cells values. We hypothesized that induced p53 function has performed differently through using mutant p53 levels for normalization. As an overview, in BL41 wtp53 cells foci per nucleus levels were higher than those in BL41 mutant p53, while BL41 mutant p53 levels used the same levels as in Figure 4.9. Photon 5 Gy foci per nucleus levels in BL41 wtp53 were found 2.5-fold ($p \leq 0.05$) higher than BL41 mutant p53 cells levels at 1 h post-irradiation. Proton 2 Gy, the foci per nucleus levels of BL41 wtp53 cells were found to be 2-fold and 9-fold higher than BL41 mutant p53 cells foci per nucleus levels at 1h and 72 h post-irradiation. After increasing the dose to Proton 5 Gy, in BL41 wtp53 cells foci per nucleus levels were determined 9.6-fold higher than BL41 mutant p53 cells foci per nucleus levels at 72 h post-irradiation ($p \leq 0.05$). Carbon 1 Gy treated BL41 wtp53 cells levels were demonstrated significantly ($p \leq 0.01$) higher than BL41 mutant p53 cells levels at 72 h post-irradiation. In BL41 wtp53 cells, Carbon 3 Gy at 1 h post-irradiation foci per nucleus levels were recorded as 1.5-fold higher and at 24 h-72 h post-irradiation were found to be 3-fold and 4.8-fold higher than BL41 mutant p53 cells foci per nucleus levels.

Another observation is comparison of radiation qualities following the increase of BL41 wtp53 values. Since mutant p53 values were used the same, the comparison between radiation qualities was performed only for wtp53 values. Proton 5 Gy foci per nucleus levels at 1 h post-irradiation was as the highest while Carbon 3 Gy foci per nucleus levels were demonstrated to be the highest levels at 24 h and 72 h post-irradiation in BL41 wtp53 cells. Significant differences between radiation qualities were found such as; Carbon 1 Gy foci per nucleus levels of BL41 wtp53 cells were determined significantly higher than Photon 2 Gy levels at 1 h ($p \leq 0.001$) and 72 h ($p \leq 0.01$) post-irradiation (Figure 4.10).

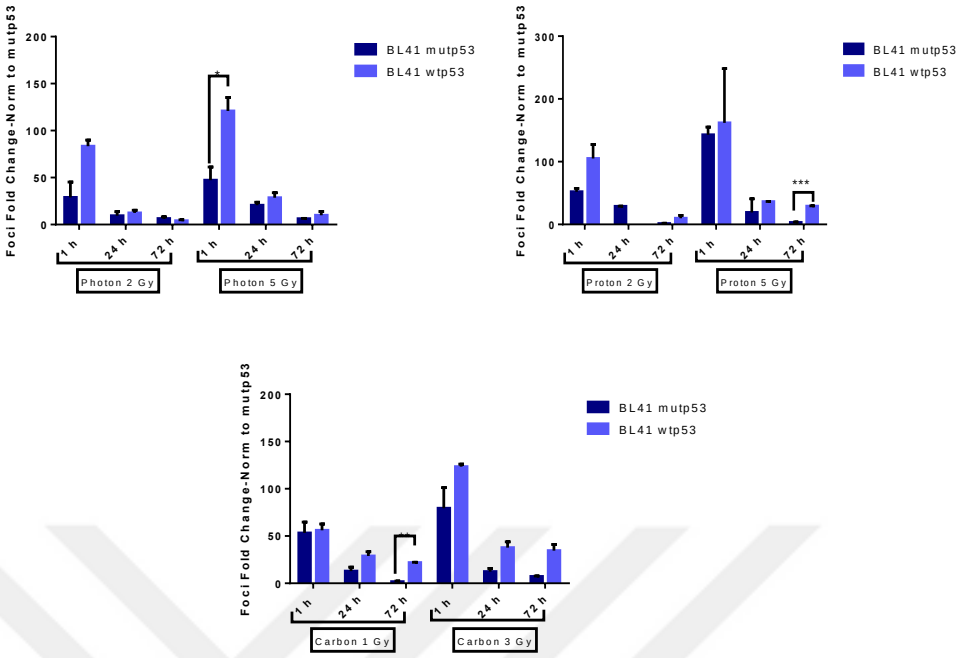

Figure 4.10. Effect of re-activated p53 on BL41 cell lines after exposing Photon, Proton and Carbon IR in the γ-H2AX signaling response based on normalization to mutant p53 background. The sum of foci was divided by the total number of cells counted to calculate the average of each time point from two replicates. The data from the untreated levels of γH2AX foci area was used to normalize the whole data to enable the comparison of the DNA repair kinetics of the BL41 mutant p53 and BL41 wtp53 cell lines. The standard deviation is represented by the error bars for independent replicates per time point.

As in the analysis of BL41 cells foci per nucleus levels of, first we observed differences between J3D wtp53 and mutant p53 cell lines. However, in Photon 2 Gy treated J3D mutant p53 and wtp53 foci per nucleus levels were recorded no major difference at each time point ($p > 0.05$) (Figure 4.11A).

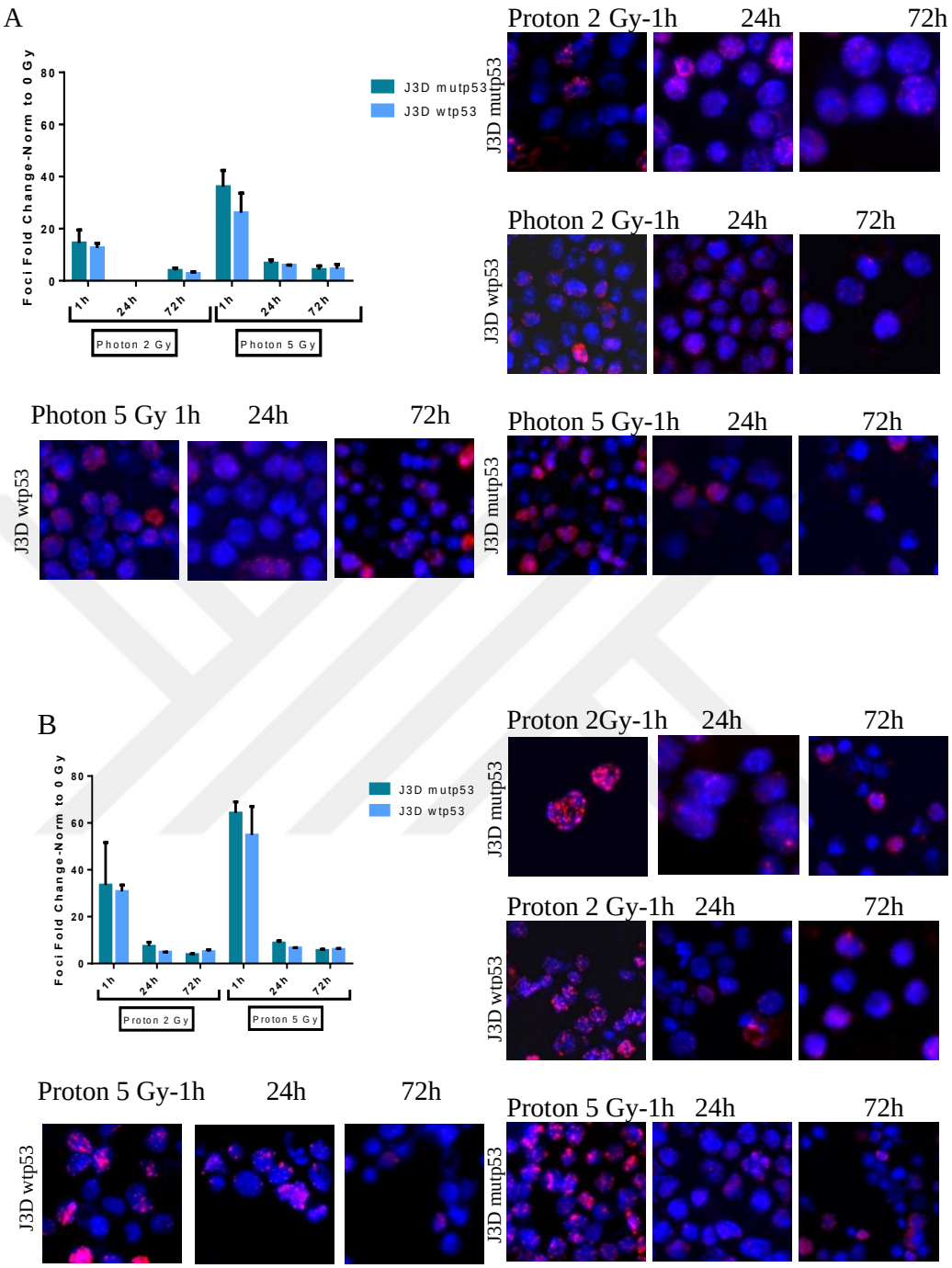
A
Foci Fold Change-Norm to 0 Gy
J3D mutp53
J3D wtp53
1h
24h
72h
Photon 2 Gy
Photon 5 Gy
Proton 2 Gy-1h
Photon 2 Gy-1h
Photon 5 Gy 1h
Photon 5 Gy-1h
B
Proton 2Gy-1h
Proton 2 Gy-1h
Proton 5 Gy-1h
Proton 5 Gy

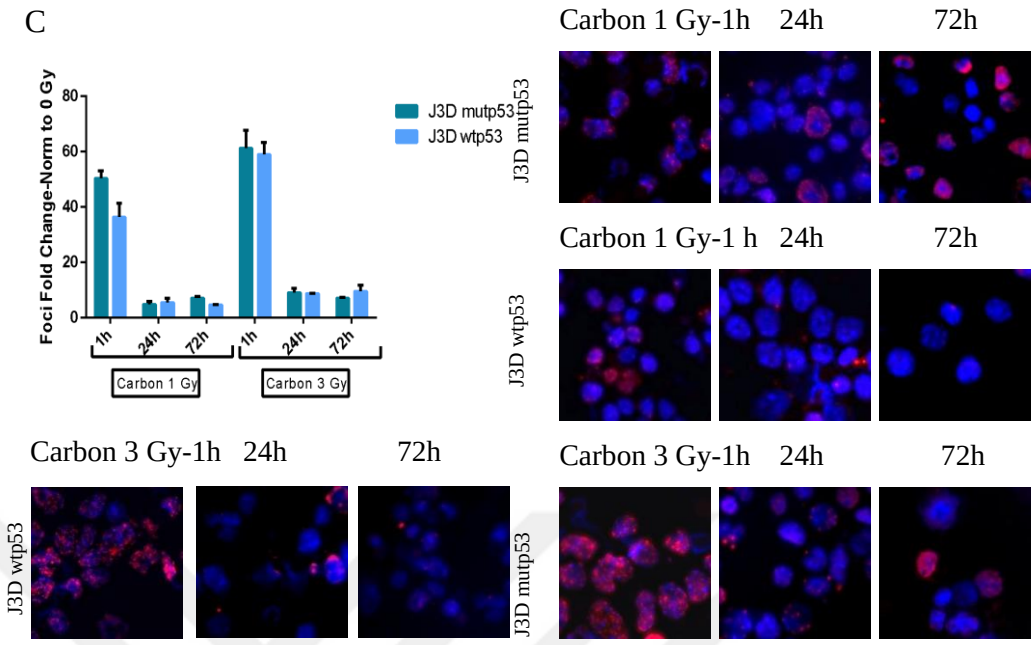

Figure 4.11. A, B, C. The Frequency of γH2AX foci per cell in J3D lymphoma cell lines expressing wild type and mutated p53 after Photon, Proton and Carbon irradiation. The sum of foci was divided by the total number of cells counted to calculate the average of each time point from two replicates. The data from the untreated levels of γH2AX foci area was used to normalize the whole data to enable the comparison of the DNA repair kinetics of the J3D mutant p53 and wtp53 cell lines. The standard deviation is represented by the error bars for independent replicates per time point.

Similar to Photon IR foci per nucleus levels, Proton 2 Gy IR 1 h post-irradiation levels were found nearly similar ($p > 0.05$) between J3D mutant p53 and wtp53 cells levels. After 24 h post-irradiation Proton 2 Gy foci per nucleus levels in J3D mutant p53 cells was determined as approximately 2-fold higher than J3D wtp53 cells foci per nucleus levels (Figure 4.11B). Also, after Carbon 1 Gy and 3 Gy IR, there were no major differences ($p > 0.05$) at 1h, 24 h, and 72 h post-irradiation in both J3D mutant p53 and wtp53 cells levels (Figure 4.11C).

Another comparison was performed between doses for each radiation quality and there were significant differences such as; in J3D wtp53 cells Proton 5 Gy levels were significantly ($p \leq 0.01$) higher than Proton 2 Gy levels at 24 h post-irradiation. Besides that, Carbon 3 Gy foci per nucleus levels were found not significantly higher than Carbon 1 Gy levels in both J3D mutant p53 and wtp53 cells for each time point (Figure 4.11).

Comparison Photon IR levels with particles, there are significant changes such as; Proton 5 Gy foci per nucleus levels in J3D mutant p53 cells were demonstrated significantly ($p \leq 0.05$) higher than Photon 5 Gy foci per nucleus levels at 1 h post-irradiation whereas at 24 h and 72 h post-irradiation foci per nucleus levels were detected nearly similar ($p > 0.05$). Also, Carbon 1 Gy levels were significantly higher ($p \leq 0.05$) than Photon 2 Gy levels while Carbon 3 Gy levels were determined also significantly higher ($p \leq 0.01$) than Photon 5 Gy levels at 1 h post-irradiation in J3D mutant p53 cells. In the case of J3D wtp53 cells, Carbon 3 Gy levels were found significantly ($p \leq 0.05$) higher than Photon 5 Gy levels at 1 h and 24 h post-irradiation (Figure 4.11).

In order to analyze the role of p53 in J3D cells, as done with the BL41 wtp53 cells foci per nucleus analysis, in J3D wtp53 cells foci per nucleus levels were normalized according to the J3D mutant p53 backgrounds levels. The same J3D mutant p53 foci per nucleus levels were used in Figure 4.12. In J3D wtp53 cells foci number values increased compared to J3D wtp53 cell foci number levels. Although Photon 2 Gy at 1h post-irradiation, J3D wtp53 cells foci per nucleus level was found to be approximately 1.5-fold higher than J3D mutant p53 cells levels, there were no major ($p > 0.05$) differences at 1 h, 24 h and 72 h post-irradiation. In J3D wtp53 cells Proton 2 Gy levels foci per nucleus levels were recorded as 1.4-fold and 2-fold higher than J3D mutant p53 cells levels at 1 h and 72 h post-irradiation, respectively. Proton 5 Gy treated J3D wtp53 cells foci per nucleus levels were approximately 1.5-fold, 1.7-fold and 2-fold ($p \leq 0.05$) higher than J3D mutant p53 cells levels at 1 h, 24 h, and 72 h post-irradiation, respectively. There were no significant ($p > 0.05$) differences detected at each time point between J3D mutant p53 and wtp53 cells levels which were irradiated with Carbon 1 Gy.

When comparing dose effect, in J3D wtp53 cells, Proton 5 Gy radiation at 1 h post-irradiation foci per nucleus levels were found to be 1.8-fold higher than those of Proton 2 Gy 1 h post-irradiation. At 72 h post-irradiation, Proton 5 Gy treated J3D wtp53 cells were also significantly ($p \leq 0.05$) higher than Proton 2 Gy levels.

In the case of Carbon 1 Gy foci per nucleus levels J3D wtp53 were determined higher than J3D mutant p53 cells at 1h and 24 h post-irradiation.

Carbon 3 foci per nucleus levels displayed to be highest when compared between J3D mutant p53-wtp53 lines and compared with other radiation qualities at 1 h, 24h, and 72 h post-irradiation (Figure 4.12).

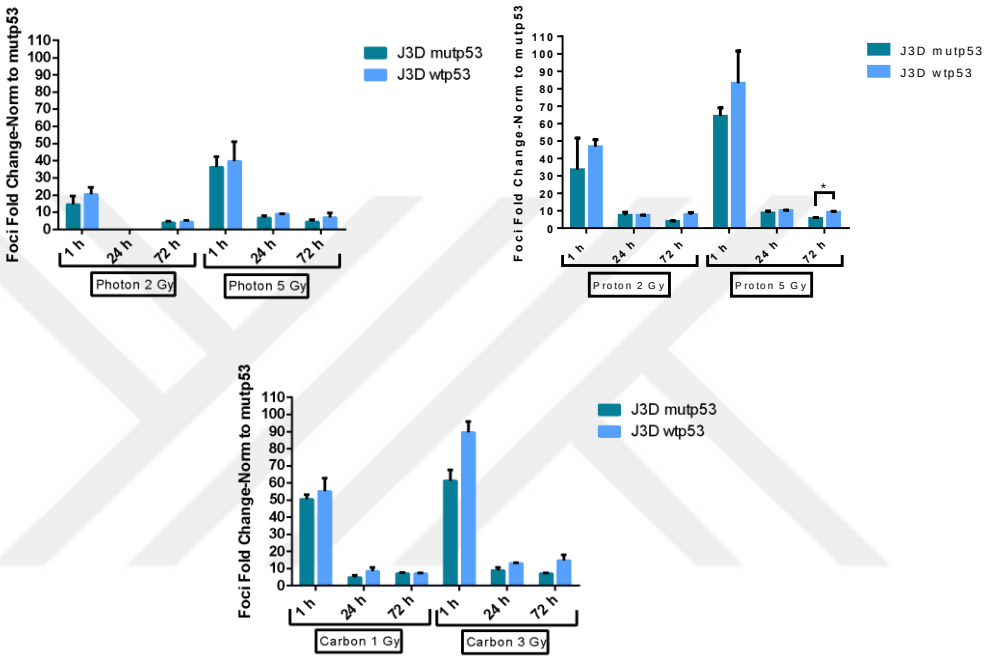

Figure 4.12. Activated p53 effect on the γH2AX signaling response to a higher and lower dose after three different radiation based on normalization to mutant p53 background in J3D cell lines. The sum of the foci was divided by the total number of cells counted to calculate the average of each time point from two replicates. Mutant p53 levels were used similar to Figure 13. The data from the background levels of γH2AX foci area was used to normalize the whole data to enable the comparison of the DNA repair kinetics of the J3D mutant p53 and J3D wtp53 cell lines. The standard deviation is represented by the error bars for independent replicates per time point.

4.4. Foci Area Analysis in BL41 and J3D cell lines

Previous reports state that the γ-H2AX foci number is related to the number of DNA double-strand breaks while the area of γ-H2AX foci can give estimates about the complexity of the DSB (56). Since it is known that Ion particles, especially Carbon beams induce more complex DSB, we tried to investigate whether we can measure these characteristics by quantifying the area of γ-H2AX in a sequential manner. To determinate foci area levels, the data was divided by

the total cell number of each replicate. Later for normalization, foci levels were divided to background levels (0 Gy) for each cell line. First comparison was performed between BL41 mutant p53 and wtp53 cells levels. Figure 4.13 below illustrates that the foci area value in Photon 2 Gy treated BL41 mutant p53 cells levels at 1h post-irradiation was found to be 3.7-fold higher than the foci area levels of BL41 wtp53 cells. Photon 5 Gy treated BL41 mutant p53 cells foci area levels were determined 4.8-fold and 2.5-fold higher than BL41 wtp53 foci area levels at 24 h and 72h post-irradiation ($p \leq 0.01$), respectively while there was no significant differences between BL41 mutant p53 and wtp53 cells at 1 h post-irradiation (Figure 4.13).

In BL41 mutant p53 cells, Proton 2 Gy foci area levels were determined as 2.8-fold higher ($p \leq 0.05$) than foci area values of BL41 wtp53 cells at 1 h post-irradiation. After increasing the dose to Proton 5 Gy, foci area levels in BL41 mutant p53 cells at 1 h post-irradiation were determined 4.7-fold ($p \leq 0.05$) higher than foci area levels of BL41 wtp53 cells. After 72 h post-irradiation, Proton 5 Gy treated BL41 mutant p53 cells foci area levels were found 4-fold higher ($p \leq 0.05$) than foci area levels of BL41 wtp53 cells (Figure 4.13). In a similar manner, Carbon 1 Gy foci area levels in BL41 mutant p53 cells were recorded to be 7-fold ($p \leq 0.05$) higher than foci area levels of BL41 wtp53 cells at 1 h post-irradiation. Nevertheless, Carbon 3 Gy treated BL41 mutant p53 cells foci area levels were determined significant ($p \leq 0.05$) higher than BL41 wtp53 cells foci area levels at 1 h post-irradiation (Figure 4.13).

Additional observation is, as a result of increasing dose, in BL41 wtp53 cells, Photon 5 Gy foci values were found significantly ($p \leq 0.01$) higher than Photon 2 Gy foci area values in BL41 wtp53 cells at 1 h and 24 h post-irradiation. Proton 5 Gy treated BL41 foci area levels were determined significantly ($p \leq 0.05$) higher than Proton 2 Gy levels at 72 h post-irradiation in BL41 mutant p53 and wtp53 cells. Also, it was found that Carbon 3 Gy levels in BL41 wtp53 cells were significantly higher ($p \leq 0.05$) than Carbon 1 Gy levels at 1 h and 72 h post-irradiation (Figure 4.13).

In regard, Proton 5 Gy IR 1 h post-irradiation foci area levels were determined to be the highest foci area levels among all radiation qualities and doses in BL41 mutant p53 and wtp53 cells. At 24 h and 72 h post-irradiation, foci area levels Carbon 3 Gy IR was found as to be the highest level in BL41 wtp53 and mutp53 cells. Additionally, in BL4 mutant p53 cells, Proton 5 Gy levels were found significantly ($p \leq 0.01$) higher than Carbon 3 Gy levels when Carbon 3 Gy levels also were determined significantly ($p \leq 0.05$) higher than Photon 5 Gy levels at 1 h post-irradiation (Figure 4.13).

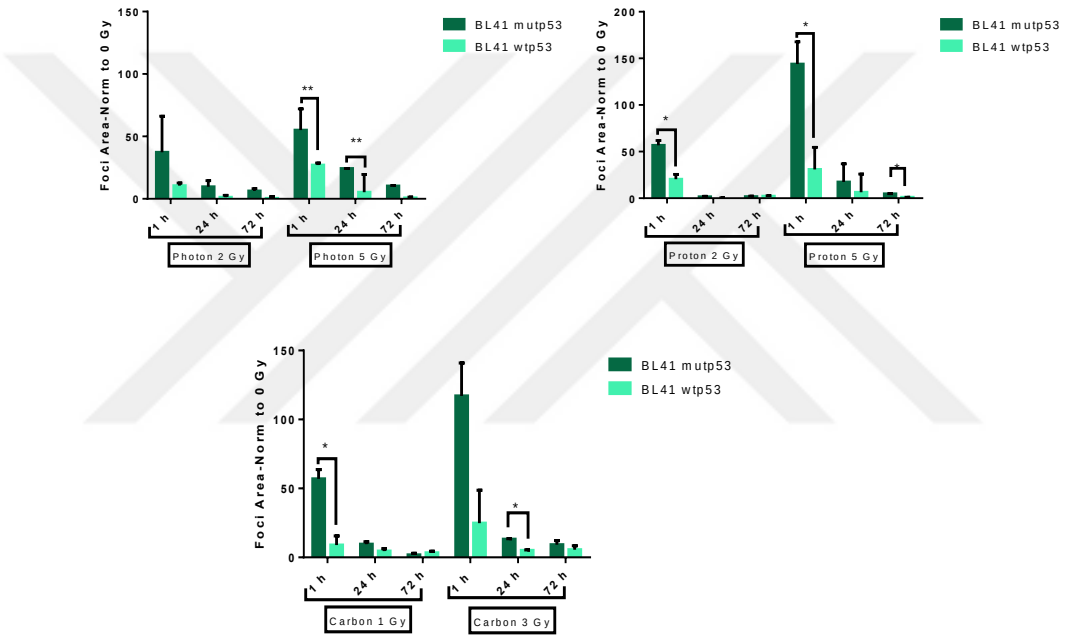

Figure 4.13. Dose and different radiation responses of γH2AX foci area in BL41 lymphoma cell lines that expressing wild type and mutated p53. The total foci area was divided by the total number of cells counted to calculate the average of each time point. The data from the untreated levels of γH2AX foci area was used to normalize the whole data to enable the comparison of the DNA repair kinetics. The standard deviation is represented by the error bars for independent replicates per time point.

In order to determine the effect of (the presence of) p53 on foci area levels, similar to the analysis of foci per nucleus, BL41 wtp53 cells foci area levels normalization was performed with the BL41 mutant p53 backgrounds foci area levels. With this, BL41 wtp53 cells area levels increased when compared to Figure 4.13 BL41 wtp53 foci area levels. Additionally, BL41 mutant p53 foci area levels were used the same as in Figure 4.13. In Photon 2 Gy, at 1h post-

irradiation foci area levels in BL41 wtp53 cells was found to be 3.7-fold higher than the levels of BL41 mutant p53 cells at 1 h post-irradiation. Following this, in BL41 mutant p53 cells, Photon 5 Gy foci area levels were determined to be 3.5-fold higher ($p \leq 0.01$) than BL41 mutant p53 levels at 1h post-irradiation. As a result of increasing dose to Photon 5 Gy, there was significant ($p \leq 0.01$) differences between Photon 5 Gy and Photon 2 Gy foci area levels in BL41 wtp53 cells (Figure 4.14). Proton IR (2 Gy and 5 Gy) area levels in BL41 wtp53 cells were higher than BL41 mutant p53 cells foci area levels and the significant differences ($p \leq 0.01$) between BL41 mutant p53 and wtp53 cells foci area levels were observed in treated with Proton 2 Gy at 1 h and Proton 5 Gy 72 h post-irradiation. Also, there are significant differences after exposed Carbon IR, such as; Carbon 1 Gy treated BL41 wtp53 cells foci area levels were determined 18-fold higher ($p \leq 0.01$) than BL41 mutant p53 cells levels at 72 h post-irradiation. Also, Carbon 3 Gy treated BL41 wtp53 cells foci area levels were demonstrated approximately 2-fold higher ($p \leq 0.05$) than BL41 mutant p53 cells levels at 24 h post-irradiation (Figure 4.14).

Another observation from Figure 4.14 is at 1 h and 24 h post-irradiation, the highest level of foci area levels was in Proton 5 Gy treated BL41 wtp53 cells. At 72 h post-irradiation, Carbon 3 Gy IR foci area levels were observed as the highest foci area levels when compared all levels in BL41 wtp53 cells (Figure 4.14).

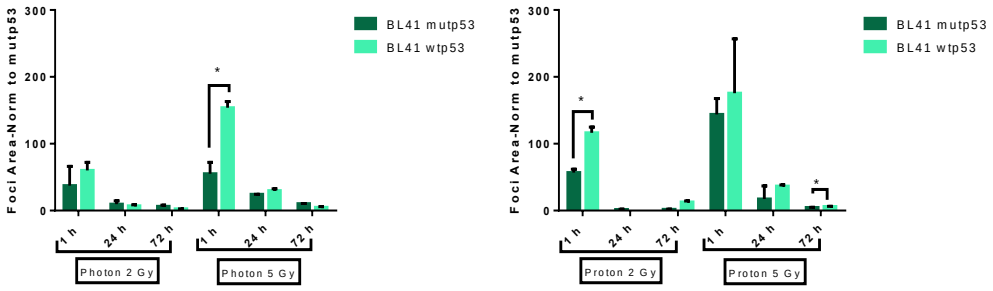

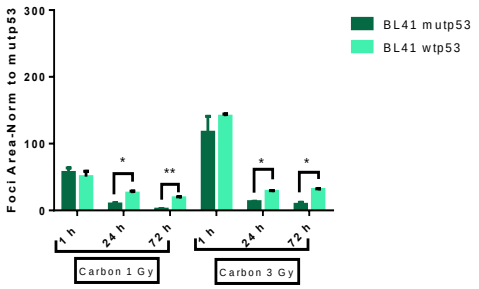

Figure 4.14. γ-H2AX foci area levels of BL41 cells exposed to three different radiation levels normalized by mutant p53 background levels. The total foci area was divided by the total number of cells counted to calculate the average of each time point. The data from the untreated levels of γH2AX foci area was used to normalize the whole data to enable the comparison of the DNA repair kinetics. The standard deviation is represented by the error bars for independent replicates per time point.

In a similar manner with BL41 foci area analysis, we start to compare with differences between J3D mutant p53 and wtp53 cells foci area levels. Regarding this, results depicted in Figure 4.15 shows that Photon 2 Gy treated J3D mutant p53 cells foci area levels at 1h post-irradiation were found 2-fold higher than the foci area levels in J3D wtp53 cells. The use of Proton 2 Gy and Proton 5 Gy resulted in higher levels of J3D mutant p53 cells foci area levels at 1 h post-irradiation compared to J3D wtp53 cells levels. Carbon IR to 3 Gy, at 1 h post-irradiation foci area levels in J3D mutant p53 cells were shown to be as 1.4-fold higher ($p \leq 0.01$) than J3D wtp53 cells.

General observation in Figure 4.15, Proton 5 Gy treated J3D mutant p53 cells levels were recorded significantly higher than Photon 5 Gy levels at 1 h ($p \leq 0.05$) and 72 h ($p \leq 0.01$) post-irradiation. At 1 h post-irradiation, Carbon 1 Gy and Carbon 3 Gy foci area levels were detected significantly ($p \leq 0.05$) higher than Photon 2 Gy and Photon 5 Gy, respectively in J3D mutant p53 cells. In the case of J3D wtp53 cells, Proton 2 Gy foci area levels which were found significantly ($p \leq 0.01$) higher than Photon 2 Gy levels at 72 h post-irradiation. In regard, Photon IR foci area values were found the lowest values when compared the other radiation qualities for each time points and both cell lines (Figure 4.15).

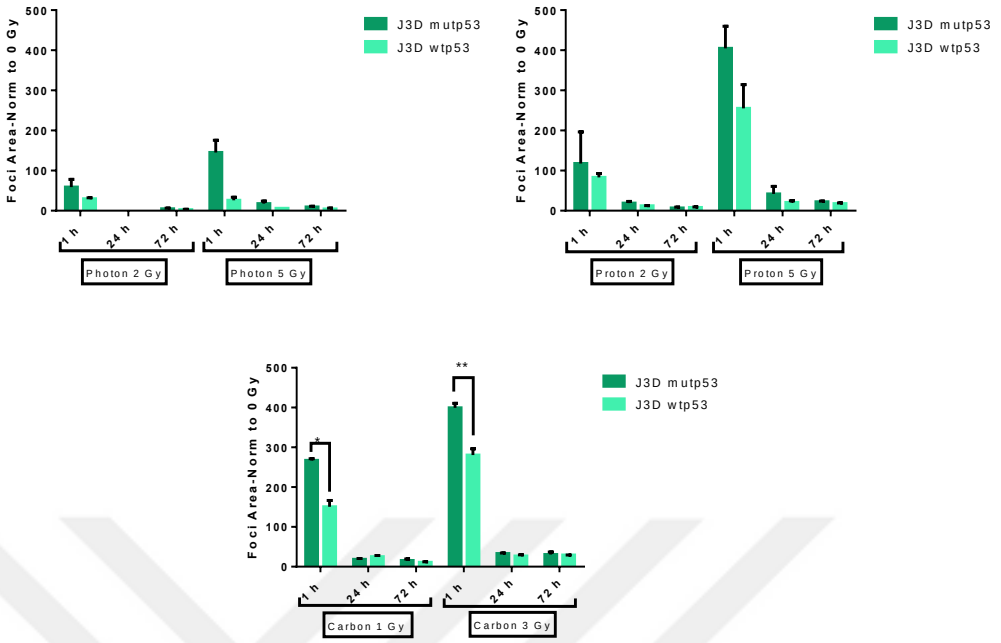

Figure 4.15. Dose and different radiation responses of γH2AX foci area in J3D lymphoma cell lines that expressing wild type and mutated p53. The total foci area was divided by the total number of cells counted to calculate the average of each time point. The data from the untreated levels of γH2AX foci area was used to normalize the whole data to enable the comparison of the DNA repair kinetics. The standard deviation is represented by the error bars for independent replicates per time point.

To determine differences between mutant p53 cells and wtp53 cells, J3D mutant p53 background foci area values were used to normalize J3D wtp53 cells foci area values. As a result of this, J3D wtp53 cells foci area levels increased in comparison to J3D wtp53 foci area levels in Figure 4.15. In J3D wtp53 cells when treating with Photon (2-5 Gy) IR, there were no major differences ($p > 0.05$) compared to J3D mutant p53 cells foci area levels. Following this, Proton 2 Gy IR treated J3D wtp53 cells were shown to be as 1.5-fold, 1.3-fold and 2-fold higher than J3D mutant p53 cells foci area levels at 1 h ,24 h and 72 h post-irradiation, respectively. In J3D wtp53 cells, Carbon 3 Gy 1 h, 24 h, and 72h post-irradiation foci area levels were demonstrated 1.5-fold, 1.7-fold, and 2-fold ($p \leq 0.05$) higher than J3D mutant p53 cells foci area levels, respectively. In addition to that, as a result of comparing three radiation qualities, it was observed that Carbon 3 Gy foci area levels were found to be as the highest level in both J3D mutant p53 and wtp53 cell lines for each time points Figure 4.16).

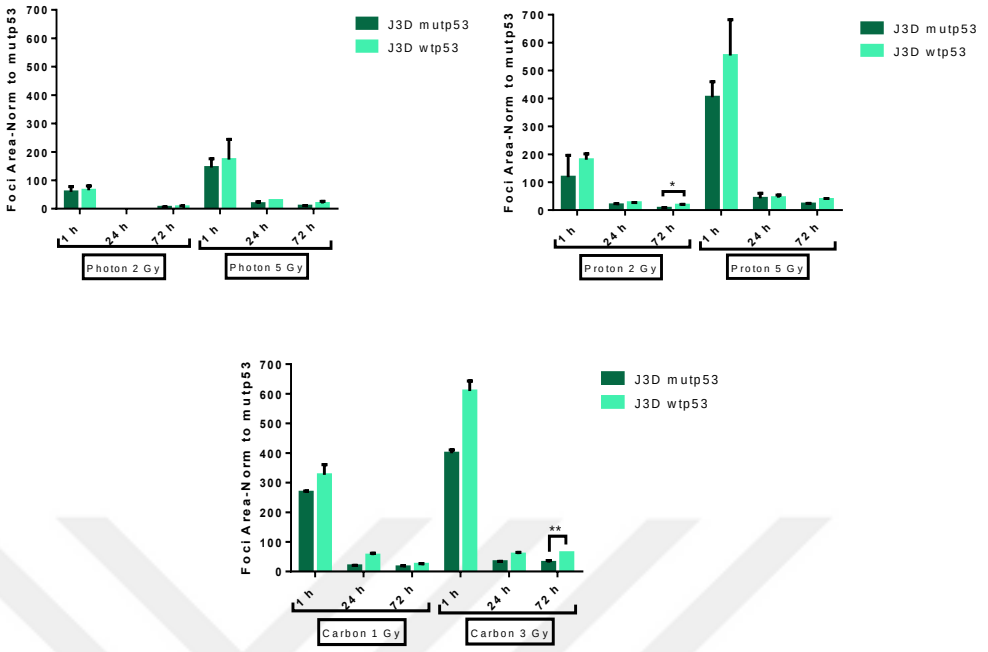

Figure 4.16. γ-H2AX foci area levels of J3D cells exposed to three different radiation levels normalized by mutant p53 background levels. The total foci area was divided by the total number of cells counted to calculate the average of each time point. The data from the untreated levels of γH2AX foci area was used to normalize the whole data to enable the comparison of the DNA repair kinetics. The standard deviation is represented by the error bars for independent replicates per time point.

4.5. Analyzing the Intensity of γH2AX Signals and Foci Distributions in BL41 and J3D Lymphoma Cell Lines which were irradiated by Photon, Proton and Carbon Beams

In respect to γ-H2AX foci per nucleus and foci area levels, we quantified the γ-H2AX foci intensity by dividing them through the total cell number of each replicate. For normalization, foci intensity levels were divided by background levels for each cell line. Similar to the quantification of γH2AX foci per nucleus and area levels, all-time points γH2AX foci intensity levels of BL41 mutant p53 were determined to be higher than γH2AX foci intensity levels of BL41 wtp53 cells. However, Photon 2 Gy and 5 Gy foci intensity levels were not found significant ($p > 0.05$) difference between BL41 mutant p53 and wtp53 cells at each time point. After increasing dose Proton IR to 5 Gy, foci intensity levels in BL41 mutant p53 cells were determined as 18-fold and 9-fold higher ($p > 0.05$)

than BL41 wtp53 cells at 1 h and 24 h post-irradiation, respectively. Nevertheless, after 72 h post-irradiation, there were significant ($p \leq 0.05$) difference foci intensity values between BL41 mutant p53 and wtp53 cells. In case of Carbon 1 Gy treatment, in BL41 mutant p53 cells foci intensity at 1h, 24 h, and 72 h post-irradiation values were found 14-fold, 9-fold, and 3-fold higher ($p > 0.05$) than BL4 wtp53 cells foci intensity levels, respectively. Also, Carbon 3 Gy foci intensity values were demonstrated to be significantly ($p \leq 0.01$) higher than BL4 wtp53 cells at 72 h post-irradiation (Figure 4.17).

Following dose differences, there was significant increase between Photon 5 Gy and Photon 2 Gy in BL41 wtp53 cells foci intensity levels at 24 h ($p \leq 0.05$) post-irradiation. Carbon 3 Gy were determined significantly ($p \leq 0.05$) higher than Carbon 1 Gy levels at 72 h post-irradiation in BL41 mutant p53 cells (Figure 4.17).

Another observation is the comparison of radiation qualities. There is also significant ($p \leq 0.05$) differences between Proton 2 Gy and Photon 2 Gy foci intensity levels in BL41 mutant p53 cells at 1 h post-irradiation (Figure 4.17).

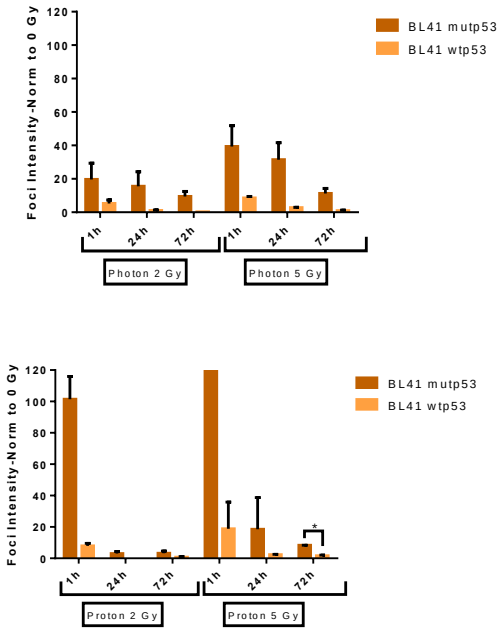

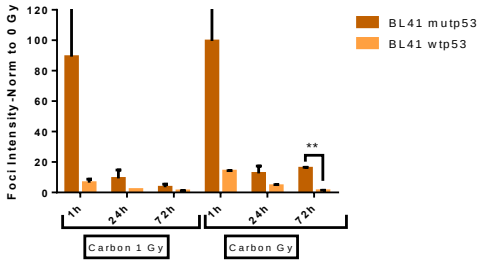

Figure 4.17. Comparison of foci intensity levels detection for the condition different doses after irradiation Photon, Proton and Carbon IR in BL41 mutant and wild type p53 cells. Following Image J analysis, the intensity of γH2AX foci per cell was determined by dividing the total detected foci intensity by the number of counted cells. The average γH2AX foci intensity of duplicates was normalized to the background levels of each cell lines separately.

As described above, second step is for comparing mutant p53 and wtp53 cells foci intensity levels, normalization of BL41 wtp53 cells levels was performed using mutant p53 backgrounds foci intensity levels and the BL41 mutant p53 foci intensity levels used are the same as in Figure 4.17. Parallel to foci per nucleus and area analysis, with normalization based on BL41 mutant p53 backgrounds, BL41 wtp53 cells foci intensity value levels increased compared to Figure 4.17. General observation is BL41 wtp53 mostly foci intensity levels were found to be higher than BL41 mutant p53. Photon 2 Gy foci intensity levels in BL41 wtp53 cells was determined approximately 3.5-fold higher than BL41 mutant p53 cells at both 1 h post-irradiation. In the case of Photon 5 Gy BL41 wtp53 levels were found 2.7-fold higher ($p \leq 0.01$) than BL41 mutant p53 cells foci intensity levels at 1 h post-irradiation. Additionally, Carbon 1 Gy treated BL41 wtp53 cells foci intensity levels were found 4.3-fold higher ($p \leq 0.05$) than BL41 mutant p53 cells levels at 72 h post-irradiation. BL41 wtp53 cells foci intensity levels in the case of Carbon 3 Gy were demonstrated 4.5-fold higher ($p \leq 0.05$) than BL41 mutant p53 cells levels at 24 h post-irradiation (Figure 4.18).

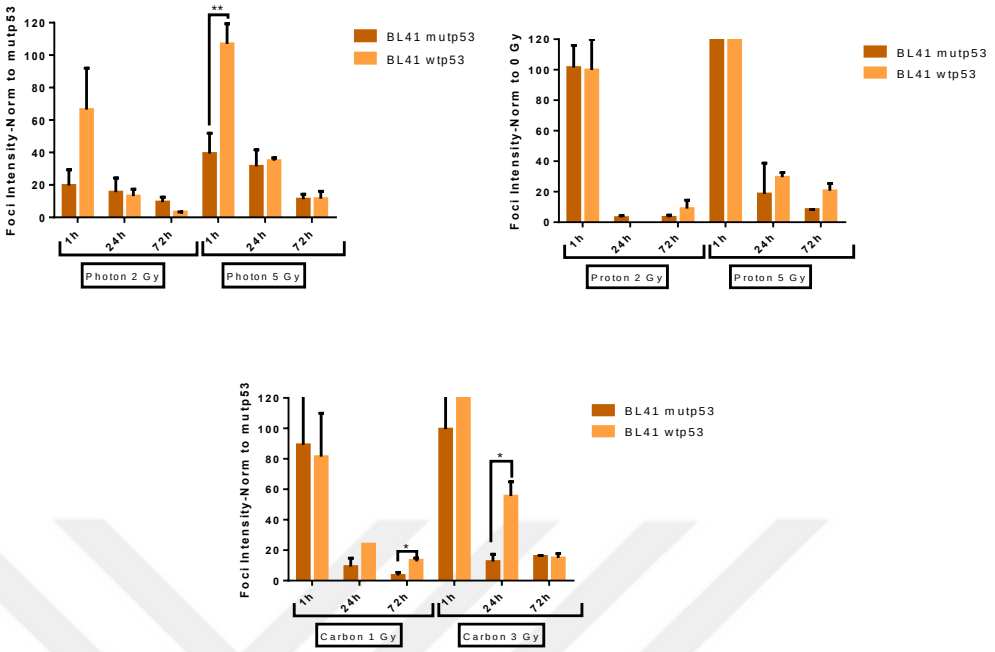

Figure 4.18. Investigation of foci intensity effect of the p53 role by normalization with BL41 mutant p53. γH2AX foci intensity was determined by dividing by the number of counted cells. The average γH2AX foci intensity of duplicates was normalized to the background levels of BL41 mutant p53 cells levels. The standard deviation is represented by the error bars for independent replicates per time point.

Later, in this experiment, we started to compare with J3D mutant p53 and wtp53 cells foci intensity levels and it was observed that J3D wtp53 foci intensity levels were found mostly higher than J3D mutant p53 cells foci intensity levels. Photon 2 Gy IR intensity foci levels detected no major ($p > 0.05$) differences between both J3D mutant p53 and wtp53 cell lines for each time point. In comparison to J3D wtp53 foci intensity levels, the Proton 2 and 5 Gy foci intensity levels of J3D mutant p53 was demonstrated higher than the J3D wtp53 cells foci intensity level for each time points (Figure 4.19).

Another significant ($p \leq 0.05$) difference was found between Carbon 3 Gy and Carbon 1 Gy at 24 h post-irradiation in J3D wtp53 cells (Figure 4.19).

On the other hand, as a result of comparing three radiation qualities, there were significant differences such as; in J3D mutant p53 and wtp53 cells, Proton 2 Gy were higher ($p \leq 0.01$) than Photon 2 Gy foci intensity levels at 72 h post-

irradiation. Following this, Carbon 1 Gy and Carbon 3 Gy levels were demonstrated significantly ($p \leq 0.01$) higher than Photon 2 Gy and Photon 5 Gy levels, respectively at 1 h post-irradiation in J3D mutant p53 cells. Besides that, in J3D wtp53 cells, Carbon 1 Gy foci intensity levels were determined significantly ($p \leq 0.01$) higher than Proton 2 Gy levels which were found higher than Photon 2 Gy levels at 72 h post-irradiation (Figure 4.19).

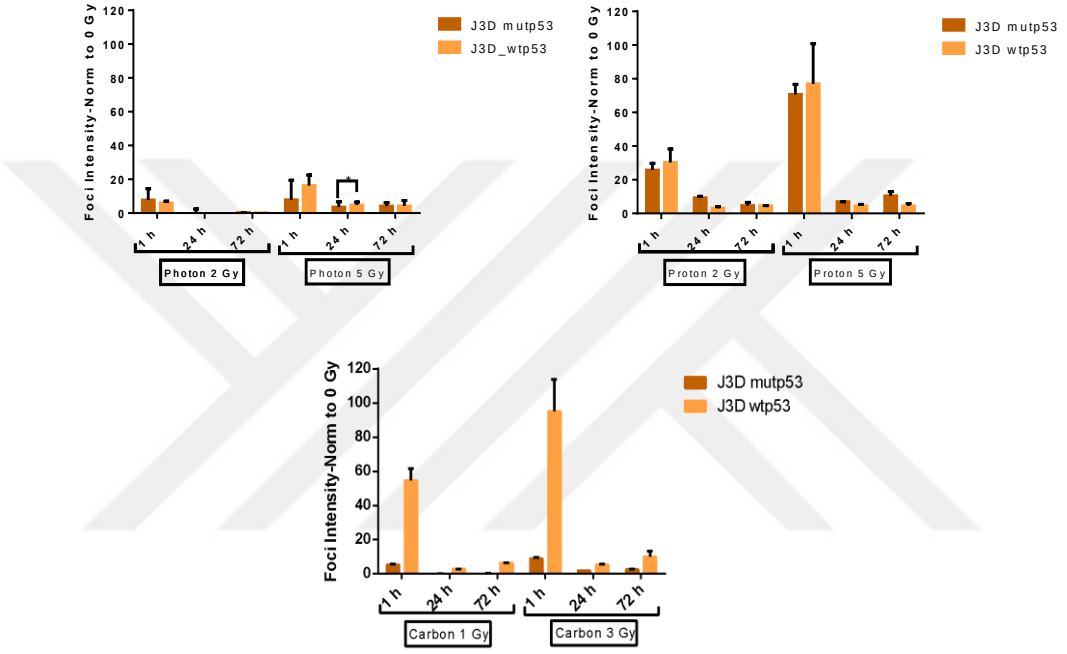

Figure 4.19. Comparison of foci intensity levels detection for the condition different doses after irradiation Photon, Proton and Carbon IR in J3D mutant and wild type p53 cells. The intensity foci levels were detected by dividing the total detected foci intensity to the number of counted cells. The average γH2AX foci intensity of duplicates was normalized to the background levels for each cell lines separately. The standard deviation is represented by the error bars for independent replicates per time point.

Similar to other analysis, for the detection of the effect of (the presence of) p53, J3D mutant p53 cells background (0 Gy) foci intensity levels were used when measuring foci intensity levels of J3D wtp53 cells. The result depicted in Figure 4.20 shows that foci intensity levels of J3D wtp53 were increased when comparing them with the J3D wtp53 foci intensity levels in Figure 4.19. As was presented in Figure 4.20, foci intensity levels in J3D wtp53 cells were already higher than J3D mutant p53 cells, therefore there was remained unchanged ($p > 0.05$) comparison between J3D wtp53 and mutant p53 cells. One of the significant

differences was found Proton 2 Gy at 72 post-irradiation, J3D wtp53 cells levels were determined significantly ($p \leq 0.05$) higher than J3D mutant p53 cells at 72 h post-irradiation. J3D wtp53 cells, Carbon 3 Gy was found as the highest value at 1 h post-irradiation when compared with all levels for each time point (Figure 4.20).

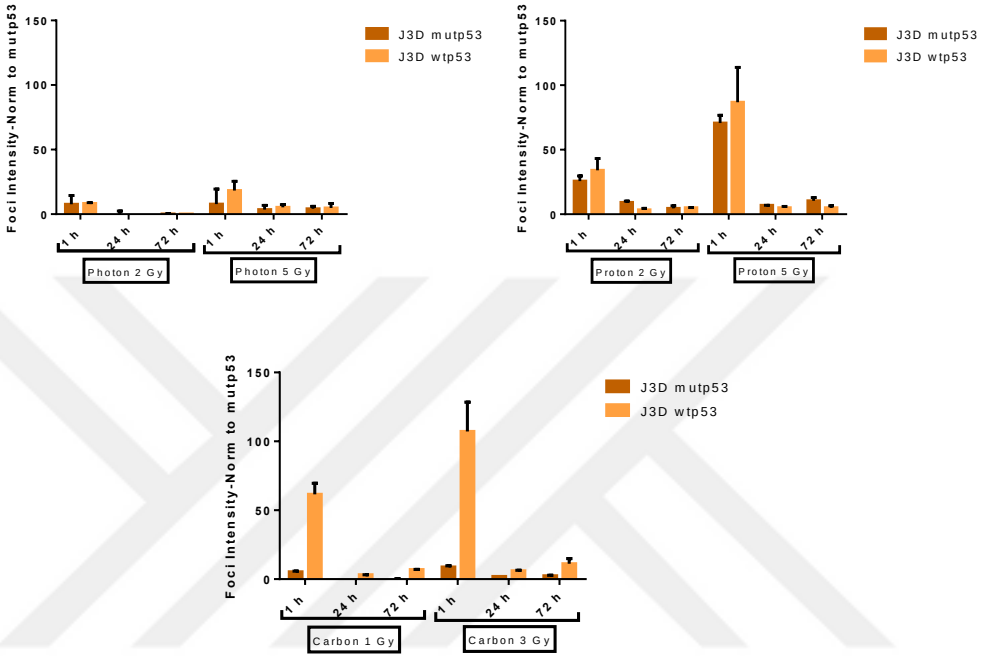

Figure 4.20. Investigation of foci intensity effect of the p53 role by normalization with J3D mutant p53. To investigate foci intensity, total detected foci intensity values was divided to cell number. Later, normalization was performed using J3D mutant p53 cells background levels. The standard deviation is represented by the error bars for independent replicates per time point.

Later, we showed the foci distribution values of each radiation quality at different doses and times. Considering the values obtained by Image-J analysis, cell numbers which include from 1 to 100 foci and we showed that this distribution is related to foci per nucleus levels. We evaluated this distribution by taking the sum of the cell's numbers containing foci 1-5, 6-10, 11-15 and above 16, respectively and separately each radiation time point. Following this, the average calculated for each replicate. As we compared in foci per nucleus, area, and intensity, here, we started to compare with mutant p53 and wtp53 cells levels. At 1h post-irradiation, there were detected several significant differences between BL41 mutant p53 and wtp53 cells such as; Photon 2 Gy in BL41 mutant p53

number of cells containing 11-15 foci, were shown to be as 34-fold higher ($p \leq 0.01$) than BL41 wtp53 number of cells at 1 h post-irradiation. Photon 5 Gy treated BL41 mutant p53 cells levels which include 6-10 foci and 11-15 foci were found significantly ($p \leq 0.05$) 101-fold and 8-fold higher than BL41 wtp53 cells levels, respectively at 1 h post-irradiation (Figure 4.21).

At 1 h post-irradiation, 11-15 foci containing cell numbers, Proton 2 Gy BL41 mutant p53 number of cells were shown as 44-fold higher ($p \leq 0.05$) than BL41 wtp53 cells levels. In a similar manner, Carbon IR (1 and 3 Gy) treated cells BL41 mutant p53 levels were higher than BL41 wtp53 cells numbers. One of significant difference is Carbon 1 Gy treated BL41 mutant p53 cells levels (6-10 foci) were demonstrated 6.9-fold higher ($p \leq 0.01$) than BL41 wtp53 cells levels at 1 h post-irradiation. Another significant was found in Carbon 3 Gy treated BL41 mutant p53 cells numbers which include 11-15 foci as 56-fold higher ($p \leq 0.01$) than BL41 wtp53 cells levels (Figure 4.21).

The general observation is that the majority of cells numbers which were exposed to Photon, Proton and Carbon irradiation showed in average the presence of 16 foci and above per cell. However, Proton and Carbon IR cell numbers which containing 11-15 foci was higher than Photon IR levels. As an example of this, in Carbon 1 Gy treated BL41 mutant p53 cells numbers which include 11-15 foci, were determined significantly ($p \leq 0.05$) higher than Photon 2 Gy levels. In the case of BL41 wtp53 cells, Proton 5 Gy levels (6-10 foci) were significantly ($p \leq 0.05$) higher than Photon 5 Gy levels. For above 16 foci, BL41 wtp53 Photon 5 Gy and Carbon 3 Gy at 1h post-irradiation foci levels were recorded to be the highest levels (Figure 4.21).

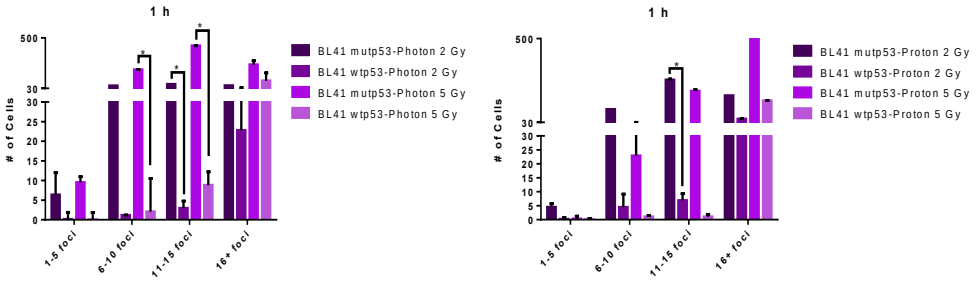

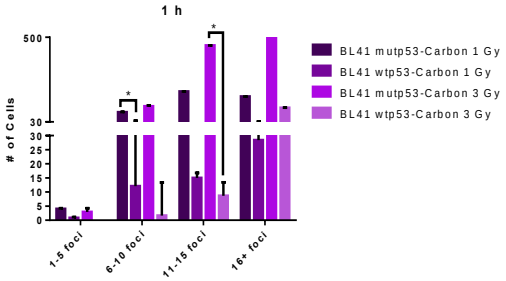

Figure 4.21. Frequency of foci distributions per BL41 wild type and mutant p53 cells exposed to Photon, Proton and Carbon IR after 1 h post-irradiation. The foci distribution was demonstrated based on Image J analysis. The cell number which have foci between 1-5, 6-10, 11-15 and above 16 foci, average was taken. The standard deviation is represented by the error bars for independent replicates per time point.

As shown in foci per nucleus, area, and intensity levels graphs, 24 h post-irradiation levels (foci include cell number) were demonstrated lower levels than 1 h post-irradiation levels. The only significant ($p \leq 0.01$) differences between BL41 mutant p53 and wtp53 cells numbers levels were determined Photon 5 Gy (1-5 foci) at 24 h post-irradiation. Following Figure 4.22, Photon 5 Gy treated BL41 mutant p53 cell numbers which include 6-10 and 11-15 foci, were found also higher than BL41 wtp53 cells levels. Regarding this, after 24 h post-irradiation. Proton 2 Gy treated BL41 mutant p53 levels were found significantly ($p \leq 0.01$) higher than BL41 wtp53 levels which contains 1-5 foci. Likewise, Proton 5 Gy treated BL41 mutant p53 cell number levels were 3-fold ($p \leq 0.05$) higher than BL41 wtp53 levels which contains 1-5 foci. In the case of Carbon IR treated BL41 mutant p53 cells number levels mostly were found higher than BL41 wtp53 cells levels. In Carbon 1 Gy treated BL41 mutant p53 cell number levels (1-5 foci) were demonstrated significantly ($p \leq 0.05$) higher than BL41 wtp53 cells levels (Figure 4.22).

Comparing of three radiation qualities, the cell numbers which include 11-15 foci, Carbon 1 Gy and Proton 2 Gy were recorded significantly ($p \leq 0.05$) higher than Photon 2 Gy in BL41 mutant p53 cells. In general, the cell numbers were contained 6-10 and 11-15 foci at 24 h post-irradiation for three radiation qualities (Figure 4.22).

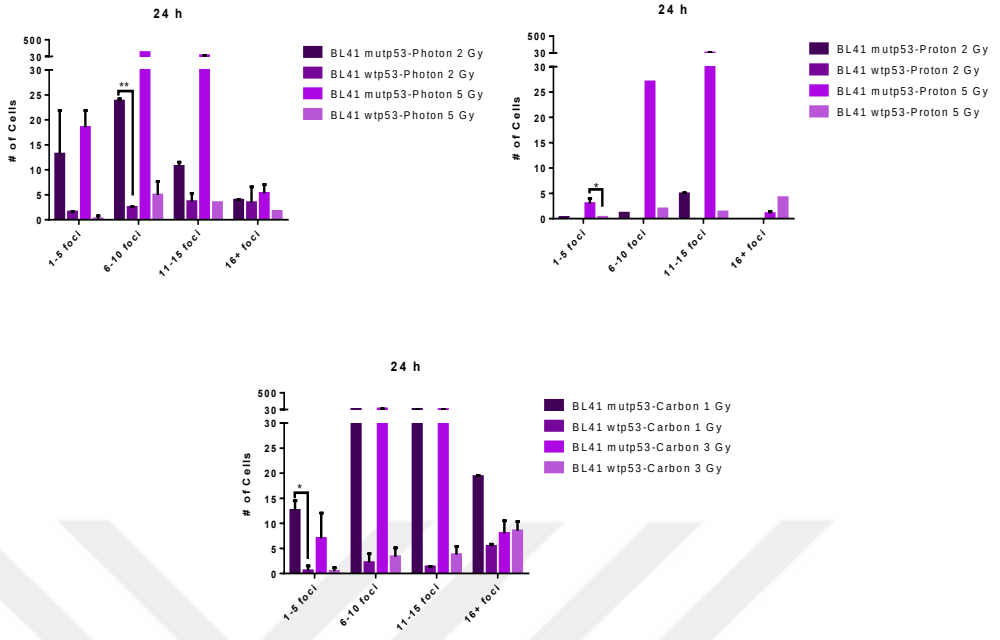

Figure 4.22. Frequency of foci distributions per BL41 wild type and mutant p53 cells exposed to Photon, Proton and Carbon IR after 24 h post-irradiation. The foci distribution of γH2AX foci per cell was calculated by some of number of cells and taken average of two replicates. The average γH2AX foci intensity of triplicates was normalized to the untreated level. The standard deviation is represented by the error bars for independent replicates per time point.

After 72 h post-irradiation, in the case of Photon treated, there were no major ($p > 0.05$) differences between BL41 mutant p53 and wtp53 cell number levels which include 1-5, 6-10, 11-15 and more than 16 foci, except, Photon 2 Gy treated BL41 mutant p53 cells numbers levels (11-15 foci) were found 9-fold ($p \leq 0.05$) higher than BL41 wtp53 cell levels.

Another observation is that Proton 2 Gy cell number levels (11-15 foci and above 16 foci) were determined significantly ($p \leq 0.05$) higher than Photon 2 Gy levels. Additionally, Carbon IR treated cells numbers were determined higher than Photon and Proton R treated cells numbers for each foci range when 16 and more foci values were taken into consideration (Figure 4.23). Generally, at 72 post-irradiation levels were found lower than 24 h and 1 h post-irradiation levels.

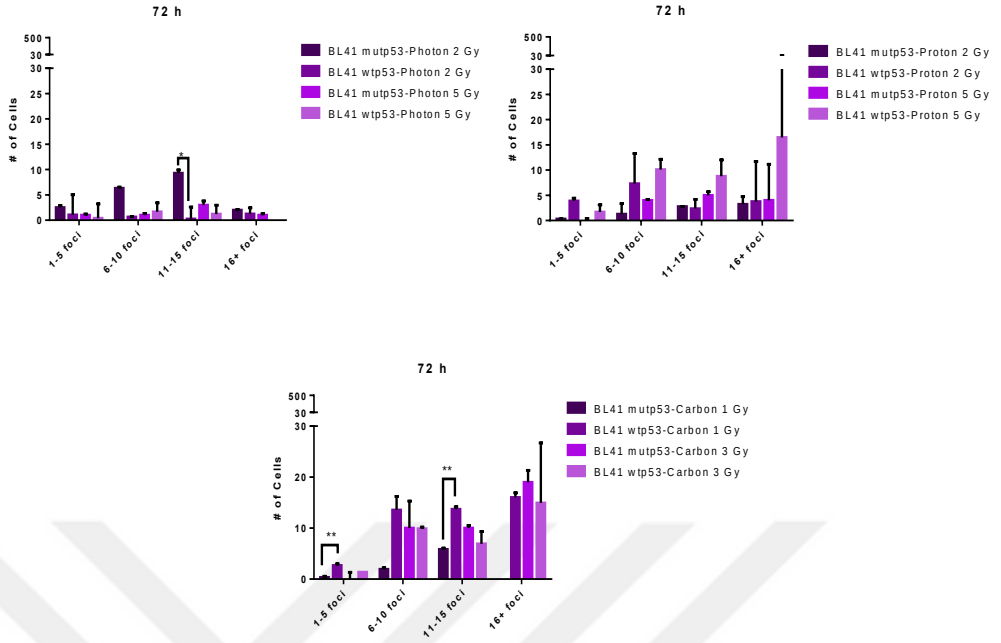

Figure 4.23. Frequency of foci distributions per BL41 wild type and mutant p53 cells exposed to Photon, Proton and Carbon IR after 72 h post-irradiation. The foci distribution of γH2AX foci per cell was calculated by some of number of cells and taken average of two replicates. The average γH2AX foci intensity of triplicates was normalized to the untreated level. The standard deviation is represented by the error bars for independent replicates per time point.

Foci distributions and determination of foci containing cell numbers were carried out in the same manner as analysis of BL41 cells foci distribution. Cell counts were evaluated considering that they contain a range of foci; 1-5, 6-10, 11-15 and 16 above, respectively. Firstly, mutant p53 and wtp53 cell lines were compared at different time intervals, and then significant differences between the three radiation qualities were shown. When Photon IR treated the cell numbers containing between 1-5 foci, 6-10 foci, and 11-15 foci are compared, there was found no significant ($p > 0.05$) difference between J3D mutant p53 and wtp53 cells levels. However, Photon 5 Gy treated J3D mutant p53 cells levels (more than 16 foci) were found 4.6-fold ($p \leq 0.05$) higher than J3D wtp53 cells levels at 1 h post-irradiation. Following this, Proton 2 Gy cell numbers levels in J3D mutant p53 was determined significantly ($p \leq 0.05$) higher than J3D wtp53 cells numbers which are containing 11-15 foci. Besides that, Proton 5 Gy treated J3D mutant p53 cells number levels were found also significantly ($p \leq 0.05$) higher

than BL41 wtp53 cells levels (6-10, 11-15, and 16 above foci). Carbon 1 Gy treated significant ($p \leq 0.001$) differences between BL41 mutant p53 and wtp53 were found in cell numbers which include more than 16 foci. Furthermore, Carbon 1 Gy and 3 Gy values were recorded as the highest value when compared Photon and Proton IR treated cells for both cell lines (Figure 4.24).

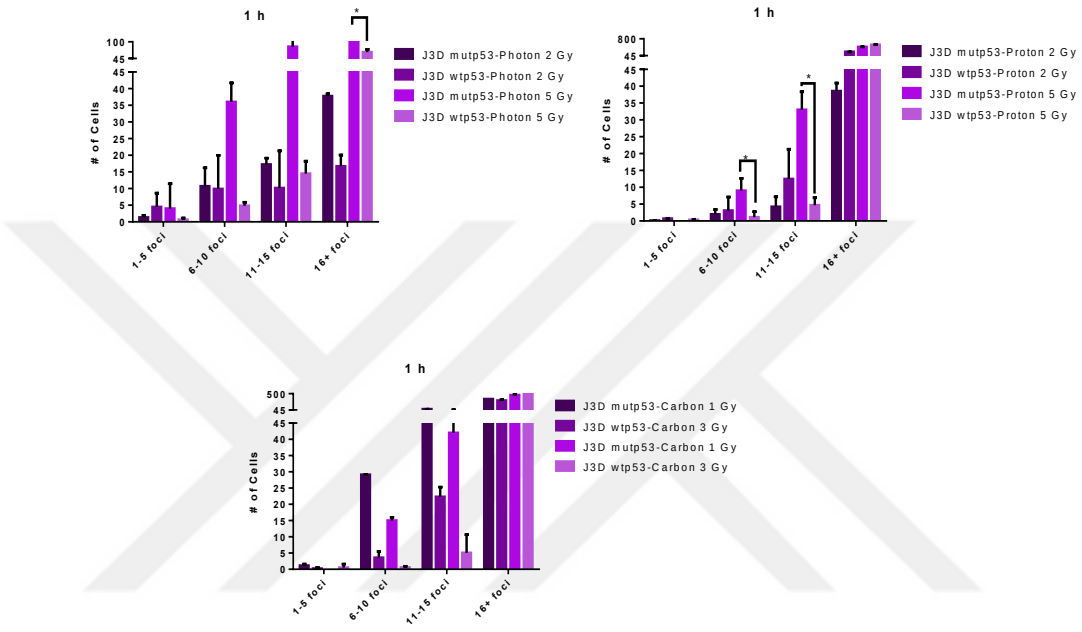

Figure 4.24. Quantification of γH2AX foci distribution after 1 h post- exposed Photon, Proton and Carbon IR in the J3D mutant p53 and wild type p53 cells. The foci distribution of γH2AX foci per cell was calculated by some of number of cells and taken average of two replicates. The average γH2AX foci intensity of triplicates was normalized to the untreated level. The standard deviation is represented by the error bars for independent replicates per time point.

After 24 h post-irradiation, there were no significant ($p > 0.05$) differences between J3D mutant p53 and wtp53 cells numbers levels for each foci range. In the case of Proton 2 Gy and Proton 5 Gy treated J3D mutant p53 cells number levels were found 2.5-fold ($p \leq 0.01$) higher than J3D wtp53 cells numbers which are containing 6-10 foci. Carbon 1 Gy, the number of cells levels detected in J3D mutant p53 cells was significantly ($p \leq 0.001$) higher than J3D wtp3 cells numbers (above 16 foci), while after increasing the dose to Carbon 3 Gy, the number of cells levels in J3D mutant p53 cells was found to be approximately 3-fold higher than in the J3D wtp53 cells (6-10 foci).

A comparison between the different radiation qualities were found, that Carbon IR treated cell numbers have a higher value for each foci range compared to Proton and Photon IR treated cell numbers levels and this observation is valid for both cell lines. It was also found that in J3D mutant p53 cells, Proton 2 Gy cell number levels (1-5 and 6-10 foci) were determined significantly ($p \leq 0.05$) higher than Photon 2 Gy levels. In addition, Proton 5 Gy cell number levels (1-5 foci) were demonstrated significantly ($p \leq 0.05$) higher than Photon 5 Gy levels. In the case of J3D wtp53 cells, as seen in foci per nucleus, area, and intensity, Carbon IR treated levels were higher than Proton and Photon. Carbon 1 Gy cell numbers which include 11-15 foci, were recorded significantly ($p \leq 0.05$) higher than Proton 2 Gy which significantly higher than Photon 2 Gy. In addition, each level of the number of cells decreased compared to the 1 h post-irradiation number of nucleus cells (Figure 4.25).

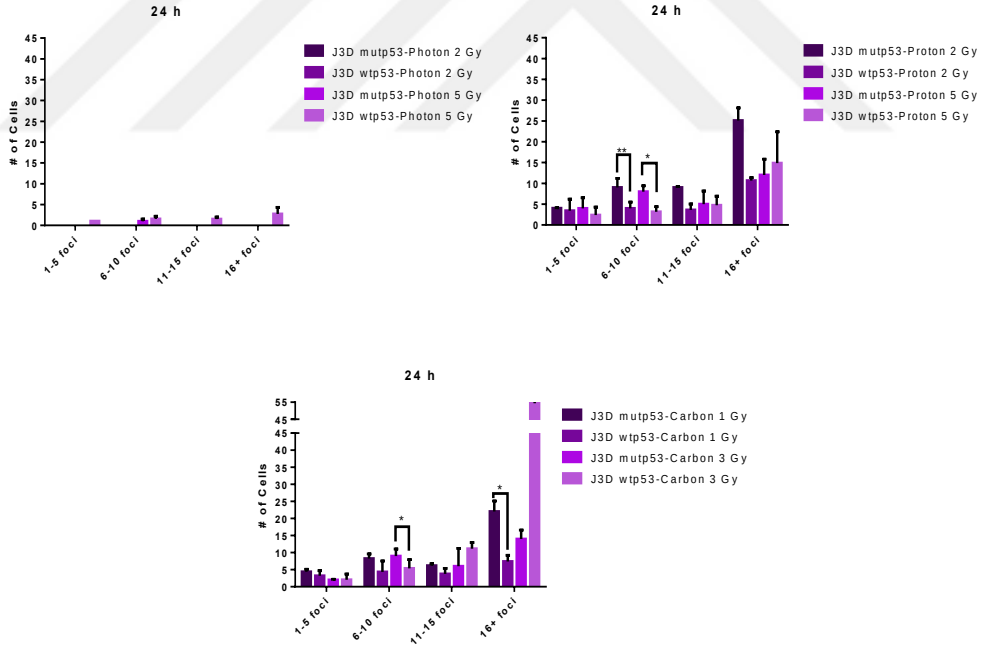

Figure 4.25. Quantification of γH2AX foci distribution after 24 h post- exposed Photon, Proton and Carbon IR in the J3D mutant p53 and wild type p53 cells. The foci distribution of γH2AX foci per cell was calculated by some of number of cells and taken average of two replicates. The average γH2AX foci intensity of triplicates was normalized to the untreated level. The standard deviation is represented by the error bars for independent replicates per time point.

At 72 h post-irradiation, Photon IR treated cell numbers had lower levels when compared to Proton and Carbon treated cells numbers for both cell lines, therefore there were no major ($p > 0.05$) differences between J3D mutant p53 and wtp53 levels for each foci range except, Photon 2 Gy treated J3D mutant p53 cells number levels (1-5 and 11-15 foci) were found significantly higher than J3D wtp53 cells levels. Even though some of Proton IR and Carbon IR treated J3D mutant p53 cell levels were detected higher than J3D wtp53 cells levels, there was no significant ($p > 0.05$) differences between J3D mutant p53 and wtp53 cells levels.

As a final observation, among the 3 radiation qualities, the number of cells levels found at 72 h post-irradiation had low levels comparing with Figure 4.24 and 4.25. Besides that, there are significant ($p \leq 0.05$) differences between radiation qualities such as; in J3D mutant p53 cells, Carbon 1 Gy cell number levels (1-5, 11-15 and more than 16 foci) were found significantly higher than Photon 2 Gy levels at 72 h post-irradiation. Also, in J3D wtp53 cells, Carbon 1 Gy cell number levels (1-5 and 6-10 foci) were determined also significantly ($p \leq 0.05$) higher than Photon 2 Gy levels (Figure 4.26).

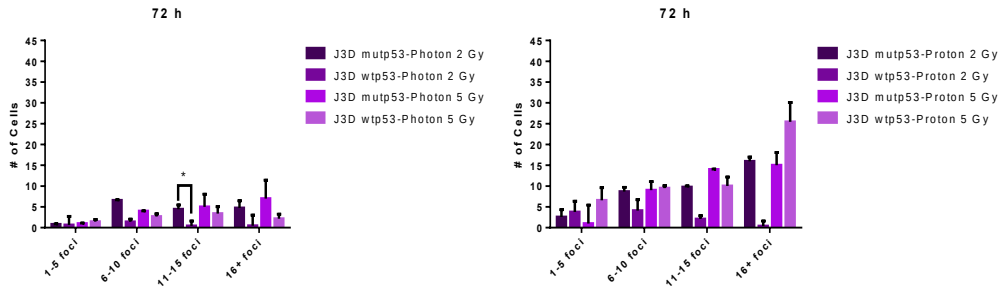

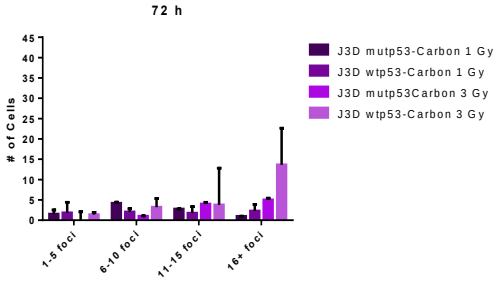

Figure 4.26. Quantification of γH2AX foci distribution after 72 h post- exposed Photon, Proton and Carbon IR in the J3D mutant p53 and wild type p53 cells. The foci distribution of γH2AX foci per cell was calculated by some of number of cells and taken average of two replicates. The average γH2AX foci intensity of triplicates was normalized to the untreated level. The standard deviation is represented by the error bars for independent replicates per time point.

4.6. Kinetics of The Decline of γH2AX Residual Foci: Analysis and Comparison of Photon, Proton and Carbon IR in Mutant and Wild Type Cell Lines

To investigate how the p53 activation would affect the DNA damage repair capacity, the residual of γ-H2AX foci was investigated by comparing the level of residual foci 24 h and 72 h following Photon, Proton and Carbon irradiation. Hence, 24 h and 72 h residual levels were calculated with proportion to 1 h post-irradiation levels: for foci number, foci area, and foci intensity residual percentages levels. The residual γH2AX foci levels in BL41 mutant p53 cells, following exposure of Photon 2 Gy was 37% after 24 h and 28% 72h post-irradiation. Nevertheless, in the BL41 wtp53 cell line, the residual foci were found 14% and 4% after 24 h and 72 h post-irradiation. Similar reduction between values over time also were obtained in BL41 mutant p53 cells and BL41 wtp53 cells for the Photon 5 Gy residual foci percentages, namely 48% to 16% and 23% to 10% at 24h and 72h post-irradiation, respectively. For the Proton 2 Gy treated BL41 wtp53 cell lines, we were not able to calculate residual foci of γH2AX foci at 24 h post-irradiation. Besides that, BL41 mutant p53 residual foci values of Proton 2 Gy and Proton 5 Gy were found similar compared to 24 h and 72 h post-irradiation. However, in Proton 5 Gy treated BL41 wtp53 cells the residual foci

between 24 h and 72 h post-irradiation were observed as 22% and 18 %, respectively. In Carbon 1 Gy treated BL41 mutant p53 cells at 24h post-irradiation residual foci percentages levels were found to be 35% and at 72h post-irradiation was found 4%. However, Carbon 1 Gy treated BL41 wtp53 cells residual foci decreased from 51% to 38% at 24 h and 72 h post-irradiation. In Carbon 3 Gy treated BL41 mutant p53 cells, the residual foci at 24 hours were 23% and 11% at 72 hours post-irradiation. Another significant differences between BL41 mutant p53 and wtp53 cells residual foci levels were found in Carbon 1 Gy levels at 72 h post-irradiation. The residual foci Photon 5 Gy treated BL41 mutant p53 cell lines decreasing was slower as a function of time, however, Carbon 3 Gy treated BL41 mutp53 decreasing over time was much faster (Figure 4.27).

Another observation is comparing three radiation qualities. Following this, in BL41 mutant p53 cells residual foci levels, Proton 2 Gy levels were significantly ($p \leq 0.05$) higher than Photon 2 Gy levels at 24 h post-irradiation. In similar manner, Carbon 3 Gy levels were demonstrated higher than Photon 5 Gy levels at 24 h and 72 h post-irradiation. In BL41 wtp53 cells, Carbon 1 Gy levels were determined Photon 2 Gy levels at 72 h post-irradiation (Figure 4.27).

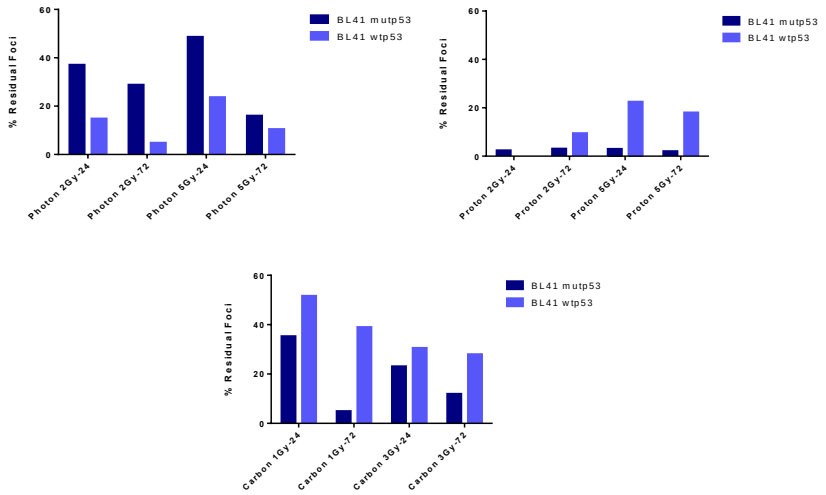

Figure 4.27. Overview of the residual foci percentages of BL41 cell lines. The percentages of the residual foci following ionizing radiation were calculated based on the data from the average foci number at 1 h post-irradiation.

In a similar manner, Photon, Proton and Carbon IR treated residual foci percentages were found to be decreasing over time for both J3D wtp53 and mutp53 cells. Addition of observation which reduction over time, Photon 2 Gy 72h post-irradiation residual percentages levels were determined as 29% and 27% in J3D mutant p53 and wtp53 cells, respectively. In J3D mutant p53 cells Proton 2 Gy and 5 Gy residual foci levels at 24 h post-irradiation was demonstrated higher than residual foci levels at 72 h post-irradiation. However, in Carbon treated cells did not decrease significantly in both cell lines (Figure 4.28).

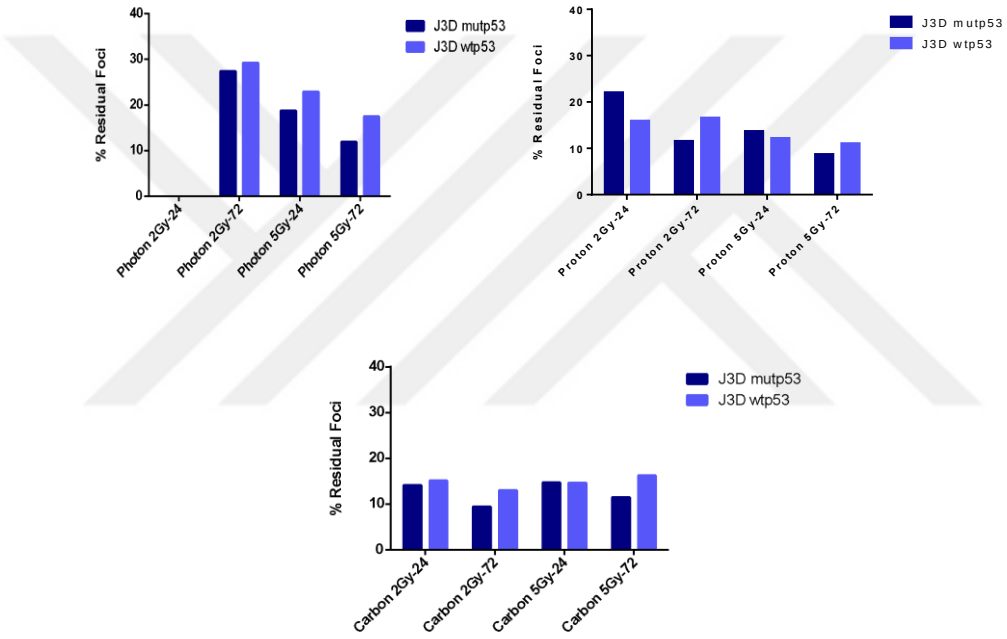

Figure 4.28. Overview of the residual foci percentages in J3D cell lines. The percentages of the residual foci following ionizing radiation were calculated based on the data from the average foci number. Percentage values were calculated based on 1 h post- irradiation values.

To investigate the repair kinetics of BL41-J3D cell lines following exposure to Photon, Proton and Carbon IR, the residual area percentage levels of γ-H2AX foci were compared at 24 h and 72 h post-irradiation and also between mutant p53 and wtp53-cell lines. Based on foci area levels, residual area levels were calculated. The residual area percentages were determined 36% and 29% in Photon 2 Gy treated BL41 mutant p53 cells. BL41 mutant p53 cells levels were detected as 11% and 4% at 24 h and 72 h post-irradiation, respectively.

In the Photon 5 Gy treated BL41 mutp53 residual area levels were demonstrated to be 56% and 24%. Proton 5 Gy treated BL41 wtp53 residual area levels were 20% at 24 h post-irradiation and decreased to 10% at 72 h post-irradiation. In Carbon 1 Gy treated BL41 mutant p53 cells were 20% and 4% at 24 h and 72 h post-irradiation, respectively. Nevertheless, Carbon 1 Gy treated BL41 mutant p53 cells were 20% and 4% at 24h and 72 h post-irradiation. These levels were lower than BL41 wtp53 cells residual area levels which were found 50% and 25% at 24h and 72 h post-irradiation, respectively. Carbon 3 Gy treated BL41 mutant p53 cell lines behaved nearly similarly at 24 h and 72 h post-irradiation (Figure 4.29).

As a final observation, comparing three radiation qualities there is significant difference between radiation qualities such as; Carbon 1 Gy and Proton 2 Gy residual foci area levels were demonstrated significantly higher than Photon 2 Gy levels at 72 h post-irradiation (Figure 4.29).

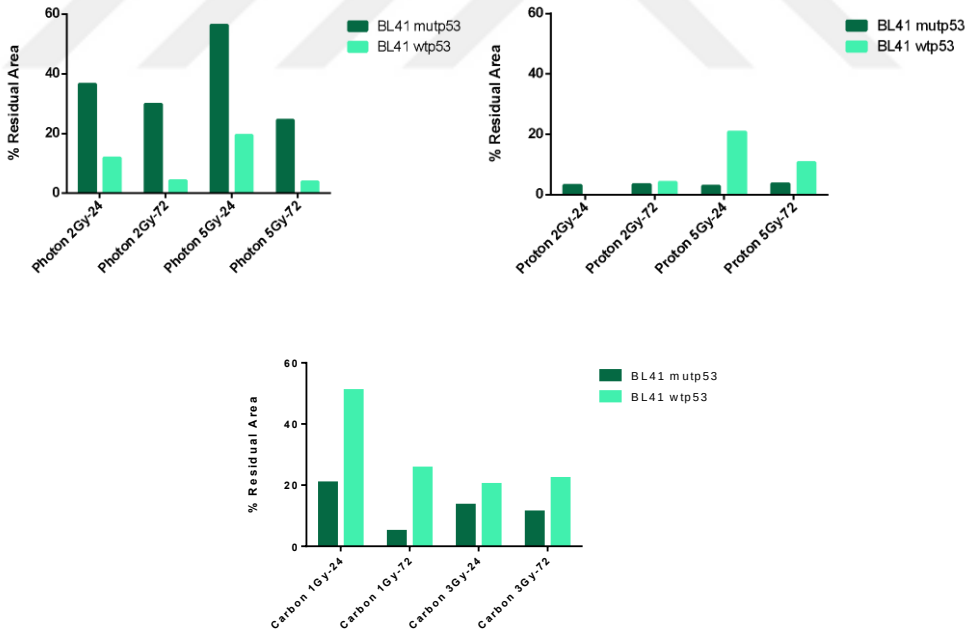

Figure 4.29. Comparison of the 24h and -72 h post-irradiation residual foci area levels in BL41 mutant p53 and wild type p53 cells. The percentages of the residual foci following ionizing radiation were calculated based on the data from average foci area. Percentage values were calculated based on the situation 1 h post-irradiation.

In the case of J3D cells residual area levels, we calculated them similar to BL41 residual area levels based on 1 h post-irradiation foci area levels. Photon 5 Gy residual area percentages were detected 12% and 6% at 24 h and 72 h post-irradiation in J3D mutant p53 cells, respectively, whereas in J3D wtp53 cells, the Photon 5 Gy residual foci area percentages were found to be 22% and 17% at 24 h and 72 h post-irradiation. The residual foci in Proton IR treated J3D wtp53 cell lines after 24 h and 72 h were nearly similar which Proton 2 Gy treated J3D mutant p53 cells levels were demonstrated 6% and 5% at 24 h and 72 h post-irradiation, respectively. Finally, both Carbon IR treated J3D mutant p53 and J3D wtp53 cell levels showed no decrease at 24 h and 72 h post-irradiation. However, J3D wtp53 cells residual area levels were found higher than J3D mutant p53 cells levels for each time points (Figure 4.30).

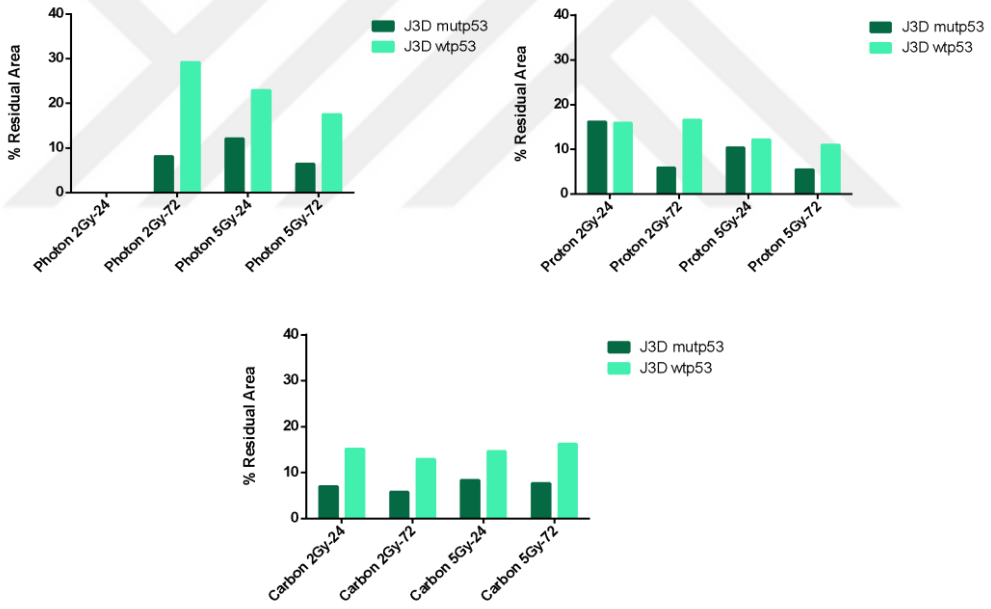

Figure 4.30. Comparison of the 24h and -72 h post-irradiation residual foci area levels in J3D mutant p53 and wild type p53 cells. The percentages of the residual foci following ionizing radiation were calculated based on the data from average foci area. Percentage values were calculated based on the situation 1 h post-irradiation.

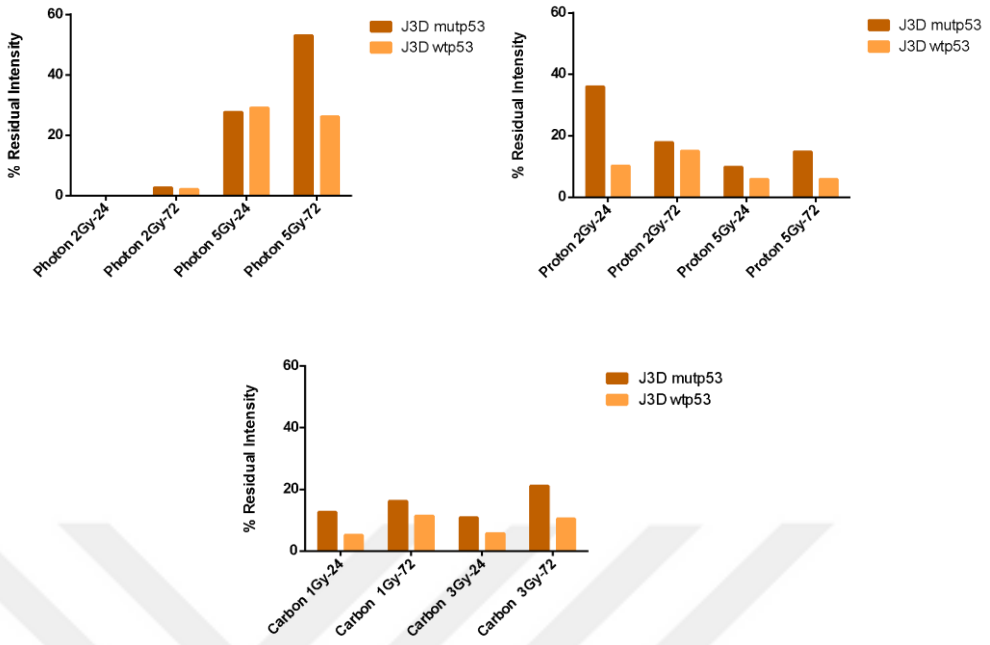

Figure 4.31. γ-H2AX signaling kinetics determination with foci intensity residual levels in J3D mutant and wild type p53 lymphocyte cells after exposure to different radiation qualities. The percentages of the residual foci following ionizing radiation were calculated based on the data from average foci area. Percentage values were calculated based on the situation 1 h post-irradiation.

Due to technical reasons, we are not able to present BL41 wtp53 and mutp53 residual intensity percentages. For the J3D wtp53 and mutp53 cell lines, residual intensity values were calculated based on foci intensity values. Additionally, like foci and area levels, we were not able to calculate Photon 2 Gy treated levels at 24 h post-irradiation. The residual intensity levels in J3D mutp53 cells after 24 h was 27%, however, we had the impression that residual intensity levels started to increase at 72 h post-irradiation. Interestingly, Proton 2 Gy 24 h post-irradiation foci intensity residual percentages were 35% in J3D mutant p53 cells, while at 72 h post-irradiation foci intensity residual percentage levels in J3D mutant p53 cell line were found 17%. The measurement of Carbon IR treated residual intensity levels in both J3D wtp53 and mutp53 cell lines, showed a similar trend at 24 h and 72 h post-irradiation (Figure 4.32).

5. DISCUSSION AND CONCLUSION

Radiotherapy is used as a treatment for different types of cancer and can have dangerous effects on patients. There are sufficient studies which have investigated and determined the effects of the risks associated with radiotherapy (87). We present a comprehensive comparison of the differences between the mechanisms of DNA repair, where we investigated three radiation qualities (Photon, Proton, and Carbon) used in wild type and mutant p53 lymphoma cell lines. Our hypothesis was that reactivation of the wild type p53 protein increases the RBE of radiotherapy. We showed that different radiation qualities effect in cells is DBSs and that, accordingly, monitoring γ-H2AX focus numbers can be a useful biomarker to detect the individual ionizing radiation (IR) effect on B-cells. The ability to detect DSBs by measuring γ-H2AX-foci protocol has been described by Rogakou et al (38) providing an opportunity to assess the induction and repair of DNA damage in vivo after relevant radiation doses. Besides that, to quantify DNA damage with γ-H2AX is more accurate through to use fluorescent microscopy. With this method, the number of foci per cell and/or the size of the foci can be measured through to a high-throughput imaging system. Unlike early studies quantifying the total amount of γH2AX-phosphorylation in tissue or cell area (57), we counted the absolute number of γH2AX-foci formed per nucleus. In addition, it is a very sensitive method due to its ability to stimulate the γ-H2AX foci at low doses up to 1.2 mGy in-vitro in cell culture. Also, it was shown that a linear relationship exists between the number of foci and doses (58).

An alternative method for γ-H2AX analysis is flow cytometry and is often the preferred method when analyzing large sample sizes (i.e. >10,000 cells). The main difference between these methods is that microscopy allows the scoring of individual foci while flow cytometry detects total fluorescence intensity in each cell (59). Hence, the microscopy method is a better alternative to quantify DNA damage with γ-H2AX. In this study experimental data sets were generated through staining procedures, imaging, and γH2AX foci quantification. In order to

understand the potential DNA damage response and optimization of particle radiation therapy, we used this measurement technique (60).

In this study, the cell lines which was used in the measurement of the γ-H2AX method, are temperature sensitive. When the cells are grown at 37°C, the mutated non-functional form of p53 is expressed. To induce the formation of the functional wild type p53, the cells can be grown at a lower temperature (32°C). We used the cells with low the temperature and exposing them 2 and 5 Gy for Photon and Proton and 1 and 3 Gy for Carbon radiation qualities. All cell numbers counted as a result of analyzes obtained by monitoring γ-H2AX were compared between wild type and mutant p53 cell types. The BL41 mutant p53 cell number was 4.4-fold higher than the BL41 wild-type p53 cell number, while no major difference was observed between J3D wild-type and mutant p53 cell numbers. The reason of this could be J3D cell lines delivered from mouse whereas BL41 cell lines human cell models. Also, these results imply that the functional activation of wild type p53 results in a decrease in cell viability of the BL41 cells. It was well known that p53 takes the cell to apoptosis when it is active, and therefore it achieved fewer cells (61). Ramqvinst et al (55) already showed that activation of wild type cell lines might result in an increase in the frequency of apoptosis.

Previous studies showed that the γ-H2AX response can be measured at later post-irradiation times to follow the progression of DNA repair (62). To study whether the functional activation of p53 would affect the DNA damage response capacity of BL41 and J3D cell lines following the exposure to three irradiations, we quantified the initial induction of γ-H2AX foci at the 1 h, 24 h, and 72 h post-irradiation. Firstly, the cells containing foci were proportioned with cell numbers as a percentage and the foci percentage levels were determined for each replicate of samples. Based on these foci percentage levels, mutant p53 and wild type p53 species of BL41 and J3D cell lines were shown to show time-dependent foci change. However, we were not able to analysis Photon 2 Gy 24 h foci levels in J3D mutant p53 and wtp53 cells levels and in BL41 mutant p53 cells, Proton 2 Gy

at 24h foci levels. The general observation from our results was found that the initial radiation-induced γ-H2AX foci substantially decreased at the late time points. The significant decrease in time was observed in exposed BL41 mutant p53 cells in each radiation quality.

As a confirmation of our results, Bylicky et al. showed that radiation-induced γ-H2AX foci display a statistically significant decrease between 24 h, 48 h, and 72 h and suggest that a significant percentage of γ-H2AX foci have resulted in the activation of the repair mechanism (63). Following radiation exposure, H2AX phosphorylation occurs to trigger DDR activation and initiate repair. After the DNA repair mechanism is activated, H2AX phosphorylation is not required for DDR activation, which results in a decrease in γ-H2AX foci formation over time (65). This is also in accordance with the findings of Rogakou et al. who observed that following DSB formation, γ-H2AX foci induction occurs rapidly. Moreover, repair of DSBs were started after 1 and 3 hours and afterward it caused the dephosphorylation and loss of the γ-H2AX foci within the nucleus (38). In cells which exhibit signs of defective DNA repair mechanisms, there is a persistence of γ-H2AX foci seen which is due to failure to resolve these DNA DSBs (66).

After foci positive levels were determined, regarding this, the γ-H2AX foci number, foci area, and foci intensity levels were calculated in unirradiated (which was shown as background levels) samples for both BL41 and J3D cells mutant p53 and wtp53 types. These unirradiated samples levels (background levels) were used as the control for each cell lines separately. Foci per nucleus, foci area, and foci intensity values were higher in unirradiated both BL41 and J3D wtp53 cells as compared to unirradiated BL41 and J3D mutant p53 cells. Even though these were not exposed the IR, γ-H2AX foci were recorded. Indeed, foci levels in unirradiated samples can occur momentarily e.g. through sunlight (67).

However, the reason of the differences between mutant p53 and wild type p53 cell lines could be, as described above, wtp53 presents p53 protein, whereas mutant p53 has a loss of p53 function. wtp53 induced apoptosis and this leads to increasing the γ-H2AX foci. Also, Rogakou et al. (38) showed evidence that

apoptotic DNA fragmentation induces γ-H2AX formation. In the case of DNA repair, this would keep the two DNA ends in close, whereas apoptosis γ-H2AX might facilitate the packaging of fragmented DNA into apoptotic bodies. Besides that, γ-H2AX have a role to recruit other endonucleases that may mediate both DNA repair and/or apoptosis. In the presence of damage, ATMs may be active through mediators and cause phosphorylation of H2AX. This phosphorylation by ATM may be increased through the activation of p53 (68).

To investigate the response of the cells to three different types of radiation, γ-H2AX foci number, area, and intensity were measured post-IR by fluorescence imaging. The superior RBE of Proton and Carbon beams are measurable based on the kinetics of DNA repair. Following this hypothesis, in general, we observed that Proton IR and Carbon IR were found higher than Photon IR for each time point. In regard to this matter, there are several significant observations when compared to three different radiation qualities. The first result was observed as Proton 5 Gy foci per nucleus levels were significantly higher than Photon 5 Gy levels at 1 h and 72 h post-irradiation in BL41 mutant p53 cells. In BL41 wtp53 cells, Carbon 1 Gy foci per nucleus levels were higher than Photon 2 Gy levels at 1 h and 72 h post-irradiation. In the case of J3D mutant p53 cells, Proton 5 Gy and Carbon (1 Gy-3 Gy) were demonstrated significantly higher than Photon 5 Gy levels at 1 h post-irradiation. Finally, in J3D wtp53 cells, Proton 2 Gy foci per nucleus levels were recorded higher than Photon 2 Gy levels at 1 h and 72 h post-irradiation. Also, Carbon 1 Gy foci per nucleus levels were significantly higher than Photon 5 Gy levels at 1 h and 24 h post-irradiation.

Similar to these observations in γ-H2AX foci per nucleus results, the measurement of γH2AX foci area and intensity levels were detected the similar trend as the obtained from the foci per nucleus levels.

The high γ-H2AX foci of Carbon and Proton IR may be due to they caused more complex damage and higher RBE. Carbon ions slow down and stop the growth rate within the tumor in time before causing damage to healthy tissue. Carbon ions are different from Photons and Protons in terms of accumulating high

LET concentration at the Bragg peak. Just like Proton beams, Carbon beams can also provide normal tissue protection to its narrow Bragg peak (69)(21). Carbon IR and Proton IR produce dense ionization and create clustered DNA damage if compared to Photon IR, which produce diffuse ionization and DNA damage. Thus, it can be said that Carbon and Proton IR have more tumor-killing potential than Photon IR. In addition to that, even when using a higher dose of Photon radiation, Carbon and Proton ion beams still lead to more severe damage (56).

Furthermore, according to Suit H. et al showed also Carbon and Proton IR result in higher cell damage than Photon IR. When compared to Photon IR, particle therapy for cancer performed either with Proton or Carbon ions offers the advantage of their distinct physical characteristics exploits greater RBE (70). Greater RBE, in turn, may lead to better tumor control and improve patient survival. Additionally, up to date, there are no convincing clinical data that confirm the effects of particle therapy (either with Protons or Carbon ions) in lymphoma treatment (71). Therefore, in this thesis, we have shown that this treatment may be useful againstlymphoma cancer.

Our other goal in this thesis was to investigate the IR response with re-activation of p53. From this, we first normalized the foci per nucleus, foci area and foci intensity values with their own unirradiated levels (background levels). We compared mutant p53 and wtp53 values in this manner. In general, we showed that mutant p53 values were higher than wild type values (Norm to 0 Gy) such as; Carbon 1 Gy BL41 mutant p53 foci per nucleus levels were determined significantly higher than BL41 wtp53 cells at 72 h post-irradiation. In the case of J3D mutant p53 cells were higher than wtp53 cells in Photon 5 Gy at 1 h post-irradiation.

Later, wtp53 cell lines levels of foci per nucleus, foci area, and foci intensity were investigated with normalization using mutated p53 unirradiated (background) values. Using mutated p53 values as control, all values increased after normalization in Bl41 and J3D wtp53 cell lines. There were several significant foci levels after using mutant p53 background levels for normalization.

Regarding this, we compared same mutant p53 levels with wtp53 levels which were normalized to mutant p53 background levels. As an example of this, BL41 wtp53 cells Photon 5 Gy at 1h post-irradiation foci per nucleus values were found to be significantly higher than BL41 mutant p53 values. Also, in J3D wtp53 cells, Proton 5 Gy levels were significantly higher than J3D mutant p53 levels at 72 h post-irradiation. This trend was also observed for the different radiation qualities, as well as the foci area and intensity values. This result provides experimental evidence that functional p53 increase the kinetics of repair while p53 presents in wild type p53 cells.

One explanation why this wild type p53 values are much higher than mutated p53 could be because wild type p53 related to the H2AX protein. In the case of DNA damage, H2AX proteins are phosphorylated. Min-Kyoung et al. showed that after exposure to irradiation, DSBs occur and it leads to activation of p53 protein which rapidly co-localizes with γ-H2AX (74). Therefore, in the case of activation p53 caused higher γ-H2AX as a response of DNA damage. Moreover, after DSBs occurred, histone H2AX is phosphorylated by ATM. DSBs induction, a fraction of the nuclear ATM pool relocates to the damaged DNA and colocalizes with γ-H2AX foci. Besides, the p53 binding protein 1 (53BP1) also colocalizes with γ-H2AX foci and also this protein can be phosphorylated by ATM in response to DNA damage (88). Thus, activation of p53 is observed to provide more γ-H2AX foci formation.

Considering γH2AX foci area results, the dose responses for the number of foci per nucleus were fitted with the area of foci levels. The foci area and foci intensity values present size and extent of radiation-induced DNA double-strand breaks, respectively. We observed that mutant p53 levels were higher than wild type p53 levels in both BL41 and J3D cells. The differences between Photon IR and particles were also demonstrated similar in foci area levels. Radiation has the effect of starting the cell cycle or inducing a change in chromatin condensation. A change in nucleus size due to an alteration in the cell cycle would be reflected by an average increase or decrease of the nucleus area. Additionally, the size of the

nucleus may change depending on dose and time. After high dose exposure, intensification can occur at G2 phase cell cycle. Thereby, in this thesis, we showed alterations of the nucleus area distribution depending on the experimental setting and time after irradiation (72).

The intensity and kinetics of the resulting cellular DNA damage signaling were determined using γH2AX focus scoring to verify if this response varied with clinical radio sensitivity. Normally, in foci per nucleus and foci area analyzes, when normalization is performed with 0 Gy, mutant p53 levels are generally higher than wt p53 levels, while wtp53 levels are higher than mutant p53 values when normalized with 0 Gy of mutant p53 levels. J3D wtp53 values were higher than mutant p53 values in both cases. One explanation of this measurement of intensity depends on staining quality (60). However, even though foci intensity values of wtp53 were also increased after normalization to mutated p53, wild type p53 values were not found higher than mutated p53 values, similar to the foci per nucleus and foci area. One reason could be due to foci intensity values are somewhat dependent on the staining quality, which this highlights the necessity for conducting experimental replicates.

Later, we also showed the foci distribution at each time points. At 1 h post-irradiation, all radiation qualities have mostly above 16 foci. The reason for this, as discussed above, 1 h post-irradiation levels were found to be highest compared to 24 h and 72 h post-irradiation levels for all radiation qualities. After 24 h post-irradiation, the levels of cells which contain foci decreased compared to 1 h post-irradiation. At 72 h post-irradiation, the levels of the cell were decreased more and determined for each foci range. These levels shifting can be observed due to DNA damage breaks are repaired over time (76). In irradiated cells at the highest dose and radiation quality, we found that the average number of foci per cell increased with the irradiation dose and quality. We analyzed the number of foci per cell to show that there is no saturation effect caused by overlapping focus signals as shown by Hernandez et al. (89).

In the final part of this work, we investigated the decay kinetics of the foci in J3D and BL41 cell lines by calculating the level of residual γ-H2AX foci at 24- and 72-hours post-IR. Residual percentages give information about the DNA repair kinetics of the cell. In BL41 and J3D cells, we observed that after 24 hours the radiation-induced γ-H2AX foci level decreased to a value comparable to the endogenous values and remained on this levelfor the next 72 hours. In J3D mutant p53 cells, the significant reduction was found Proton 2 Gy and 5 Gy over time. However, there was no significant reduction in Photon and Carbon IR in J3D cells.

Residual foci and foci area, in Photon IR treated BL41 mutant p53 levels were demonstrated higher than BL41 wtp53 cells levels whereas Proton IR and Carbon IR treated BL41 wtp53 residual levels were determined higher than BL41 mutant p53 cells levels at each time point. The general observation is Carbon IR residual damage frequency was higher than Photon and Proton IR at late time points, this related to Carbon IR caused complex damage in BL41 cells.

In contrast, in J3D cells, there were no significant residual levels between J3D mutant p53 and wtp53. Also, for three radiation qualities was not showed significant decreasing as a function of time except Proton 2 Gy and 5 Gy residual foci levels.

The particles have much more resistant DSB still at the late time points thereby, they are declining less. Repair of complex DSB breaks may require longer time and shows the slow repair. Radiation-type like Photon induces rapid repair and particles need slower repair (64). The lower levels of γ-H2AX at late time points might imply that the cells have a decreased capacity to repair IR-induced DNA lesions. Our results intimate a reduction in the kinetics of DNA repair as a function of time depicted by the retention of γH2AX residual foci.

The results in this thesis have clearly shown the higher efficiency of particle therapy compared to traditional Photon IR and how the radio-sensitivity varies

largely with dose, as well as highlighting the important role that p53 plays in DNA repair for all types of IR.

Since over 50% of human cancers have p53 mutations, mutational inactivation is a major molecular mechanism behind p53 dysfunction. As such the difference between the expression levels of wild type p53 and mutant p53 might be a critical determinant of cell fate in response to DNA damage as a result of IR. In this study, it was shown that inducing p53 caused killing cells better. Thus, the development of novel strategies to re-activate mutant p53 is required to provide clues to effectively treat malignant cancers bearing p53 mutations (83). This could be an idea as a therapy of lymphoma. Radiation may induce apoptosis in case of loss of function of the p53 protein (77). With respect to further clinical treatments, the detection of γ-H2AX with other scales could provide a new way of treatment for patients who are exposed to IR. These findings can be expanded to the identification of new druggable pathways and the development of more precise diagnostics and therapies based on the genetic profile of individual tumors.

Although further validation of these findings is required, we have provided evidence that particular cancer-specific mutations in the DDR pathway alter DNA repair kinetics and respond differently to ionizing radiation. Our findings may prove to be valuable in the context of clinical data and may potentially identify novel biomarkers for personalized radiotherapy.

6. REFERENCES

1. Jiang M, Bennani NN, Feldman AL. Lymphoma classification update: T-cell lymphomas, Hodgkin lymphomas, and histiocytic/dendritic cell neoplasms. Expert Rev Hematol. 2017 Mar; 10(3): 239–249. 239-249.

2. Swerdlow SH, Campo E, Pileri SA, Harris NL, Stein H, Siebert R, Advani R, Ghielmini M, Salles GA, Zelenetz AD and Jaffe ES. The 2016 revision of the World Health Organization classification of lymphoid neoplasms. 2016; Blood 127, s. 2375-2390. 2375-2390.

3. Yustein CV, JT and Dang. Biology and treatment of Burkitt's lymphoma. Curr Opin Hematol. 2007: 4. 375-81.

4. Love C, Sun Z, Jima D, Li G, Zhang J, Miles R, Richards KL, Dunphy CH, Choi WWL, Srivastava G, Lugar PL, Rizzieri DA, Lagoo AS, Bernal-Mizrachi L, Mann KP, Flowers CR, Naresh KN, Evens AM, Chadburn A, Gordon LI, Czader MB, Grill JI,Hsi ED, Dave SS. The genetic landscape of mutations in Burkitt lymphoma. 2012: Nature Genetics, 14. 1321-1325.

5. Maifrede S, Martin K, Podszywalow-Bartnicka P, Katherine S, Langer S, Nejati R, Dasgupta Y, Gritsyuk D, Nieborowska-Skorska M, Lupey L, Piwocka K, Wasik MA, Tempera I and Skorski T. IGH/MYC Translocation in Burkitt Lymphoma Is Associated with BRCA2 Deficiency and Synthetic Lethality By PARP1 Inhibitors. 2016: Blood, 2016, 128. 4111.

6. Chong LC, Ben-Neriah S, Slack GW, Freeman C, Ennishi D, Mottok A, Collinge B, Abrisqueta P, Farinha P, Boyle M, Meissner B,Kridel R , Gerrie AS,Villa D, Savage KJ,Laurie H. Sehn,Siebert R, Morin RD, Gascoyne RD, Marra MA, Connors JM, Mungall AJ, Steidl C. High-resolution architecture and partner genes of MYC rearrangements in. 20, 2018: Blood, 2018, 2. 2755–2765.

7. Sandlund JT. Burkitt lymphoma: staging and response evaluation 6. 2012: Br. J. Haematol. 156. 761-5.

8. Jacobson A, LaCasce and C. How I treat Burkitt lymphoma in adults. 19. 2014: Blood, 124. 2913-2020.

9. Zimmermann M, Oehler C, Mey U,Ghadjar P. and Zwahlencorresponding DR. Radiotherapy for Non-Hodgkin's lymphoma: still standard practice and not an outdated treatment option. 2016: Radiat Oncol. 11. 10.

10. Stephens FO, Aigner KR. Basics of Oncology. 2009: Springer.

11. International Agency for Reseach on Cancer (IARC). World Cancer Report *2008*. Organization World Health.

12. Hausmann, Sebastian. Antisense studies on base excision repair genes and their effects. Prof. Dr. Christoph Plass, Ruprecht-Karls-Universität. Division: Epigenomics and Cancer Risk Factors: 2011.

13. Holland J. New treatment modalities in radiation therapy. 2001: J Intraven Nurs, 24. 95-101.

14. Ikushima H. Radiation therapy: state of the art and the future. The Journal of Medical Investigation, 2010, 57.

15. Baskar R, Dai J, Wenlong N, Yeo R, and Yeoh KW. Biological response of cancer cells to radiation treatment. Front Mol Biosci, 2014.

16. Hall EJ, Giaccia AJ. Radiobiology for the Radiobiologist. 2012, 7. p.9-10.

17. Greubela C, Ilicic K, Rösch T, Reindl J, Siebenwirth C, Mosera M, Girsta S, Walsh DWM, Schmid TE, Dollinger G. Low LET proton microbeam to understand high-LET RBE by shaping spatial dose distribution. Nucl. Instr.Meth.B., 2017, 404. 155-161.

18. Allen C, Borak TB, Tsujii H, and Nickoloff JA. Heavy Charged Particle Radiobiology: Using Enhanced Biological Effectiveness and Improved Beam Focusing to Advance Cancer Therap. 1-2, Mutat Res., 2011, 711. 150–157.

19. Gameiro SR, Malamas AS, Bernstein MB, Tsang KY, Vassantachart A, Sahoo N, Tailor R, Pidikiti R, Guha CP, Hahn SM, Krishnan S, Hodge JW. Tumor Cells Surviving Exposure to Proton or Photon Radiation Share a Common Immunogenic Modulation Signature, Rendering Them More Sensitive to T Cell-Mediated Killing. Int J Radiat Oncol Biol Phys. 2016, 95. 120-130.

20. Trikalinos T, Terasawa T, Raman G, and Lau J. Particle Beam Radiation Therapies for Cancer. Comparative Effectiveness Technical Briefs, 2009.

21. Nickoloff J. K. Photon, light ion, and heavy ion cancer radiotherapy: paths from physics and biology to clinical practice. Ann Transl Med, 2015, 3. 336.

22. Alticozzi L. Radiotherapy with scanning carbon ions beams: biological dose analysis for partial treatment delivery. Bologna: Università di Bologna, 2016.

23. Scalliet J, P and Gueulette. Radiobiological Characterization of Clinical Proton and Carbon-Ion Beams. 2018. 1-11.

24. Mavragani I.V, Nikitaki Z.,Souli M.P, Aziz A, Nowsheen S, et al. Complex DNA Damage: A Route to Radiation-Induced Genomic Instability and Carcinogenesis. Cancers, 2017, 18.

25. Tommasino M, F and Durante. Proton Radiobiology. Cancers, 2015, 7. 353-381.

26. Holley AK, Miao L, St. Clair DK, and St. Clair WH. *Redox*-Modulated Phenomena and Radiation Therapy: The Central Role of Superoxide Dismutases. Antioxid Redox Signal. 2014, 20. 1567–1589.

27. Shuryak D. J, I and Brenne. A model of interactions between radiation-induced oxidative stress, protein and DNA damage in Deinococcus radiodurans. J Theor Biol. 2009, 261. 305–317.

28. Srinivas US, Tan BWQ, Vellayappan BA, Jeyasekharan AD. ROS and the DNA damage response in cancer. Redox Biol, 2018, 101084.

29. Olive PL. The role of DNA single- and double-strand breaks in cell killing by ionizing radiation. Radiat Res, 1998, 150. 42-51.

30. Yu, Wei Han and K. N. Ionizing Radiation, DNA Double Strand Break and Mutation. 2010, 4.

31. Schimid T, Dollinger G, Beisker W, Hable V, Greubel C, Auer S, Mittag A, Tarnok A, Friedl AA, Molls M, Ropper B. Differences in the kinetics of c-H2AX fluorescence decay after exposure. Int. J. Radiat. Biol., 2010, 86. 682–691.

32. Nakamura AJ1, Rao VA, Pommier Y, Bonner WM. The complexity of phosphorylated H2AX foci formation and DNA repair assembly at DNA double-strand breaks. Cell Cycle, 2010. 9. 389–397.

33. Stucki M, Clapperton JA, Mohammad D, Yaffe MB, Smerdon SJ, Jackson SP. MDC1 Directly Binds Phosphorylated Histone H2AX to Regulate Cellular Responses to DNA Double-Strand Breaks. Cell, 2005. 123. 1213-26.

34. Fernandez-Capetillo O1, Allis CD, Nussenzweig A. Phosphorylation of histone H2B at DNA double-strand breaks. J Exp Med., 2004, 199. 1671-7.

35. Bartova E, Krejci J, Harnicarova A, Galiova G & Kozubek S. Histone modifications and nuclear architecture: a review. J. Histochem. Cytochem. 2008, 56. 711–721.

36. Kinner A1, Wu W, Staudt C, Iliakis G. γ-H2AX in recognition and signaling of DNA double-strand breaks in the context of chromatin17, Nucleic Acids Res. 2008, 36. 5678-94.

37. Bonner W. M, Redon C. E, Dickey J.S. et all. γH2AX and cancer. Nature reviews cancer, 2008.

38. DNA double-stranded breaks induce histone H2AX phosphorylation on serine 139. J Biol Chem, 1998, 273 (5858-68)

39. Ivashkevich A, Redon CE, Nakamura AJ, Martin RF, and Martin OA. Use of the γ-H2AX Assay to Monitor DNA Damage and Repair in Translational Cancer Research. Cancer Lett, 2011, 123–133.

40. Podhorecka M, Skladanowski A, and Bozko P. H2AX Phosphorylation: Its Role in DNA Damage. Journal of Nucleic Acids, 2010.

41. Stiff T. et al. ATR-dependent phosphorylation and activation of ATM in response to UV treatment or replication fork stalling, EMBO J, 2006, 5775–5782.

42. Nikitaki Z, Nikolov V, Mavragani I.V, Plante I, Emfietzoglou D, Iliakis G, and Georgakilas A.G. Non-DSB Clustered DNA lesions: Does theory colocalize with the experiment? Radiat. Phys. Chem, 2016, 26–35.

43. Bassing C. H. et al. Histone H2AX: a dosage-dependent suppressor of oncogenic translocations and tumors. Cell, 2003, 359–370.

44. Sedelnikova O. A. and Bonner W. M. γH2AX in cancer cells: a potential biomarker for cancer diagnostics, prediction and recurrence. Cell Cycle, 2006, 2909–2913.

45. Ciccia A, Elledge SJ. The DNA damage response: making it safe to play with knives. Mol Cell, 2010, 179-204.

46. Giglia-Mari G, Zotter A and Vermeulen W. DNA Damage Response. Cold Spring Harb Perspect Biol, 2011.

47. Lovejoy CA, Cortez D. Common mechanisms of PIKK regulation. DNA Repair (Amst). 2009, 1004-1008.

48. Christmann M, Tomicic MT, Roos WP, Kaina B. Mechanisms of human DNA repair: an update. Toxicology, 2003,193. 3-34.

49. Morimura H, Fishman GA, Grover SA, Fulton AB, Berson EL, Dryja TP. Mutations in the RPE65 gene in patients with autosomal recessive retinitis pigmentosa or leber congenital amaurosis. Proc Natl. Acad. Sci. USA, 1998, (3088-93)

50. Rassool FV. DNA double strand breaks (DSB) and non-homologous end joining (NHEJ) pathways in human leukemia. Cancer Lett, 2003, 1-9.

51. Helleday T, Lo J, van Gent DC, Engelward BP. DNA double-strand break repair: from mechanistic understanding to cancer treatment. DNA Repair (Amst), 2007, 923.

52. WS, Fei P, and El-Deiry. P53 and radiation responses. Nature, 2003, 5774-5783.

53. Levine A. J. Targeting Therapies for the p53 Protein in Cancer Treatments. Annu. Rev. Cancer Biol. 2018.

54. Meek D. W. Tumour suppression by p53: a role for the DNA damage response? Nat. Rev. Cancer. 2009, 714-723.

55. Ramqvist T, Magnusson KP, Wang Y, Szekely L, Klein G, Wiman KG. Wild-type p53 induces apoptosis in a Burkitt lymphoma (BL) line that carries mutant p53. Oncogene, 1993, 1495-500.

56. Schmid TE, Zlobinskaya O, Multhoff G. Differences in Phosphorylated Histone H2AX Foci Formation and Removal of Cells Exposed to Low and High Linear Energy Transfer Radiation. Current Genomics. 2012, 418-25.

57. Olive PL, Banath JP, Sinnott LT. Phosphorylated histone H2AX in spheroids, tumors, and tissues of mice exposed to Etoposide and 3-Amino-1,2,4-Benzotriazine-1,3-Dioxide. Cancer Res, 2004, 5363–5369.

58. Rübe CE, Grudzenski S, Kühne M, Dong X, Rief N, Löbrich M, Rübe C. DNA double-strand break repair of blood lymphocytes and normal tissues analysed in a preclinical mouse model: implications for radiosensitivity testing. Clin Cancer Res. 2008, 6546-6555.

59. Barsoom SH. Studies to validate the Comet assay in measuring differential radiationinduced DNA damage in cancer cells. Leicester Cancer Research Centrer, 2018.

60. Rothkamm K1, Horn S. Gamma-H2AX as protein biomarker for radiation exposure. Ann Ist Super Sanita. 2009, 265-271.

61. Parrales T, and Iwakuma A. Targeting Oncogenic Mutant p53 for Cancer Therapy. Front Oncol. 2015.

62. Bana´th JP, MacPhail SH, and Olive PL. Radiation Sensitivity, H2AX Phosphorylation, and Kinetics of Repair of DNA Strand Breaks in Irradiated Cervical Cancer Cell Lines. Cancer Res October. 2004, 7144-7149.

63. Bylicky MA, Mueller GP, Day RM. Radiation resistance of normal human astrocytes: the role of non-homologous end joining DNA repair activity. Journal of Radiation Research. 2019, 37–50.

64. Markova E, Schultz N, Belyae IY. Kinetics and dose-response of residual 53BP1/gamma-H2AX foci: co-localization, relationship with DSB repair and clonogenic survival. Int J Radiat Biol, 2007, 319-29.

65. Mariotti LG, Pirovano G, Savage KI, Ghita M, Ottolenghi A, Prise KM. Use of the γ-H2AX Assay to Investigate DNA Repair Dynamics Following Multiple Radiation Exposures. PLoS One, 2013.

66. Bourton EC, Plowman PN, Zahir SA, Senguloglu GU, Serrai H, Bottley G, and Parris CN. Multispectral imaging flow cytometry reveals distinct frequencies of γ-H2AX foci induction in DNA double strand break repair defective human cell lines. Cytometry A. 2012 Feb. 130–137.

67. Schuch AP, Moreno NC, Schuch NJ, Menck CFM, Garcia CCM. Sunlight damage to cellular DNA: Focus on oxidatively generated lesions. Free Radic. Bio.l Med. 2017, 110-124

68. Aubrey BJ, Kelly GL, Janic A, Hero MJ and Strasser A. How p53 triggers apoptosis and its association with p53-mediated tumor suppression. Cell Death and Differentiation. 2017, 104-113.

69. Plastaras J. P. P, Berman A. T, Freedman G. M. Special Cases for Proton Beam Radiotherapy: Re-irradiation, Lymphoma, and Breast Cancer. Semin Oncol. 2014, 807-819.

70. Suit H, DeLaney T, Goldberg S, Paganetti H, Clasie B, Gerweck L, Niemierko A, Hall E, Flanz J, Hallman J, Trofimov A. Proton vs carbon ion beams in the definitive radiation treatment of cancer patients. Radiother Oncol. 2010, 3-22.

71. Chernov MF, Muragaki Y, Kesari S, McCutcheon. Proton and Carbon Ion Therapy of Intracranial Gliomas, IE (eds): Intracranial Gliomas. Part III-Innovative Treatment Modalities. Prog Neurol Surg. Basel Karger. 2018, 57-65.

72. Rassamegevanon T, Löck S, Baumann M, Krause M, Neubeck C. Heterogeneity of γH2AX Foci Increases in Ex Vivo Biopsies Relative to In Vivo Tumors. Int J Mol Sci. 2018.

73. Xia L, Paik A, and Li JJ. p53 Activation in Chronic Radiation-Treated Breast Cancer Cells. Regulation of MDM2/p14ARF. Cell and Tumor Biology, 2004.

74. Kim TM, Shin JM, Eun HC, Chung JO. He Role of p300 Histone Acetyltransferase in UV-Induced Histone Modifications and MMP-1 Gene Transcription. PLoS One, 2009.

75. Capoulade C, Bressac-de Paillerets B, Lefrère I, Ronsin M, Feunteun J, Tursz T and Wiels J. Overexpression of MDM2, due to enhanced translation, results in inactivation of wild-type p53 in Burkitt's lymphoma cells. Oncogene 1998, 1603–1610.

76. Martina O. A, Ivashkevich A, Chooe S, Woodbine L, Jeggo P.A. J, Martin R. F, Lobachevsky P. Statistical analysis of kinetics, distribution and co-localisation of DNA repair foci in irradiated cells: Cell cycle effect and implications for prediction of radiosensitivity. DNA Repair (Amst). 2013, 844-855.

77. Chowdhury D. et al. γH2AX dephosphorylation by protein phosphatase 2A facilitates DNA double-strand break repair. Mol. Cell. 2005, 801–809.

78. Stucki M, Clapperton JA, Mohammad D, Yaffe MB, Smerdon SJ, Jackson SP. MDC1 Directly Binds Phosphorylated Histone H2AX to Regulate Cellular Responses to DNA Double-Strand Breaks. Cell 2005, 1213-26.

79. Kinner A, Wu W, Staudt C, Iliakis G, γ-h2ax in recognition and signaling of DNA double-strand breaks in the context of chromatin. Nucl. Acids Res, 2008, 5678–5694.

80. Syed A, Tainer JA. The MRE11–RAD50–NBS1 Complex Conducts the Orchestration of Damage Signaling and Outcomes to Stress in DNA Replication and Repair. Annu Rev Biochem.2018, Jun 20; 87: 263–294.

81. Moulder DE, Hatoum D, Tay E, Lin Y, McGowan EM.The Roles of p53 in Mitochondrial Dynamics and Cancer Metabolism: The Pendulum between Survival and Death in Breast Cancer?Cancers (Basel). 2018 Jun 8;10(6): E189.

82. Donehower L.A., Harvey M., Slagle B.L., McArthur M.J., Montgomery C.A., Jr., Butel J.S., Bradley A. Mice deficient for p53 are developmentally normal but susceptible to spontaneous tumours. Nature. 1992. ;356:215–221.

83. Ozaki T and Nakagawara A.Role of p53 in Cell Death and Human Cancers. Cancers (Basel). 2011 Mar; 3(1): 994–1013.

84. Moroni MC, Hickman ES, Denchi EL, Caprara G, Colli E, Cecconi F, Muller H and Helin K. Apaf-1 is a transcriptional target for E2F and p53. Nat. Cell Biol. 2001. .3: 552–558.

85. Prives C and Hall PA. The p53 pathway. J. Pathol. 1999; 187, 112–126.

86. Williams AB, Schumacher B.p53 in the DNA-Damage-Repair Process. Cold Spring Harb Perspect Med. 2016 May 2;6(5).

87. Brown LC, Mutter RW, Halyard MY. Benefits, risks, and safety of external beam radiation therapy for breast cancer. Int J Womens Health. 2015; 7: 449–458.

88. Moon SH1, Lin L, Zhang X, Nguyen TA, Darlington Y, Waldman AS, Lu X, Donehower LA. Wild type p53-induced phosphatase 1 dephosphorylates histone variant gamma-H2AX and suppresses DNA double strand break repair.J Biol Chem. 2010 Apr 23;285(17):12935-47.

89. Laia Hernández L, Terradas M, Flix MM.Highly Sensitive Automated Method for DNA Damage Assessment: Gamma-H2AX Foci Counting and Cell Cycle Sorting. August 2013, International Journal of Molecular Sciences 14(8):15810-2.

CURRICULUM VITAE

Personal Information

Name	Fatma	Surname	Pınar
Place of Birth	Kadıköy, İstanbul	Date of Birth	26.11.1993
E-mail	fatmapinar993@gmail.com		

Education

Level	Institution Name	Graduation Year
Master of Science	Acıbadem Mehmet Ali Aydınlar University	2019
Undergraduate	Istanbul University	2016
High School	Üsküdar Ahmet Keleşoğlu Anadolu Lisesi	2011

Work Experience

Position	Corporation	Duration
Master Thesis	DKFZ	08.2018-03.2019
Research Scholar	Acıbadem Mehmet Ali Aydınlar University	09.2016-07.2018
Laboratory Intern	Heidelberg University, Center of Molecular Biology (ZMBH)	07.2015-08.2015
Laboratory Intern	Aziz Sancar Institute of Experimental Medicine	01.2014-02.2014
Laboratory Intern	Çapa Medicine Faculty, Istanbul University Department of Histology-Embrylogy	08.2013-09.2013
Laboratory Intern	Cerrahpaşa Medicine Faculty, Istanbul University Department of Histology-Embrylogy	01.2013-02.2013

Foreign Languages

Language	Reading*	Speaking*	Writing*
English	Advanced	Good	Advanced
German	Intermediate	Beginner	Intermediate

* Evaluated as advanced, good, intermediate, beginner

Exams

Name of the Exam	Quantitative	Equally Weighted	Verbal
ALES**	81	82	

**ALES: Akademik Personel ve Lisansüstü Eğitimi Giriş Sınavı

Computer Skills

Program	Ability to Use
Microsoft Office	Advanced
MATLAB	Beginner
R Studio	Beginner

* Evaluated as advanced, good, intermediate, beginner

Scholarships

Type	Institution	Years
MSc. Program of Medical Biotechnology, 100% Scholarship	Acıbadem Mehmet Ali Aydınlar University	2016-2019